

50  
10

**SINGULAR TRAJECTORIES IN AIRPLANE CRUISE-DASH OPTIMIZATION**

by

1960

Karl D. Bilimoria

Dissertation submitted to the Faculty of the  
Virginia Polytechnic Institute and State University  
in partial fulfillment of the requirements for the degree of  
Doctor of Philosophy  
in  
Aerospace Engineering

APPROVED:

~~\_\_\_\_\_~~  
Eugene M. Cliff, Chairman

~~\_\_\_\_\_~~  
Henry J. Kelley

~~\_\_\_\_\_~~  
Frederick H. Lutze

~~\_\_\_\_\_~~  
Harold L. Stalford

~~\_\_\_\_\_~~  
James F. Marchman III

January 1987

Blacksburg, Virginia

# **SINGULAR TRAJECTORIES IN AIRPLANE CRUISE-DASH OPTIMIZATION**

by

Karl D. Bilimoria

Eugene M. Cliff, Chairman

Aerospace Engineering

(ABSTRACT)

The problem of determining cruise-dash trajectories is examined for the case of time-fuel optimization using a linear combination of time and fuel as the performance index. These trajectories consist of a transient arc followed by a steady-state arc. For cases where the steady-state arc is flown with full throttle the associated skeletal transient trajectories are also flown with full throttle, and approach the cruise-dash points monotonically in an asymptotic fashion.

When the steady-state arc is flown at an intermediate throttle setting, the transient trajectories follow a singular control law and exhibit a complex structure that is different from the full-throttle transients. Singular transients in the vicinity of singular cruise-dash points are confined to a bounded singular surface. In state-space these trajectories trace out asymptotic spirals on the singular surface as they approach the steady-state arc. If the initial operating point lies outside the singular surface, then the transient trajectories are composites consisting of a full-throttle or zero-throttle segment flown until the singular surface is met, followed by a singular segment that fairs into the cruise-dash point.

Addressing the question of optimality of the steady-state arc, it was found that although steady-state cruise fails a Jacobi-type condition, steady-state cruise-dash can satisfy this condition if the emphasis on time is sufficiently large. The outcome of the Jacobi-type test appears to be connected with the eigenstructure of the linearized state-adjoint system.

## **Dedication**

To my parents      and  
and my sister

## **Acknowledgments**

I am indebted to Dr. Eugene Cliff and Dr. Henry Kelley for the help and guidance they have given me, and for their constant interest in this work. I wish to thank Dr. Frederick Lutze for making several helpful suggestions. Thanks are also due to Dr. Harold Stalford and Dr. James Marchman for serving on my committee.

This research was supported by NASA Langley Research Center under grant  
served as NASA Technical Officer.

I take this opportunity to thank all my friends for their help and advice,  
especially

# Table of Contents

<b>Chapter 1: Introduction.....</b>	<b>1</b>
<b>Chapter 2: Problem Formulation .....</b>	<b>6</b>
2.1 Aircraft Equations of Motion in the Point-Mass Model .....	6
2.2 Formulation of Problem in Terms of Optimal Control Theory .....	9
2.3 Determination of Singular Control .....	14
2.4 The Reduced Order Cruise-Dash Model .....	21
<b>Chapter 3: Necessary Conditions .....</b>	<b>25</b>
3.1 Classical Legendre-Clebsch Condition .....	26
3.2 Generalized Legendre-Clebsch Condition .....	28
3.3 Erdmann Corner Condition .....	32
3.4 McDannell-Powers Junction Condition .....	32

<b>Chapter 4: Numerical Results and Discussion .....</b>	<b>34</b>
4.1 General Structure of Cruise-Dash Trajectories .....	35
4.2 Full-Throttle Cruise-Dash Trajectories .....	36
4.3 Partial-Throttle Cruise-Dash Trajectories .....	39
4.4 Eigenvalue Analysis of the Linearized System .....	40
4.5 Concept of Singular Manifold .....	44
4.6 Singular Trajectories to the Equilibrium Point .....	46
4.7 Composite Bang-Singular Trajectories .....	48
4.8 Necessary Conditions .....	50
4.9 Bang-Bang Transient Trajectories.....	50
4.10 A Jacobi-type Condition.....	52
<b>Chapter 5: Conclusions .....</b>	<b>55</b>
5.1 Structure of Optimal Cruise-Dash Trajectories .....	56
5.2 Future Work .....	58
<b>References .....</b>	<b>59</b>
<b>Vita.....</b>	<b>104</b>

## List of Symbols

$C$ .....Thrust-Specific Fuel Consumption

$D$ .....Total Drag

$D_0$ .....Zero-Lift Drag

$D_i$ .....Level-Flight Induced Drag

$g$ .....Acceleration due to gravity

$H$ .....Hamiltonian

$h$ .....Altitude

$L$ .....Lift

$M$ .....Mach Number

$n$ .....Load Factor

$Q$ .....Fuel Flow Rate

$q$ .....Dynamic Pressure

$S$ .....Switching Function

$T$ .....Thrust



$t$  .....Time  
 $\underline{u}$  .....Control Vector  
 $V$  .....Airspeed  
 $W$  .....Weight  
 $W_F$  .....Weight of Fuel Consumed  
 $x$  .....Range  
 $\underline{z}$  .....Generalized State Vector

### Greek Symbols

$\gamma$  .....Flight Path-Angle  
 $\eta$  .....Throttle Setting  
 $\lambda_h$  .....Altitude Co-state Variable  
 $\lambda_\gamma$  .....Path-Angle Co-state Variable  
 $\lambda_v$  .....Velocity Co-state Variable  
 $\lambda_x$  .....Range Co-state Variable  
 $\lambda_w$  .....Fuel-Weight Co-state Variable  
 $\mu$  .....Fuel-Time Tradeoff Parameter  
 $\Phi$  .....Cost Function  
 $\rho$  .....Air Density

## Superscripts

.....Time Derivative

*o* .....Steady-state Outer Solution

*T* .....Transpose

\* .....Transpose-conjugate

## Subscripts

Except for those defined above, subscripted variables denote the partial derivative of that variable with respect to the subscript.

## List of Figures

Figure 1. Cruise-Dash Points in the (h,V) Plane.....	65
Figure 2. Altitude Time History for $\mu = 0$ sec/lb.....	66
Figure 3. Path-Angle Time History for $\mu = 0$ sec/lb .....	67
Figure 4. Velocity Time History for $\mu = 0$ sec/lb .....	68
Figure 5. Range Time History for $\mu = 0$ sec/lb.....	69
Figure 6. Fuel-Weight Time History for $\mu = 0$ sec/lb.....	70
Figure 7. Load-Factor Time History for $\mu = 0$ sec/lb .....	71
Figure 8. Normalized State Histories for $\mu = 0$ sec/lb .....	72
Figure 9. Altitude Time History for $\mu = 0.0095$ sec/lb.....	73
Figure 10. Path-Angle Time History for $\mu = 0.0095$ sec/lb.....	74
Figure 11. Velocity Time History for $\mu = 0.0095$ sec/lb.....	75
Figure 12. Range Time History for $\mu = 0.0095$ sec/lb .....	76
Figure 13. Fuel-Weight Time History for $\mu = 0.0095$ sec/lb .....	77
Figure 14. Load-Factor Time History for $\mu = 0.0095$ sec/lb .....	78

Figure 15. Normalized State Histories for $\mu = 0.0095$ sec/lb.....	79
Figure 16. Full-Throttle Cruise-Dash Trajectories in the (h,V) Plane .....	80
Figure 17. Eigenvalues of Linearized System with $\mu = 1000$ sec/lb.....	81
Figure 18. Eigenvalues of Linearized System with $\mu = 320$ sec/lb.....	82
Figure 19. Altitude Time History for $\mu = 320$ sec/lb.....	83
Figure 20. Path-Angle Time History for $\mu = 320$ sec/lb.....	84
Figure 21. Velocity Time History for $\mu = 320$ sec/lb.....	85
Figure 22. Throttle Time History for $\mu = 320$ sec/lb .....	86
Figure 23. Load-Factor Time History for $\mu = 320$ sec/lb.....	87
Figure 24. Singular Surface in $(\gamma, V, h)$ Space .....	88
Figure 25. Altitude Time History for (Full)Bang-Singular Control .....	89
Figure 26. Path-Angle Time History for (Full)Bang-Singular Control.....	90
Figure 27. Velocity Time History for (Full)Bang-Singular Control .....	91
Figure 28. Throttle Time History for (Full)Bang-Singular Control .....	92
Figure 29. Load-factor Time History for (Full)Bang-Singular Control .....	93
Figure 30. Altitude Time History for (Zero)Bang-Singular Control.....	94
Figure 31. Path-Angle Time History for (Zero)Bang-Singular Control .....	95
Figure 32. Velocity Time History for (Zero)Bang-Singular Control .....	96
Figure 33. Throttle Time History for (Zero)Bang-Singular Control.....	97
Figure 34. Load-Factor Time History for (Zero)Bang-Singular Control .....	98
Figure 35. Altitude Time History for Bang-Bang Control.....	99
Figure 36. Path-Angle Time History for Bang-Bang Control.....	100
Figure 37. Velocity Time History for Bang-Bang Control.....	101

Figure 38. Throttle Time History for Bang-Bang Control .....	102
Figure 39. Load-Factor Time History for Bang-Bang Control .....	103

## **Chapter 1: Introduction**

The problem of determining optimal flight trajectories for aircraft has been investigated by many researchers for a variety of performance indices. Time-optimal flight for a climb-dash mission has been investigated for the case of symmetric flight and is presented in Reference 1. A (non-trivial) extension of this problem to a turn-climb-dash mission involving 3-D flight is reported in Reference 2. Both studies used the point-mass model for the airplane dynamics and realistic aero-propulsive models. These studies revealed that optimal dash trajectories funnel rapidly into a skeletal or nominal path that leads to the dash-point. Although such trajectories can be described by optimal open-loop control laws, these studies concentrated on the synthesis of near-optimal closed-loop feedback laws for on-board implementation. For the case of time-optimal flight, the fuel consumed has no effect on the value of the performance index and for maneuvers of practical interest the throttle control is set at its maximum limit.

In contrast, fuel-optimal flight [3-8] minimizes the fuel consumed while generally covering a specified range and may require operation at an intermediate throttle-setting. The optimality of steady-state cruise (operation at a fixed altitude and velocity pair) has been the subject of some debate. Using the energy-model [9-13], Schultz and Zagalsky [14] showed that intermediate values of thrust violate the Legendre-Clebsch condition and are hence non-minimizing. With an intermediate vehicle model [15] featuring the flight-path angle as an additional control, Schultz and Zagalsky showed that the state-Euler equations are satisfied along a cruise arc. However, Speyer [16] showed that for this model the Generalized Legendre-Clebsch condition is not satisfied, indicating that the cruise arc is non-minimizing. Using the full point-mass model Schultz [17] showed that the cruise arc satisfies both the state-Euler equations and the Generalized Legendre-Clebsch condition. Speyer [18] then used the same point-mass dynamic model and showed that for certain aero-propulsive models, steady-state cruise fails to satisfy a Jacobi-like condition obtained by a transformation to the frequency domain [19] and is therefore non-optimal. He also showed that periodic (cyclic) cruise can result in improved fuel economy over steady-state cruise. The concept of periodic control has been used by other researchers to study the problem of fuel-optimal flight [20-23].

Between the two extremes of time-optimal and fuel-optimal flight (with range specified) is a spectrum of time-fuel-optimal flight conditions which may be regarded as members of a cruise-dash family. Such a situation arises when a

linear combination of time and fuel is used as a performance index and can be regarded as an exercise in time-fuel tradeoff. The present study focuses on the cruise-dash optimization problem with the aim of achieving an understanding of the nature and structure of this family.

It is well known [24-26] that aircraft dynamics may be separated into “fast” and “slow” dynamics corresponding to “inner” and “outer” solutions in a singular-perturbations approach [27]. The outer solution corresponds to steady-state operation at constant altitude and velocity with zero path-angle. The inner solution corresponds to a transient that takes the system to the steady-state and can be regarded as a boundary layer which may contain a sub-layer. By ignoring the dynamics of certain fast variables, a reduced-order model may be obtained and used to analyze the behavior of the system in those segments of the trajectory where the fast dynamics have no significant effect. The energy model [9-13] is a reduced-order model that has been used to study aircraft performance problems, although it was originally obtained from an *ad hoc* engineering approach. Order-reduction within the framework of singular perturbations was first applied to airplane trajectory optimization problems by Kelley [28-30].

Singular perturbation techniques can be used to extend the validity of reduced-order models (such as the energy-state and cruise-dash models) by correcting for the fast dynamics ignored in the order-reduction process. Separation of the system dynamics into fast and slow modes permits the



solution of a higher-order problem in terms of a series of lower-order problems. The inner and outer solutions obtained from a singular perturbations approach may then be joined together to form a composite by using the method of matched asymptotic expansions. Kelley [31], Ardema [32-33] and Calise [34-36] have employed this method to study airplane performance problems.

Although attractive, the singular perturbations approach does have its limitations. The fast dynamics of the system cannot be ignored in missions where the aircraft indulges in violent or “hard” maneuvers such as loop [37] or high angle-of-attack [38] maneuvers. In some treatments the separation of state variables, which is usually based on an *ad hoc* judgement, may lead to an effective decoupling of system dynamics that are actually closely coupled (e.g. altitude and path-angle dynamics). Since the separation of states is rarely distinct, the singular perturbation solution is generally only sub-optimal. It is possible to improve accuracy by making higher-order corrections at the expense of increased complexity of the problem.

The approach taken in this study is to make use of the time-scale separation and analyze the reduced-order cruise-dash model. Rather than using a singular perturbations approach to determine the inner solution, the “exact” point-mass model is used to study the transient dynamics. A first cut at the cruise-dash optimization problem was made [39] by considering the cruise-dash model which gives the steady-state or outer solution. In view of

Speyer's findings [18] regarding the non-optimality of steady-state cruise, one might question the wisdom of such an approach. However, this point is addressed in a later chapter where Speyer's analysis is re-traced for steady-state operation at a cruise-dash point. In the cruise-dash study [39] a family or locus of optimal steady-state operating points was obtained; each operating point corresponded to a particular value of a time-fuel tradeoff parameter. This provides a starting point for the present study where an attempt is made at understanding the nature of the transient trajectories that lead to the steady-state operating points. For cases with a heavy emphasis on fuel, it is likely that the throttle control would not be fixed at its upper bound, but may assume intermediate values. From the point of view of optimal control theory, this is a singular optimization problem and this feature lends an additional level of complexity to the problem. The problem of singular trajectories for time-range-fuel optimization of an ascending rocket is discussed in Reference 40.

The following chapter formulates the cruise-dash problem in terms of optimal control. An analysis of the problem is made and it is set up as a Two Point Boundary Value Problem. A singular control law is derived for the throttle control. Chapter 3 discusses the various necessary conditions for optimality with particular attention to the singular nature of the problem. Numerical results for a high-performance fighter aircraft are discussed in Chapter 4, and Chapter 5 summarizes the principal results obtained regarding the nature and structure of the cruise-dash family.

## Chapter 2: Problem Formulation

### 2.1 Aircraft Equations of Motion in the Point-Mass Model

The equations of motion in the point-mass model may be written as:

$$\dot{h} = V \sin \gamma \quad (2.1)$$

$$\dot{\gamma} = \frac{g}{V} (n - \cos \gamma) \quad (2.2)$$

$$\dot{V} = \frac{g}{W} [\eta T_{\max}(h, V) - D_o(h, V) - n^2 D_i(h, V)] - g \sin \gamma \quad (2.3)$$

$$\dot{x} = V \cos \gamma \quad (2.4)$$

$$\dot{W}_F = \eta Q_{\max}(h, V) \quad (2.5)$$

These equations are for symmetric flight in still air over a flat, non-rotating earth. In these equations,  $h$  is the altitude,  $V$  is the velocity (true airspeed),  $\gamma$  is the flight path-angle,  $x$  is the down-range and  $W_f$  is the weight of fuel consumed.  $g$  is the gravitational acceleration at sea level.  $n$  is the load-factor and is equal to the lift divided by the aircraft weight  $W$ . The maximum values of thrust and fuel flow-rate are  $T_{\max}$  and  $Q_{\max}$ , respectively. Both are represented as functions of altitude and velocity and are scaled by the throttle parameter  $\eta$ . This model embodies the assumption of constant aircraft weight, and thrust along the flight-path (small angle-of-attack).

The atmospheric data (air density and sonic velocity as functions of altitude) and aerodynamic data (zero-lift drag coefficient, induced drag coefficient and maximum lift coefficient as functions of Mach number) are represented by cubic splines [41]. The propulsive data (maximum thrust and fuel-flow as functions of altitude and Mach number) are represented by cubic spline lattices [42]. These data are a realistic representation of a high-performance interceptor aircraft. Since this aircraft is equipped with an afterburner there are two sets of propulsive data; one corresponds to maximum afterburning operation and the other corresponds to maximum non-afterburning operation (military thrust). The drag is modelled as a square-law with lift, and features realistic Mach-number dependence. The only assumption made is that the thrust-specific fuel consumption (TSFC) is independent of the throttle parameter  $\eta$ , and hence the thrust  $T$  and fuel flow-rate  $Q$  at any given altitude

and velocity pair are each sectionally linear functions of the throttle parameter  $\eta$ .

The state variables in the dynamical equations (2.1 - 2.5) are  $h$ ,  $\gamma$ ,  $V$ ,  $x$  and  $W_F$ , and the control variables are  $n$  and  $\eta$ . The system is subjected to certain inequality constraints involving state and control variables:

$$\beta_1 = (h - h_T) \geq 0 \quad (\text{terrain limit})$$

$$\beta_2 = (q_{\max} - 0.5 \rho V^2) \geq 0 \quad (\text{dynamic pressure limit})$$

$$\beta_3 = (M_{\max} - M) \geq 0 \quad (\text{Mach limit})$$

$$\beta_4 = (q S C_{L_{\max}}(M) - n W) \geq 0 \quad (\text{aerodynamic load-factor limit})$$

$$\beta_5 = (n_{\max} - n) \geq 0 \quad (\text{positive structural load-factor limit})$$

$$\beta_6 = (n - n_{\min}) \geq 0 \quad (\text{negative structural load-factor limit})$$

$$\beta_7 = (\eta - \eta_{\min}) \geq 0 \quad (\text{lower throttle limit})$$

$$\beta_8 = (\eta_{\max} - \eta) \geq 0 \quad (\text{upper throttle limit})$$

## 2.2 Formulation of Problem in Terms of Optimal Control Theory

The problem under consideration is the determination of an atmospheric flight-path that satisfies given initial and final conditions while minimizing a linear combination of time-elapsd and fuel-consumed. It is assumed that the range is sufficiently large to allow the decomposition of the trajectory into an initial transient, a steady-state and a terminal transient. In optimal control terms, this problem may be stated as:

Determine the controls  $n$  (load factor) and  $\eta$  (throttle setting) to transfer the dynamical system given by equations (2.1 - 2.5) and subject to the constraints  $\beta_i \geq 0$  from a given set of initial states  $(h_o, \gamma_o, V_o, x_o)$  to a given set of final states  $(h_f, \gamma_f, V_f, x_f)$  while minimizing a Mayer-type cost function

$$\Phi = t_f + \mu W_F(t_f)$$

The parameter  $\mu$  is specified as various values effecting a trade-off between time and fuel.

By varying the parameter  $\mu$ , a family of trajectories is obtained with varying amounts of emphasis on time and fuel. In particular with  $\mu = 0$ , a minimum-time trajectory is obtained. As  $\mu$  is increased, the emphasis on fuel

is correspondingly increased. The limiting case where  $\mu \rightarrow \infty$  corresponds to a best cruise (minimum fuel per unit distance) trajectory. The trajectories lying between these two extremes are termed cruise-dash trajectories. Negative values of  $\mu$  correspond to operating points between best cruise operation and best endurance (minimum fuel per unit time) operation [39].

The variational Hamiltonian [43-44] is formed by adjoining the right-hand sides of the system state differential equations (2.1 - 2.5) with the co-state variables (or Lagrange multipliers)  $\lambda_h, \lambda_\gamma, \lambda_V, \lambda_x, \lambda_W$ :

$$H = \lambda_h V \sin \gamma + \lambda_\gamma \frac{g}{V} (n - \cos \gamma) + \lambda_x V \cos \gamma + \lambda_W \eta Q_{\max} + \lambda_V \left[ \frac{g}{W} (\eta T_{\max} - D_o - n^2 D_i) - g \sin \gamma \right] \quad (2.6)$$

Constraints of the form  $\beta_i = 0$  are not adjoined to the Hamiltonian (with appropriate multipliers) since they are either absorbed into the aero-propulsive data or are found to be inactive. The co-state differential equations are obtained from:

$$\dot{\lambda}_h = - \frac{\partial H}{\partial h} \quad (2.7)$$

$$\dot{\lambda}_\gamma = - \frac{\partial H}{\partial \gamma} \quad (2.8)$$

$$\dot{\lambda}_V = - \frac{\partial H}{\partial V} \quad (2.9)$$

$$\dot{\lambda}_x = - \frac{\partial H}{\partial x} \quad (2.10)$$

$$\dot{\lambda}_W = - \frac{\partial H}{\partial W_F} \quad (2.11)$$

Substituting (2.6) in equations (2.7 - 2.11):

$$\dot{\lambda}_h = - \lambda_V \frac{g}{V} \eta T_{\max h} - \lambda_W \eta Q_{\max h} \quad (2.12)$$

$$\dot{\lambda}_\gamma = - \lambda_h V \cos \gamma + \lambda_\gamma \frac{g}{V} \sin \gamma + \lambda_V g \cos \gamma + \lambda_x \sin \gamma \quad (2.13)$$

$$\dot{\lambda}_V = - \lambda_h \sin \gamma + \lambda_\gamma \frac{g}{V^2} (n - \cos \gamma) - \lambda_x \cos \gamma \quad (2.14)$$

$$- \lambda_V \frac{g}{W} \left( \eta T_{\max v} - D_{o_v} - n^2 D_{i_v} \right) - \lambda_W \eta Q_{\max v}$$

$$\dot{\lambda}_x = 0 \quad (2.15)$$

$$\dot{\lambda}_W = 0 \quad (2.16)$$

Equations (2.1 - 2.5) and (2.12 - 2.16) are the state-Euler equations. The problem of solving these equations with the appropriate boundary conditions is a Two-Point-Boundary-Value-Problem (TPBVP). Generally, at the initial point, all five states are specified and the co-states are free; while at the final time, four states are specified and the fuel-weight is free. Thus at the final time all co-states are free except for  $\lambda_W$  which is specified to be equal to  $\mu$  by the



transversality condition [43]. At the final time, the transversality condition also requires that  $H = -1$ . Since the system is autonomous this condition must hold along the entire trajectory.

Using the Minimum Principle [43-44], the control vector  $\underline{u}$  may be determined from:

$$\underline{u} = \arg \left[ \min_{\underline{u}} H(\underline{u}) \right] \quad (2.17a)$$

A necessary condition for unconstrained components of  $\underline{u}$  that satisfy the Minimum Principle is:

$$\frac{\partial H}{\partial \underline{u}} = 0 \quad (2.17b)$$

Substituting (2.6) in (2.17b) with the components of  $\underline{u}$  as  $n$  and  $\eta$  yields:

$$\frac{\partial H}{\partial n} = \lambda_\gamma \frac{g}{V} - \lambda_V 2n \frac{g}{W} D_i = 0 \quad (2.18)$$

$$\frac{\partial H}{\partial \eta} = \lambda_V \frac{g}{W} T_{\max} + \lambda_W Q_{\max} = 0 \quad (2.19)$$

Equation (2.18) can be solved to obtain the control  $n$  as

$$n = \frac{\lambda_\gamma}{\lambda_V} \left( \frac{W}{2D_i V} \right) \quad (2.20)$$

However, equation (2.19) does not yield the control  $\eta$  since it appears linearly in the expression for the Hamiltonian (2.6). In order to determine the control  $\eta$ , the switching function  $S$  is defined as

$$S = \lambda_V \frac{g}{W} T_{\max} + \lambda_W Q_{\max} \quad (2.21)$$

The control  $\eta$  must be chosen so as to minimize the Hamiltonian (2.6). Noting that  $\eta$  is bounded, the throttle control law derived from the Minimum Principle (2.17a) may be stated as:

$$\text{If } S > 0, \text{ then } \eta = 0 \quad (2.22a)$$

$$\text{If } S < 0, \text{ then } \eta = 1 \quad (2.22b)$$

$$\text{If } S = 0 \text{ over a finite time interval, then } 0 \leq \eta \leq 1 \quad (2.22c)$$

If  $S = 0$  only for an isolated instant of time ( $t_s$ ), then  $t_s$  is a *switching point* and the control switches or jumps from one bound to the other. However, if  $S = 0$  over a finite interval of time  $[t_1, t_2]$ , then the control has an intermediate value that lies between its two bounds. The problem of determining the control  $\eta$  when  $S = 0$  for a finite time interval is called a singular control problem and the control  $\eta$  is a *singular control*. The segment of the trajectory over which the control is singular is termed a *singular arc*.

### 2.3 Determination of Singular Control

The problem of determining a singular arc arises when the application of the Minimum Principle in the form (2.17b) yields no information about the control, and the switching function is identically zero over a non-zero time interval. In such a case, the switching function  $S$  may be differentiated with respect to time until the singular control appears with a coefficient that is not identically zero [45-46]. If  $(2k)$  time derivatives are required, then the *order* of the singular arc is  $k$ . The singular control may then be obtained by solving the equation  $\frac{d^{2k}S}{dt^{2k}} = 0$ .

Along a singular arc one has

$$S = \lambda_V \frac{g}{W} T_{\max} + \lambda_W Q_{\max} = 0 \quad (2.23)$$

The thrust-specific fuel consumption (TSFC) is defined as the ratio

$$C(h, V) = \frac{Q_{\max}(h, V)}{T_{\max}(h, V)} \quad (2.24)$$

so that equation (2.23) may be written as

$$S = T_{\max} \left( \lambda_V \frac{g}{W} + \lambda_W C \right) = 0 \quad (2.25)$$

Hence, along a singular arc

$$\lambda_V = -\lambda_W \frac{W}{g} C \quad (2.26)$$

The time derivative of the switching function is:

$$\dot{S} = T_{\max} \left( \dot{\lambda}_V \frac{g}{W} + \lambda_W \dot{C} \right) + \dot{T}_{\max} \left( \lambda_V \frac{g}{W} + \lambda_W C \right) \quad (2.27)$$

Using  $S = 0$  (eqn. 2.26), we get

$$\dot{S} = T_{\max} \left( \dot{\lambda}_V \frac{g}{W} + \lambda_W \dot{C} \right) \quad (2.28)$$

Using (2.24, 2.26) in (2.14) we have

$$\begin{aligned} \dot{\lambda}_V = & -\lambda_h \sin \gamma + \lambda_\gamma \frac{g}{V^2} (n - \cos \gamma) + \lambda_V \frac{g}{W} (D_{oV} + n^2 D_{iV}) \\ & - \lambda_x \cos \gamma - \lambda_W C_V T_{\max} \eta \end{aligned} \quad (2.29)$$

Since  $C = C(h, V)$ ,

$$\begin{aligned} \dot{C} = & C_h \dot{h} + C_V \dot{V} \\ = & C_h V \sin \gamma + C_V \frac{g}{W} T_{\max} \eta - C_V \frac{g}{W} (D_o + n^2 D_i) - C_V g \sin \gamma \end{aligned} \quad (2.30)$$

Substituting (2.29, 2.30) in (2.28) and then using  $S = 0$  (eqn. 2.26), we get:

$$\begin{aligned} \frac{W}{g T_{\max}} \dot{S} = & -\lambda_h \sin \gamma + \lambda_\gamma \frac{g}{V^2} (n - \cos \gamma) - \lambda_x \cos \gamma \\ & + \lambda_W \left[ \left( C_h \frac{V}{g} - C_V \right) W \sin \gamma - C_V (D_o + n^2 D_i) - C (D_{oV} + n^2 D_{iV}) \right] \end{aligned} \quad (2.31)$$

Using  $S = 0$  (eqn.2.26) in  $H = -1$

$$\begin{aligned} (-\lambda_h \sin \gamma - \lambda_x \cos \gamma) = & \frac{1}{V} + \lambda_\gamma \frac{g}{V^2} (n - \cos \gamma) \\ & + \lambda_W \frac{C}{V} (D_o + n^2 D_i + W \sin \gamma) \end{aligned} \quad (2.32)$$

Substituting (2.32) in (2.31)

$$\begin{aligned} \frac{W}{g T_{\max}} \dot{S} = & \frac{1}{V} + \lambda_\gamma \frac{2g}{V^2} (n - \cos \gamma) + \lambda_W \left[ \left( C_h \frac{V}{g} - C_V + \frac{C}{V} \right) W \sin \gamma \right. \\ & \left. + \left( \frac{C}{V} - C_V \right) (D_o + n^2 D_i) - C (D_{oV} + n^2 D_{iV}) \right] \end{aligned} \quad (2.33)$$

It is convenient to define a function  $G(h, \gamma, V, \lambda_\gamma, \lambda_W)$  as the right-hand side of equation (2.33). That is,

$$\begin{aligned} G(h, \gamma, V, \lambda_\gamma, \lambda_W) = & \frac{1}{V} + \lambda_\gamma \frac{2g}{V^2} (n - \cos \gamma) + \lambda_W \left[ \left( C_h \frac{V}{g} - C_V + \frac{C}{V} \right) W \sin \gamma \right. \\ & \left. + \left( \frac{C}{V} - C_V \right) (D_o + n^2 D_i) - C (D_{oV} + n^2 D_{iV}) \right] \end{aligned} \quad (2.34)$$

Note that the function  $G$  involves the load factor  $n$ , which can be expressed by a known function of the states and co-states. We have from equation (2.20)

$$n = \frac{\lambda_\gamma}{\lambda_V} \left( \frac{W}{2D_i V} \right) \quad (2.35)$$

Using  $S = 0$  (2.26) in (2.35) we get

$$n = - \frac{\lambda_\gamma}{\lambda_W} \left( \frac{g}{2D_i C V} \right) \quad (2.36)$$

Thus, along a singular arc, the load factor  $n$  is a function of  $h$ ,  $V$ ,  $\lambda_\gamma$  and  $\lambda_W$ .

We evaluate the derivatives  $n_h$ ,  $n_V$  and  $n_{\lambda_\gamma}$  (for later use) as follows:

$$n_h = -n \left[ \frac{D_{i_h} C + D_i C_h}{D_i C} \right] \quad (2.37)$$

$$n_V = -n \left[ \frac{D_{i_V} V C + D_i C + D_i V C_V}{D_i V C} \right] \quad (2.38)$$

$$n_{\lambda_\gamma} = n \left[ \frac{1}{\lambda_\gamma} \right] \quad (2.39)$$

From equation (2.34)

$$\dot{S} = \frac{g}{W} T_{\max} \dot{G} \quad (2.40)$$

Therefore

$$\dot{S} = \frac{g}{W} T_{\max} \dot{G} + \frac{g}{W} \dot{T}_{\max} G \quad (2.41)$$

Using  $\dot{S} = 0$  (eqn. 2.40), we have

$$\ddot{S} = \frac{g}{W} T_{\max} \dot{G} \quad (2.42)$$

Hence

$$\frac{W}{g T_{\max}} \ddot{S} = \left( \dot{h}G_h + \dot{\gamma}G_\gamma + \dot{V}G_V + \dot{\lambda}_\gamma G_{\lambda_\gamma} \right) \quad (2.43)$$

where

$$\begin{aligned} G_h = & \lambda_\gamma \left[ \frac{2g}{V^2} n_h \right] + \lambda_W \left[ \left( C_{hh} \frac{V}{g} - C_{vh} + \frac{C_h}{V} \right) W \sin \gamma - C_h (D_{oV} + n^2 D_{iV}) \right. \\ & + (D_{o_h} + n^2 D_{i_h} + 2nn_h D_i) \left( \frac{C}{V} - C_V \right) \\ & \left. + (D_o + n^2 D_i) \left( \frac{C_h}{V} - C_{vh} \right) - C (D_{o_{vh}} + n^2 D_{i_{vh}} + 2nn_h D_{iV}) \right] \end{aligned} \quad (2.44)$$

$$\begin{aligned} G_V = & -\frac{1}{V^2} + \lambda_\gamma \left[ \frac{2g}{V^2} n_V - \frac{4g}{V^3} (n - \cos \gamma) \right] \\ & + \lambda_W \left[ \left( C_{hV} \frac{V}{g} + \frac{C_h}{g} - C_{VV} + \frac{C_V}{V} - \frac{C}{V^2} \right) W \sin \gamma \right. \\ & - C (D_{o_{VV}} + n^2 D_{i_{VV}} + 2nn_V D_{iV}) + \left( \frac{C}{V} - C_V \right) (D_{oV} + n^2 D_{iV} + 2nn_V D_i) \\ & \left. + \left( \frac{C_V}{V} - \frac{C}{V^2} - C_{VV} \right) (D_o + n^2 D_i) - C_V (D_{oV} + n^2 D_{iV}) \right] \end{aligned} \quad (2.45)$$

$$G_\gamma = \lambda_\gamma \left[ \frac{2g}{V^2} \sin \gamma \right] + \lambda_W \left[ \left( C_h \frac{V}{g} - C_V + \frac{C}{V} \right) W \cos \gamma \right] \quad (2.46)$$

$$G_{\lambda_\gamma} = \frac{2g}{V^2} (2n - \cos \gamma) + n \frac{g}{D_i C V} \left[ C D_{i_v} + D_i \left( C_V - \frac{C}{V} \right) \right] \quad (2.47)$$

The switching function  $S$  has now been differentiated twice with respect to time and it can be seen from equation (2.43) that the singular control appears in the expression for  $\ddot{S}$  through the  $\dot{V}$  term. Thus, the singular arc is of first order, unless the coefficient of  $\eta$  (which is  $T_{\max} G_V$ ) is identically zero.

Setting  $\ddot{S} = 0$

$$\eta = \frac{(D_o + n^2 D_i)}{T_{\max}} + \left[ \frac{W \sin \gamma}{T_{\max}} + \frac{NUM}{DEN} \right] \quad (2.48)$$

where

$$NUM = G_h \dot{h} + G_\gamma \dot{\gamma} + G_{\lambda_\gamma} \dot{\lambda}_\gamma \quad (2.49)$$

$$DEN = -\frac{g}{W} T_{\max} G_V \quad (2.50)$$

At equilibrium, the time derivatives of all states (except  $x$  and  $W_F$ ) and co-states are zero. Thus it is clear that  $NUM$  in (2.49) will be equal to zero at equilibrium. The flight-path angle  $\gamma$  is also zero at equilibrium. As a result, the



quantity in square brackets in (2.48) vanishes at equilibrium, and the steady-state control law is simply

$$\eta^o = \frac{(D_o + n^2 D_i)}{T_{\max}} \quad (2.51)$$

This is equivalent to stating that the thrust must equal drag, which is precisely what level-flight equilibrium requires.

Thus it can be seen that the singular control is made up of two distinct parts and can be represented as

$$\eta = \eta^o + \bar{\eta} \quad (2.52)$$

where

$$\eta^o = \frac{(D_o + n^2 D_i)}{T_{\max}} \quad (2.53)$$

$$\bar{\eta} = \left[ \frac{W \sin \gamma}{T_{\max}} + \frac{NUM}{DEN} \right] \quad (2.54)$$

The first part  $\eta^o$  may be regarded as a “steady-state” component, and the second part  $\bar{\eta}$  as a transient component which vanishes as the system approaches equilibrium. In fact,  $\eta^o$  is also time-varying since  $D_o$ ,  $D_i$  and  $T_{\max}$  are functions of  $(h, V)$ , and the load-factor  $n$  is varying.

## **2.4 The Reduced-Order Cruise-Dash Model**

Equations (2.1 - 2.5) are the aircraft equations of motion written in the point-mass model and include altitude, path-angle and velocity dynamics. It is known [24-26, 27-30] that the altitude and path-angle dynamics take place on a “fast” time-scale, and the velocity dynamics on an “intermediate” time-scale. The range and fuel dynamics take place on a “slow” time-scale and continue even after the “fast” and “intermediate” dynamics have died out. They may therefore be regarded as the steady-state response of the system, while altitude, path-angle and velocity dynamics form the transient response of the system. If the trajectory is sufficiently long, it can in general be decomposed into three parts:

1. An initial transient going from the prescribed initial states to the steady-state segment.
2. A steady-state segment (or cruise-dash arc) where the “fast” and “intermediate” dynamics are ignorable.
3. A terminal transient going off the steady-state segment to the prescribed final states.

The transients generally fair asymptotically into the cruise-dash arc at both ends, and together they form a composite trajectory. Since the terminal

transient can be treated as an initial transient in retro-time, any analysis made for one is valid for the other. Thus we need consider only the initial transient and the cruise-dash arc. There is evidence [18] that the transient does not always die out with “cyclic” cruise-dash [20-23]. The steady-state or cruise-dash problem has been studied and is discussed in References 39 and 47. The major results of [39] are reproduced in the remainder of the present section for the sake of continuity and completeness.

The cruise-dash model ~~model~~ may be obtained from the point-mass model (2.1 - 2.5) by setting the right-hand sides of equations (2.1 - 2.3) to zero and retaining equations (2.4 - 2.5).

$$\dot{x} = V \cos \gamma \quad (2.55)$$

$$W\dot{F} = \eta Q_{\max}(h, V) \quad (2.56)$$

There are now only two states,  $x$  and  $W_F$  ;  $\eta$  and  $n$  are still controls. The variables  $h$ ,  $\gamma$  and  $V$  (which were states in the point-mass model) now take on the role of control variables, and are required to satisfy

$$(\dot{h} = ) V \sin \gamma = 0 \quad (2.57)$$

$$(\dot{\gamma} = ) \frac{g}{V} (n - \cos \gamma) = 0 \quad (2.58)$$

$$(\dot{V} = ) \frac{g}{W} [\eta T_{\max} - D_o - n^2 D_i] - g \sin \gamma = 0 \quad (2.59)$$

Solving the above three equations yields

$$\gamma^o = 0 \quad (2.60)$$

$$n^o = 1 \quad (2.61)$$

$$\eta^o = \frac{D}{T_{\max}} \quad (2.62)$$

where

$$D = (D_o + D_i) \quad (2.63)$$

The “free controls”  $h^o$  and  $V^o$  are the values of  $h$  and  $V$  that minimize the Hamiltonian

$$H = \lambda_x V + \lambda_W C D \quad (2.64)$$

From the transversality conditions [43] it can be shown that

$$\lambda_W^o = \mu \quad (2.65)$$

$$\lambda_x^o = - \left( \frac{1 + \mu C D}{V} \right) \quad (2.66)$$

It is convenient to introduce the parameter  $v$  as

$$v = \frac{\lambda_W^o}{\lambda_x^o} \quad (2.67)$$

so that the controls  $h^o$  and  $V^o$  may now be obtained from

$$(h^o, V^o) = \arg \left[ \min_{(h,V)} (v C D - V) \right] \quad (2.68)$$

Making use of the fact that the time derivative of all the co-state variables is zero in the steady-state, one can obtain [18]

$$\lambda_h^o = - \frac{C W}{V} \quad (2.69)$$

$$\lambda_V^o = - C \frac{W}{g} \quad (2.70)$$

$$\lambda_\gamma^o = - 2 C D_i \frac{V}{g} \quad (2.71)$$

Solving equation (2.68) for  $h^o$  and  $V^o$  for various values of  $v$  yields a locus of steady-state operating points or cruise-dash points ranging from the dash-point (minimum time) through the cruise-point (minimum fuel per unit distance) to the endurance-point (minimum fuel per unit time). For the aircraft data used, it was found [39] that this locus has several breaks and excludes certain bands of velocity from the set of optimal operating points. The family of optimal cruise-dash points is presented in Fig. 1.

## Chapter 3: Necessary Conditions

The state-Euler equations discussed in the previous chapter together with the associated transversality conditions constitute a collection of first-order necessary conditions. Solutions of the state-Euler system are termed *extremals*. Further tests are required before any claim can be made with respect to the minimizing nature of these extremals. A set of necessary conditions can form [48-49, 43] a sufficiency condition for a weak or strong local minimum. It is emphasized that all the necessary conditions are local in nature and the strongest claim one can make about an extremal is that it provides a strong relative minimum - nothing can be said about the global minimizing nature of the extremal without further argument. In the following three sections, some of the necessary conditions are examined in detail. The last two sections deal with corner and junction conditions, applicable when two segments are joined at a "corner".

### 3.1 Classical Legendre-Clebsch Condition

The aircraft equations of motion involve two control variables: the load-factor  $n$  which appears quadratically and the throttle-setting  $\eta$  which appears linearly. Due to the assumption of thrust-along-flightpath (small angle-of-attack), these controls are non-coupled. The Classical Legendre-Clebsch necessary condition is that the matrix made up of the second-partials of the Hamiltonian with respect to the control variables be positive-semidefinite.

$$[H_{\underline{u}\underline{u}}] \geq 0 \quad (3.1)$$

For the problem under consideration, the control vector  $\underline{u}$  is given by

$$\underline{u} = \begin{bmatrix} n \\ \eta \end{bmatrix} \quad (3.2)$$

Hence

$$[H_{\underline{u}\underline{u}}] = \begin{bmatrix} H_{nn} & H_{n\eta} \\ H_{\eta n} & H_{\eta\eta} \end{bmatrix} \quad (3.3)$$

From the expression for the Hamiltonian (2.6) we get:

$$H_{nn} = \frac{\partial^2 H}{\partial n^2} = \lambda_V 2n \frac{g}{W} D_i \quad (3.4a)$$

$$H_{n\eta} = \frac{\partial^2 H}{\partial n \partial \eta} = 0 \quad (3.4b)$$

$$H_{\eta n} = \frac{\partial^2 H}{\partial \eta \partial n} = 0 \quad (3.4c)$$

$$H_{\eta\eta} = \frac{\partial^2 H}{\partial \eta^2} = 0 \quad (3.5d)$$

Thus the Classical Legendre-Clebsch necessary condition (3.1) becomes:

$$[H_{uu}] = \begin{bmatrix} H_{nn} & 0 \\ 0 & 0 \end{bmatrix} \geq 0 \quad (3.6)$$

In order that a  $(2 \times 2)$  matrix be positive-semidefinite, a necessary and sufficient condition [50] is that its determinant and both its diagonal elements be non-negative. Applying this condition to  $[H_{uu}]$  in equation (3.3), all of the following three conditions must be satisfied:

$$H_{nn} \geq 0 \quad (3.6a)$$

$$H_{\eta\eta} \geq 0 \quad (3.6b)$$

$$(H_{nn} H_{\eta\eta} - H_{n\eta} H_{\eta n}) \geq 0 \quad (3.6c)$$

The first condition (3.6a) is simply the Classical Legendre-Clebsch condition applied to the quadratic control  $n$ . This condition will be satisfied in the



strengthened form when the control  $n$  is not at a bound and locally minimizes the Hamiltonian  $H$ .

It can be seen that the last two conditions (3.6b, 3.6c) are satisfied only in the equality form and hence the matrix  $[H_{uu}]$  is not positive-definite, but only positive-semidefinite. Therefore, the Legendre-Clebsch condition is satisfied only in the weak form. As a result, additional tests are required to determine optimality over short lengths of arc.

### **3.2 Generalized Legendre-Clebsch Condition**

In the previous section, it was seen that if one of the controls appears linearly in the Hamiltonian, the Classical Legendre-Clebsch condition is satisfied only in the weak form (i.e. as an equality). Therefore, if one of the controls is singular, this test yields no information on the minimizing nature of the extremal.

For such cases, the Generalized Legendre-Clebsch condition must be satisfied along a candidate extremal. The mathematical treatment for extending the Classical Legendre-Clebsch condition to cases where one or more of the controls is singular is given in References [45-46, 51-54]. The Accessory Minimum Problem (AMP) is first formulated [51]. Since the original problem is singular, the AMP is also singular. Using Goh's transformation [51-52] of

(singular) control and state variables, the singular AMP is transformed to a non-singular AMP [53]. Application of the Classical Legendre-Clebsch condition to the transformed (non-singular) AMP yields the Generalized Legendre-Clebsch condition, which requires [54] that the matrix  $[R]$  given below be positive-semidefinite.

$$[R]_{(m \times m)} = \begin{bmatrix} R_1 & R_2^T \\ R_2 & R_3 \end{bmatrix} \geq 0 \quad (3.7)$$

For the problem under consideration  $m = 2$ , and the sub-matrices  $R_1$ ,  $R_2$  and  $R_3$  are scalars given by:

$$R_1 = \frac{\partial^2 H}{\partial n^2} \quad (3.8a)$$

$$R_2 = \frac{\partial}{\partial \eta} \left[ \frac{d}{dt} \left( \frac{\partial H}{\partial n} \right) \right] \quad (3.8b)$$

$$R_3 = - \frac{\partial}{\partial \eta} \left[ \frac{d^2}{dt^2} \left( \frac{\partial H}{\partial \eta} \right) \right] \quad (3.8c)$$

Positive semi-definiteness of the matrix  $[R]$  requires that all of the following three conditions hold:

$$R_1 = \frac{\partial^2 H}{\partial n^2} \geq 0 \quad (3.9a)$$

$$R_3 = - \frac{\partial}{\partial \eta} \left[ \frac{d^2}{dt^2} \left( \frac{\partial H}{\partial \eta} \right) \right] \geq 0 \quad (3.9b)$$

$$(R_1 R_3 - R_2^2) \geq 0 \quad (3.9c)$$

The first condition (3.9a) is the Classical Legendre-Clebsch condition applied to the non-singular (quadratic) control  $n$ , the second condition (3.9b) is the Kelley condition applied to the singular (linear) control  $\eta$ , and the third condition (3.9c) is the Goh condition which involves both singular and non-singular controls. Thus the Generalized Legendre-Clebsch condition for the problem under consideration is given by equations (3.9a-c) and is a combination of the Classical Legendre-Clebsch, Kelley and Goh conditions.

If the matrix  $[R]$  is positive-definite and equations (3.9a-c) are satisfied with a strict inequality, then no additional conditions are imposed by this treatment. This would be true for a minimizing first-order singular arc. However, if any of these equations is satisfied only as an equality then additional conditions analogous to those presented above must also be satisfied. These conditions are obtained by successive application of the Goh transform, and are applicable in the case of higher-order singular arcs.

For the problem under study the quantities  $R_1, R_2$  and  $R_3$  are evaluated as:

$$R_1 = \lambda_V 2n \frac{g}{W} D_j \quad (3.10a)$$

$$R_2 = \frac{g}{W} T_{\max} \left[ -\lambda_\gamma \frac{g}{V^2} + 2\lambda_W (CD_i n_V + C_V D_i n + CD_{i_V} n) \right] \quad (3.10b)$$

$$R_3 = \frac{g}{W} T_{\max} G_V \quad (3.10c)$$

where  $G_V$  is given by equation (2.45).

An additional condition imposed by Goh's treatment [52] is that the matrix

$$[Q]_{(m^* \times m^*)} = \left[ \frac{\partial^2 H}{\partial \underline{x} \partial \underline{u}} \right]_{(m^* \times n)} \quad \left[ \frac{\partial f}{\partial \underline{u}} \right]_{(n \times m^*)}$$

must be identically symmetric, where

$\underline{x}$  = state vector of order  $n$

$\underline{u}$  = control vector of order  $m$

$f$  = right-hand-side of the state differential equation vector

$m^*$  = number of linearly appearing controls

For the problem under consideration  $m^* = 1$ , and hence the matrix  $[Q]$  is trivially symmetric. Therefore the above condition is always satisfied.

This condition is identical to the Robbins equality condition [55].

### 3.3 Erdmann Corner Condition

The state-Euler equations employ the assumption that the state and co-state variables are continuous and have continuous first time derivatives. This will hold true for cases where the control variables are continuous. However, if any control variable *jumps* (is discontinuous), then the time derivatives of the states will, in general, be discontinuous. If this is the case we have a *broken extremal* [48] or a *corner*. At a corner (or junction of two extremals) the Erdmann Corner Condition [48-49] must be satisfied. This condition requires that all the co-state variables be continuous at a corner.

### 3.4 McDanell-Powers Junction Condition

The joining of singular and non-singular arcs generally involves a jump in the singular control variable(s) and hence the junction is a corner. Therefore the Erdmann Corner Condition applies at the junction of singular and non-singular arcs. Additionally, the McDanell-Powers Junction Condition [56, 46] stated below applies:

If  $r$  is the lowest order derivative of the (singular) control which is discontinuous at the junction and if  $q$  is the order of the singular arc, then  $(q + r)$  must be an odd integer.

For a first order singular arc ( $q = 1$ ), this condition may be interpreted as follows:

1. If the singular control is unsaturated at a junction, then it can jump to either the upper or lower bound ( $r = 0$ ).
2. If the singular control saturates at a junction with a non-zero time derivative, it *must* jump to the opposite bound ( $r = 0$ ).
3. If the singular control saturates at a junction with a zero time derivative, it can either jump to the opposite bound ( $r = 0$ ) or stay at the same bound ( $r = 2$ ).

## **Chapter 4: Numerical Results and Discussion**

It was seen in Chapter 2 that application of the Minimum Principle to the flight-path optimization problem at hand results in a nonlinear Two Point Boundary Value Problem (TPBVP) where some of the boundary conditions are known at one boundary and the rest at the other boundary. The differential equations involved are the state-Euler equations (2.1 - 2.5, 2.12 - 2.16). These are the equations for lifting atmospheric flight and are highly nonlinear. In addition, the state-Euler system is unstable, leading to errors in integration. Since a closed-form analytical solution for such problems is not known, a numerical scheme must be employed. A numerical solution of this TPBVP is far from trivial, given the nonlinear and unstable nature of the differential equations.

The numerical scheme employed in this study is the Multiple Shooting Method [57-58] which is a refinement of the Simple Shooting Method. In Simple Shooting, the unknown variables at the initial point are guessed and the

equations integrated forward. Depending on the match (or mis-match) of the boundary conditions at the terminal point, the guessed values of the unknown variables are updated and the cycle repeated until all the boundary conditions are met. In the Multiple Shooting Method, the time interval is divided into several segments thus reducing the integration time and the associated error build-up. The values of variables at all the grid points are adjusted to meet the boundary conditions at the end-points and compatibility conditions at intermediate points. Multiple Shooting may be interpreted as Simple Shooting in a higher dimensional problem. This method tames the inherent instability of the system of differential equations at the expense of computational complexity [59]. Provided that a “good” initial estimate of the states and co-states can be made at all the grid points, this method works well and has been used successfully for solving airplane trajectory optimization problems [1-2]. This study uses the Multiple Shooting package BOUNDSCO supplied by Dr. K. Well of DFVLR, West Germany and Dr. R. Bulirsch of the Technical University of Munich, West Germany.

#### **4.1 General Structure of Cruise-Dash Trajectories**

As discussed in Chapter 2, an optimal trajectory for the cruise-dash problem is a composite consisting of a transient part and a steady-state part. Steady-state cruise-dash has been studied in an earlier work [39], and optimal steady-state operating points have been computed over the entire spectrum



of interest from the dash-point through the cruise-point to the endurance-point. These are shown in Figure 1 along with the military and afterburning flight envelopes. Each of these points corresponds to a certain value of the parameter  $\mu$  which may be regarded as a measure of time-fuel tradeoff. Since the aircraft weight is assumed to be constant, the cruise-dash arc corresponds to steady-state operation at an appropriate  $(h^o, V^o)$  point which is constant with respect to time.

In general the initial operating conditions will not coincide with the appropriate steady-state conditions and the aircraft must fly a transient trajectory that leads to the cruise-dash operating point. Along this part of the trajectory the altitude, velocity and path-angle as well as the controls  $n$  and  $\eta$  will in general be time-varying. In order to obtain the time histories of the states and controls, a nonlinear TPBVP involving the state-Euler equations must be solved. This is done using the Multiple Shooting method described in the previous section.

## **4.2 Full-Throttle Cruise-Dash Trajectories**

For cruise-dash trajectories associated with small values of  $\mu$  (i.e. light emphasis on fuel), it can be seen from Fig. 1 that the associated cruise-dash points lie on the flight envelope and correspond to full-throttle operation. It is reasonable to conjecture that the transients leading to these points will also be run at full throttle. According to the control law (2.22) derived from the

Minimum Principle, a control can be at its upper bound only when the switching function is negative. Therefore it is expedient to “eliminate” the throttle control from the optimization problem by specifying  $\eta = \eta_{\max}$  in the state-Euler equations, and then monitor the sign of the switching function along the entire trajectory. Note that if  $S$  takes on positive values at any point(s) then the resulting trajectory is *not* an extremal because it does not satisfy the Minimum Principle.

Using this approach, the dash trajectory (corresponding to  $\mu = 0$  sec/lb) was recreated, using time histories generated by a previous study [1]. Using this as an initial estimate, the program BOUNDSCO was used to generate a cruise-dash trajectory corresponding to a small (positive) value of  $\mu$ . The differential equations used were the state-Euler equations (2.1 - 2.5, 2.12 - 2.16). The boundary conditions at the initial time were specified as follows: the altitude, path-angle, range and fuel weight were specified as zero, and the velocity was “specified” by the condition  $n = 1$  which ensures that the initial conditions correspond to steady-state operation. The boundary conditions at the (unspecified) final time were specified as the steady-state values of altitude and velocity ( $h^o, V^o$ ) corresponding to the parameter  $\mu$ . The path-angle was specified as zero and the fuel weight was unspecified. The value of the final range was selected as a large number (of the order of 100 miles) to ensure that all transient components vanish, and the system reaches steady-state asymptotically. It is noted that due to the asymptotic decay of the transient

components the system cannot exactly reach steady-state in a finite time (or range).

Full-throttle trajectories were computed for all values of  $\mu$  that yield *steady-state operating points* with  $\eta = \eta_{\max}$ . It was found that for all computed trajectories the switching function remained negative for all times, confirming that the computed full-throttle trajectories satisfy the Minimum Principle. These trajectories correspond to a certain range of small values of the time-fuel tradeoff parameter  $\mu$  (0.0 sec/lb to 0.1328 sec/lb) indicating a heavy emphasis on time. Each of these transient trajectories leads to a steady-state operating point that lies on the afterburning flight envelope. Representative results are presented in Figures 2 - 13. Figures 2 - 7 give the state and control (load-factor) histories for the dash-trajectory ( $\mu = 0$  sec/lb), and Figure 8 shows all the state variables (normalized with respect to their maximum value) plotted against normalized time on the same graph. Figures 9 - 15 give the corresponding histories for  $\mu = 0.0095$  sec/lb. The throttle control history is  $\eta \equiv \eta_{\max}$ .

These figures demonstrate the structure of the full-throttle cruise-dash trajectories, exhibiting a transient segment that blends into the steady-state. Figures 8 and 15 also highlight the time-scale separations inherent in aircraft dynamics. It is seen that  $h$  and  $\gamma$  reach their steady-state before the other states and are hence the "fast" variables.  $V$  reaches its steady-state later and is the "intermediate" variable. Finally,  $x$  and  $W_F$  are seen to be the "slow"

variables that make up the steady-state outer solution. Unlike the other states they are time-varying and do not settle down to constant values. Indeed the major portion of their growth occurs during the phase when all the other states have reached their steady-state values. Figure 16 shows several full-throttle cruise-dash trajectories for values of  $\mu$  ranging from 0.0 sec/lb to 0.1328 sec/lb. in the  $(h, V)$  plane along with a portion of the after-burning flight envelope.

### **4.3 Partial-Throttle Cruise-Dash Trajectories**

It can be seen from Fig. 1 that beyond a certain value of  $\mu$  the steady-state operating points lie inside the flight envelope, indicating that the throttle control is not at its bound along the cruise-dash arc. The cruise-dash arc is in fact a singular arc featuring a singular throttle control lying between its bounds. Correspondingly, the switching function and its time-derivative are zero along this arc.

It is conjectured that if the cruise-dash arc involves a singular control, then the transient arc leading to the steady-state also exhibits the same feature, at least in the vicinity of the cruise-dash arc. Proceeding with this assumption, one can in principle compute a transient trajectory that fairs into the steady-state. Along this trajectory, the singular throttle control would be evaluated by the control law (2.48) derived earlier. Also, the switching function and its first time derivative would be identically zero along the trajectory. The resulting

singular trajectory would be a candidate extremal that satisfies the Minimum Principle and the state-Euler equations.

An initial attempt to generate such a singular transient trajectory was made by backward integration of the state-Euler equations from the steady-state. This was done by making a very small perturbation in the (known) steady-state values of the states and co-states and then integrating the equations in retro-time. The steady-state operating point chosen was one corresponding to a very high value of  $\mu$  (i.e. very high emphasis on fuel) and was in the vicinity of the cruise-point. Time histories of the states and control for  $\mu = 1000 \text{ sec/lb}$  were computed and it was observed that that the trajectory appeared to oscillate about the steady-state operating point.

#### **4.4 Eigenvalue Analysis of the Linearized System**

In order to gain some insight into the behavior exhibited by the computed singular trajectory, an eigenvalue analysis of the system was performed. The system of state-Euler equations was linearized about the steady-state (or equilibrium) point. The Jacobian was evaluated numerically by perturbing the states and co-states from their equilibrium values in both directions and then using a central-difference scheme. The "slow" states  $x$  and  $W_F$  are ignorable, as are their associated co-states  $\lambda_x$  and  $\lambda_W$ . Hence the linearization was performed on a system of six equations (three states and three co-states) and

the Jacobian yielded six eigenvalues. The eigenvalues of the Jacobian matrix are shown in Figure 17. Two eigenvalues are real with a very small positive magnitude, and the other four are purely imaginary in conjugate pairs.

For the eigenstructure described above, the linearized system will exhibit a purely oscillatory solution about the equilibrium point if the modes corresponding to the imaginary eigenvalues are perturbed. However if the system is perturbed so that the modes corresponding to the real eigenvalues are excited, the linearized system will move away from the equilibrium point in an asymptotic fashion. The actual nonlinear system will behave in a similar fashion in some neighborhood of the equilibrium point. The computed singular trajectory exhibited the oscillatory component of the modes corresponding to the imaginary eigenvalues, but did not appear to have the asymptotic component associated with the real eigenvalues. This leads us to consider the possibility that the modes corresponding to the real eigenvalues are not excited along a singular trajectory.

To test this hypothesis, the following analysis was carried out. Along any singular arc (i.e.  $x(t), \lambda(t)$ ), two conditions that must hold are

$$S(x(t), \lambda(t)) = 0 \tag{4.1}$$

and

$$\dot{S}(x(t), \lambda(t)) = 0 \tag{4.2}$$

Linearizing equations (4.1, 4.2) about the equilibrium point one gets

$$\delta \underline{z}^T \left[ \frac{\partial S}{\partial \underline{z}} \right] = 0 \quad (4.3)$$

and

$$\delta \underline{z}^T \left[ \frac{\partial \dot{S}}{\partial \underline{z}} \right] = 0 \quad (4.4)$$

where

$$\underline{z} = [h \ V \ \gamma \ \lambda_h \ \lambda_V \ \lambda_\gamma]^T$$

For the linearized model the perturbation  $\delta \underline{z}$  can be represented by any linear combination of its eigenvectors  $\underline{W}_i$ . Thus equations (4.3, 4.4) will hold for a non-zero solution of the linearized model only if

$$\underline{W}_i^T \left[ \frac{\partial S}{\partial \underline{z}} \right] = 0 \quad (4.5)$$

and

$$\underline{W}_i^T \left[ \frac{\partial \dot{S}}{\partial \underline{z}} \right] = 0 \quad (4.6)$$

for some eigenvectors  $\underline{W}_i$ . On the other hand, if either (4.5) or (4.6) is violated for a particular eigenvector then a solution containing that eigenvector does not satisfy (4.1, 4.2) and does not represent a singular extremal.

Computing the expressions in equations (4.5, 4.6) for each of the six eigenvectors, it was found that only the eigenvectors corresponding to the purely real eigenvalues yielded non-zero values while the others yielded zeros. It can hence be concluded that the purely real eigenvalues correspond to modes that lead the system away from conditions (4.1 and 4.2) and are not singular extremals.

The eigenvalue analysis was repeated for several values of  $\mu$  corresponding to cruise-dash operation with decreasing emphasis on fuel, at optimized operating points close to the cruise-point. It was found that if the value of  $\mu$  was slightly decreased, the eigenvalue structure was preserved (i.e. there were four imaginary and two real eigenvalues). However if  $\mu$  was decreased beyond a certain value, then the previously purely imaginary eigenvalues turned into complex conjugates with non-zero real parts. In addition, they reflect the *Hamiltonian structure* of the Jacobian matrix, meaning that if  $\lambda$  is an eigenvalue then  $-\lambda$  is also an eigenvalue, as are their complex conjugates  $\lambda^*$  and  $-\lambda^*$ . Again, the purely real eigenvalues correspond to modes that lead the system away from the conditions (4.1 and 4.2). The eigenvalues corresponding to  $\mu = 320$  sec/lb are shown in Figure 18.



## 4.5 Concept of Singular Manifold

The transient dynamics of the system defined by the state-Euler equations involve the three “non-ignorable” states  $h$ ,  $V$  and  $\gamma$  and their associated co-states  $\lambda_h$ ,  $\lambda_V$ , and  $\lambda_\gamma$ . Therefore the transient trajectories lie in a six-dimensional state-space, the co-ordinates of which are the components of the generalized state vector  $\underline{z}$ . Correspondingly, the linearized system which approximates the actual nonlinear system in the neighborhood of the equilibrium point will have solutions that lie in a six-dimensional linear state-space.

Given a point  $(h, V, \gamma)$  in the state space, it is possible to determine whether or not it can lie on a singular arc. Making use of  $S = 0$  the co-state  $\lambda_V$  can be expressed in terms of the (known) co-state  $\lambda_W$  from equation (2.26). Substituting this into the expression  $\dot{S} = 0$  one gets equation (2.33). Making use of equation (2.36) to eliminate the control  $n$ , the resulting expression for  $\dot{S} = 0$  can be expressed as a quadratic equation in  $\lambda_\gamma$ . Keeping in mind the fact that  $\lambda_\gamma$  must be real, the “solvability” of this quadratic equation determines if a singular arc can pass through the  $(h, V, \gamma)$  point under scrutiny. If the value of  $\lambda_\gamma$  determined from the quadratic equation is real, then one can substitute the values of the states and co-states into equation (2.48) and attempt to evaluate the value of the singular throttle control  $\eta$ . If the resulting value of  $\eta$  is admissible (i.e. it lies between the prescribed upper and lower bounds) then

the  $(h, V, \gamma)$  point under consideration will satisfy conditions (4.1 - 4.2) in an admissible fashion and can lie on a singular arc. Thus in the three-dimensional  $(h, V, \gamma)$  state-space, singular trajectories must lie in a subset of this space where the conditions described above are satisfied.

It has been found that two modes of the linearized system violate the conditions (4.1 and 4.2) which all singular arcs must satisfy. Therefore all singular arcs in the linearized system must be confined to a four-dimensional linear subspace state-space where the two “nonsingular” modes are inactive. For the linearized system this is a four-dimensional plane, corresponding to a four-dimensional *singular manifold* in the actual nonlinear system.

In the linearized system, singular trajectories lying in the four-dimensional plane may be generated by exciting the modes corresponding to the four complex-conjugate eigenvalues. Out of these four modes, only two will be stable due to the Hamiltonian structure of the associated eigenvalues. Hence all singular trajectories *that lead to the equilibrium point* in the linearized system must lie in a two-dimensional linear subspace (i.e. on a plane). Thus in the actual nonlinear system the singular manifold may be regarded as a *singular surface* in  $(h, V, \gamma)$  space.

It is conjectured that this singular surface plays a key role in determining the nature and structure of transient trajectories leading to a singular cruise-dash arc. If the specified initial conditions  $(h_i, V_i, \gamma_i)$  are near the cruise-dash point

and happen to lie on the singular surface, it is possible to reach the equilibrium point with a purely singular trajectory characterized by a partial-throttle control along its entire length. If on the other hand, the initial conditions correspond to a point that lies outside the singular surface, a purely singular trajectory cannot take the system to the equilibrium point in an optimal fashion. A full-throttle or zero-throttle trajectory must be run to take the system to a point on the singular surface, after which a singular trajectory takes the system to the equilibrium point. The optimal trajectory will thus be a composite consisting of a full-throttle or zero-throttle arc followed by a singular arc.

#### **4.6 Singular Trajectories to the Equilibrium Point**

As noted in a previous section, a singular trajectory may be computed by making a small perturbation about the equilibrium point and then integrating the state-Euler equations backwards in time. If the perturbation in the states and co-states is proportional to the eigenvectors corresponding to the complex eigenvalues, then it is guaranteed that the *linearized* system will follow a path on the singular plane and will not leave it. Although such a claim cannot be made about the behavior of the actual non-linear system, the corresponding trajectory will remain on the singular surface at least in some neighborhood of the equilibrium point if the singular plane is a good approximation to the singular surface.

Since we expect the trajectory to move away from the equilibrium point in retro-time, we choose the eigenvectors corresponding to the complex-conjugate eigenvalues with negative real parts. Since these eigenvectors are also complex-conjugates, it is clear that the perturbations can be chosen as any linear combination of their real and complex parts. Each of these combinations will correspond to a singular trajectory that fades into (or emerges from in retro-time) the equilibrium point from a certain direction on the singular surface. If all trajectories corresponding to all possible linear combinations were computed, they would form the singular surface.

Four such combinations were used to create a perturbation, and the corresponding singular trajectories were generated by backward integration of the state-Euler equations that define the actual nonlinear system with  $\mu = 320 \text{ sec/lb}$ . The integration was performed with monitoring of the value of the singular control and the values of the switching function and its time derivative, and was stopped when the control saturated at its upper bound. The switching function and its time derivative remained zero all along the trajectory. The state and control histories of one such trajectory are shown in Figs. 19 - 23. It is seen that all three (non-ignorable) states undergo damped oscillations that die out as the equilibrium point is approached, as predicted by the linearized model. In fact, it was found that the frequency of the oscillations and the damping ratio are very close to those of the linearized system. This indicates that the singular surface is almost planar and that the

linearized system is a good approximation of the nonlinear system over the singular surface.

Figure 24 shows all four trajectories in  $(h, V, \gamma)$  space. It can be seen that these trajectories approach the equilibrium point along asymptotic spirals. These spirals define a surface which is almost planar.

#### **4.7 Composite Bang-Singular Trajectories**

It was found that transient singular trajectories approach the steady-state operating point asymptotically in an oscillatory fashion. They lie on a surface which appears to be bounded by the upper throttle limit. If the initial operating point happens to lie on this surface then the transient trajectory is purely singular and describes an asymptotic spiral in  $(h, V, \gamma)$  space fairing into the equilibrium point. However, if the initial states do not correspond to a point that lies on the singular surface, the transient trajectory would have a more complex structure. In general, it would consist of two segments: an initial non-singular arc run at either full-throttle or zero-throttle (or possibly a combination thereof) until the singular surface is reached, followed by a purely singular arc that takes the system to the equilibrium point. The joining of a singular and a non-singular arc is subject to the McDanell-Powers Junction Conditions discussed in Chapter 3. According to these conditions, if the

singular control is unsaturated at a junction, then it can jump to either its upper or lower bound.

In order to compute a representative composite trajectory, a point lying within the boundary of the singular surface was selected. The value of the corresponding singular control was less than the upper throttle limit and was hence unsaturated. Using the corresponding values of the states and co-states, the state-Euler equations were integrated backwards in time with the throttle control set at its upper bound. The trajectory obtained had a switching function with the appropriate (negative) sign required by the Minimum Principle. The composite trajectory is shown in Figs. 25 - 29. A zero-throttle trajectory was computed in a similar fashion. Again, the (positive) sign of the switching function was in accordance with the Minimum Principle. This trajectory is presented in Figs. 30 - 34. It can be seen from these figures that the zero-throttle trajectory approaches the singular surface from higher altitudes and energies while the full-throttle trajectory approaches the singular surface from lower altitudes and energies. It is also noted that the states change monotonically (do not oscillate) along those segments of the trajectory where the control is at a bound.

#### **4.8 Necessary Conditions**

All the trajectories computed and discussed above were found to satisfy all the necessary conditions discussed in Chapter 3. The singular trajectories satisfy the Generalized Legendre-Clebsch Condition along their entire length, as do the singular segments of composite bang-singular trajectories. The junctions of the composite bang-singular trajectories are in accordance with the McDanell-Powers condition and the Erdmann corner condition is also satisfied (the co-states are continuous). No Jacobi-like condition was checked along the transient singular arc.

#### **4.9 Bang-Bang Transient Trajectories**

If the initial states lie outside the singular surface, a transient bang-singular trajectory can take the system to the steady-state point while satisfying all the necessary conditions discussed in Chapter 3 viz. the Generalized Legendre-Clebsch Condition, the Erdmann Corner Condition and the Junction Conditions. The total trajectory is composed of this transient and the steady-state cruise-dash arc. Note that the cruise-dash arc is itself a singular arc along which the throttle control takes on a constant intermediate value. For the computed composite trajectories, all the states, co-states and controls blend smoothly into the steady-state values.

A control variable is not subject to smoothness restrictions and may exhibit jump discontinuities or worse. With this point in mind, it is possible to construct an alternative control structure where the throttle control remains at its upper or lower bound (or any combination thereof) all along the transient trajectory. When the system states reach their steady-state values, the throttle control can jump to the intermediate (singular) value prescribed along the cruise-dash arc. This jump in control results in a corner in the trajectory and the Erdmann corner condition must be satisfied at the point where the control jumps to its steady-state value.

A candidate control for the transient trajectory is a bang-bang type of control where the throttle remains at one bound for part of the trajectory and switches to the opposite bound for the rest of the trajectory. This would be followed by a jump to the steady-state value of the throttle control, resulting in a bang-bang-singular type of composite trajectory. Starting from an initial point outside the singular surface, a bang-bang transient trajectory leading to the equilibrium point was computed. Its time history is shown in Figs. 35 - 39. This trajectory satisfies the state-Euler equations and the Minimum Principle as well as the classical Legendre-Clebsch condition. The co-state histories reveal that the Erdmann corner condition is satisfied at the first junction where the zero-throttle segment joins the full-throttle segment. However, the values of the co-states at the end of the transient trajectory do not coincide with the steady-state values of the co-states, indicating a discontinuity in the co-state variables at the corner formed by the transient and steady-state extremals.



Hence the Erdmann corner condition is not satisfied and such a composite bang-bang-singular trajectory is non-optimal.

It is, however, possible that a full-throttle or zero-throttle trajectory could arrive at the cruise-dash point with the appropriate values of the co-states and hence the joining of the transient and steady-state extremals would satisfy the Erdmann corner condition. Such a trajectory could be obtained by backward integration from the cruise-dash point with the prescribed values of states and co-states and the throttle control set to either bound. Thus there are two trajectories, one with zero-throttle and the other with full-throttle that can provide the transient segment of a composite bang-bang-singular type trajectory that satisfies the Erdmann corner condition.

#### **4.10 A Jacobi-type Condition**

In the foregoing discussion, it has been stated that the structure of candidate extremals is a transient arc followed by a steady-state cruise-dash arc. For a performance index involving fuel alone, Speyer [18] cast doubt on the optimality of a steady-state cruise arc by showing that for certain aero-propulsive models a Jacobi-type condition is not satisfied.

The Jacobi condition in the calculus of variations [48-49] is not applicable when some or all components of the controls are singular. In such cases, the

accessory minimum problem [AMP] is formulated and the Goh transform is applied. The transformed AMP is nonsingular and the classical Jacobi condition may now be applied in one of several forms [53]. The approach taken by Speyer [18] is to use Parseval's transformation [19] and then apply the Jacobi test in the frequency domain. For a specialized drag model, equation 62 of Reference 18 states this Jacobi-type condition as follows:

$$Y(\omega) = H_{LL} - \frac{\sigma}{m^2 V^2 D_{VV}(\omega^2 - \beta g)^2} \left[ \omega^2 \frac{W^2}{V^2} + V^2 D_{Vh}^2 \right] \quad (4.7)$$

must be non-negative for all values of  $\omega$ . Although  $H_{LL}$  is positive, it is seen that  $Y(\omega)$  can be made negative for values of  $\omega$  near  $\sqrt{\beta g}$ . Note that the cost function to be minimized in this problem is fuel alone.

Re-tracing Speyer's analysis for the exact same model, with a linear combination of time and fuel as the performance index, one gets:

$$Y(\omega) = H_{LL} - \frac{\sigma}{m^2 V^2 D_{VV}(\omega^2 - \beta g)^2} \left[ \omega^2 \frac{W^2}{V^2} + V^2 D_{Vh}^2 - \omega^2 \frac{V}{\mu \sigma} \right] \quad (4.8)$$

where  $\mu$  is the time-fuel tradeoff parameter. It can be shown that  $Y(\omega)$  will be non-negative for all values of  $\omega$  if

$$\frac{1}{\mu} \geq \frac{\sigma}{g\beta V} \left[ \frac{\beta g W^2}{V^2} + V^2 D_{Vh}^2 \right] \quad (4.9)$$

For the case of  $\mu \rightarrow \infty$ , there is no emphasis on time and Speyer's result is recovered. However, if there is a sufficiently heavy emphasis on time and  $\mu$  is small enough then equation (4.9) will be satisfied. As a consequence, Speyer's Jacobi-type condition will be satisfied for steady-state cruise-dash arcs corresponding to a sufficiently heavy emphasis on time. Thus it has been shown that for the model studied by Speyer, steady-state *cruise* fails a Jacobi-type test and is nonminimizing, while some types of steady-state *cruise-dash* pass this test and can be minimizing.

For the case of steady-state cruise-dash, a Jacobi-type test may be applied [53] by examining solutions of the algebraic matrix Riccati equation [60]. The Jacobi-type condition is satisfied if the solution matrix to the algebraic matrix Riccati equation is finite, real and positive semi-definite. Using the aero-propulsive data for the example aircraft, this matrix was evaluated numerically for several steady-state cruise-dash conditions corresponding to various values of  $\mu$ . It was found that for large values of  $\mu$  (conditions approximating cruise), the Jacobi-type condition was not satisfied since the solution matrix to the algebraic matrix Riccati equation had complex entries. If a substantial emphasis was placed on time (moderate values of  $\mu$ ) then the Jacobi-type condition was satisfied. An interesting feature that emerged from this study was that the Jacobi-type condition was satisfied when the eigenvalues of the linearized system had no purely imaginary values and failed the test when this structure collapsed.

## Chapter 5: Conclusions

This study explores the nature and structure of optimal cruise-dash trajectories that arise in airplane performance optimization involving time-fuel tradeoffs. In particular, a linear combination of time-elapsd and fuel-consumed was chosen as a performance index. Optimal cruise-dash trajectories generally consist of two parts - a transient arc followed by a steady-state arc. Numerical studies conducted for a high-performance aircraft reveal that the general skeletal structure of full-throttle cruise-dash trajectories is similar to that of the dash trajectory studied in an earlier work [1]. The structure of partial-throttle cruise-dash trajectories is far more complex and can in general be composed of several subarcs joined together in an optimal fashion. The salient features of cruise-dash trajectories are discussed in the following section.

## **5.1 Structure of Optimal Cruise-Dash Trajectories**

It has been established computationally that skeletal cruise-dash trajectories associated with a light emphasis on fuel (and heavy emphasis on time) are run at full-throttle. The steady-state operating points lie on the flight envelope and the skeletal transients leading to these optimal operating points are flown with the throttle at its maximum limit. These transients approach the steady-state cruise-dash points in an asymptotic fashion. Moreover, the state histories in the vicinity of the equilibrium points are monotonic with no oscillations.

Cruise-dash trajectories corresponding to a heavy emphasis on fuel (and light emphasis on time) have a different and far more complex structure. The steady-state operation points lie within the flight envelope and the corresponding cruise-dash arc is a singular arc flown with a partial-throttle setting. Studies of the transient trajectories leading to these cruise-dash points reveal that they approach the steady-state asymptotically in a damped oscillatory fashion, unlike the full-throttle trajectories studied earlier. These transient trajectories in the neighborhood of the equilibrium points are singular trajectories and are run with partial-throttle settings. A singular control law has been derived for the throttle control. It consists of a transient component that vanishes with the approach of the steady-state, and a “steady-state” component corresponding to operation along the cruise-dash arc.

Transient singular trajectories in the neighborhood of the equilibrium point lie on a two-dimensional singular surface in the three-dimensional  $(h, V, \gamma)$  state-space. On this surface, transient singular trajectories fair into the equilibrium point along an asymptotic spiral. The singular surface is bounded as a result of saturation of the throttle control at its upper limit. If the initial states lie outside the singular surface, a full-throttle or zero-throttle trajectory must be flown to the singular surface after which a singular trajectory takes the system to the steady-state. In general, initial states corresponding to altitudes and energies higher than the equilibrium values need a zero-thrust coasting arc to reach the singular surface. Similarly, initial states corresponding to altitudes and energies lower than the equilibrium need a full-thrust arc to reach the singular surface.

The computed singular trajectories satisfy the Generalized Legendre-Clebsch Condition, and the bang-singular trajectories also satisfy the Erdmann Corner Condition as well as the Junction Conditions. Except for two special cases, full-throttle or zero-throttle trajectories to the equilibrium point followed by a jump in control to the steady-state value do not satisfy the Erdmann Corner Condition. Hence bang-bang type transient trajectories are generally nonoptimal.

It has been determined that, for the example, steady-state operation at a cruise-dash point does satisfy the Jacobi-type Condition for certain values of  $\mu$  and therefore steady-state cruise-dash can be optimal. However,

steady-state cruise-dash arcs fail the Jacobi-type test for large values of  $\mu$ , and in particular the cruise arc fails the Jacobi-type test. The Jacobi-type test has a strong connection with the eigenstructure of the linearized system at the equilibrium point. Specifically, if the eigenvalues have no purely imaginary values, the Jacobi-type Condition is satisfied. Absence of this feature (presence of purely imaginary eigenvalues) results in failure of the Jacobi-type Condition.

## **5.2 Future Work**

The next logical step is to investigate the structure of optimal cruise-dash trajectories away from the equilibrium point, and determine if there are any singular trajectories outside the computed singular surface.

The oscillatory nature of partial-throttle cruise-dash trajectories and the connection of the Jacobi-type Condition with the eigenstructure of the system indicate some connection with the concept of oscillatory cruise. Instead of studying oscillatory cruise in isolation, one might better consider it as part of a cruise-dash family.

## References

1. Weston, A.R., Kelley, H.J. and Cliff, E.M., "Onboard Near-Optimal Climb-Dash Energy Management," *Journal of Guidance, Control and Dynamics*, Vol. 8, No. 3, 1985, pp. 320-324.
2. Visser, H.G., Kelley, H.J. and Cliff, E.M., "Energy Management of Three-Dimensional Minimum-Time Intercept," *AIAA Atmospheric Flight Mechanics Conference*, Snowmass CO, August 1985.
3. Erzberger, H. and Lee, H., "Constrained Optimum Trajectories with Specified Range," *Journal of Guidance and Control*, Vol. 3, No. 1, January-February 1980, pp. 78-85.
4. Erzberger, H. and McLean, J.D., "Fuel Conservative Guidance System for Powered Aircraft," *Journal of Guidance and Control*, Vol. 4, No. 3, May-June 1981, pp. 253-261.
5. Sorensen, J.A. and Waters, M.H., "Airborne Method to Minimize Fuel with Fixed Time-of-Arrival Constraints," *Journal of Guidance and Control*, Vol. 4, No. 3, May-June 1981, pp. 348-349.
6. Burrows, J.W., "Fuel-Optimal Trajectory Computation," *Journal of Aircraft*, Vol. 19, No. 4, April 1982, pp. 324-329.
7. Burrows, J.W., "Fuel-Optimal Aircraft Trajectories with Fixed Arrival Times," *Journal of Guidance and Control*, Vol. 6, No. 1, January-February 1983, pp. 14-19.



8. Chakravarty, A., "Four-Dimensional Fuel-Optimal Guidance in the Presence of Winds," *Journal of Guidance, Control and Dynamics*, Vol. 8, No. 1, January-February 1985, pp. 16-22.
9. Kaiser, F., "Der Steigflug mit Strahlflugzeugen-Teil I, Bahngeschwindigkeit für Besten Steigens," Versuchsbericht 262-02-L44, Messerschmitt A.G., Augsburg, April 1944. Translated as British Ministry of Supply RPT/TIB, Translation GDC/15/148T.
10. Lush, K.J., "A Review of the Problem of Choosing a Climb Technique with Proposals for a New Climb Technique for High Performance Aircraft," Aeronautical Research Council Report, Memo. 2557, 1951.
11. Rutowski, E.S., "Energy Approach to the General Aircraft Performance Problem," *Journal of the Aeronautical Sciences*, Vol. 21, March 1954, pp. 187-195.
12. Bryson, A.E., Desai, M.N. and Hoffman, K., "Energy-State Approximation in Performance Optimization of Supersonic Aircraft," *Journal of Aircraft*, Vol. 6, No. 6, November-December 1969, pp. 481-488.
13. Merrit, S.R., Cliff, E.M. and Kelley, H.J., "Energy-Modelled Climb and Climb-Dash - The Kaiser Technique," Ninth IFAC World Congress, Budapest, Hungary, July 1984.
14. Schultz, R. and Zagalsky, N. R., "Aircraft Performance Optimization," *Journal of Aircraft*, Vol. 9, No. 2, February 1972, pp. 108-114.
15. Menon, P.K., Kelley, H.J. and Cliff, E.M., "Optimal Symmetric Flight with an Intermediate Vehicle Model," *Journal of Guidance, Control and Dynamics*, Vol. 8, No. 3, May-June 1985, pp. 312-319.
16. Speyer J.L., "On the Fuel Optimality of Cruise," *Journal of Aircraft*, Vol. 10, No. 12, December 1973, pp.763-765.
17. Schultz, R.L., "Fuel Optimality of Cruise," *Journal of Aircraft*, Vol. 11, No. 9, September 1976, pp. 586-587.
18. Speyer, J.L., "Nonoptimality of the Steady-State Cruise for Aircraft," *AIAA Journal*, Vol. 14, No. 11, November 1976, pp. 1604-1610.
19. Bittanti, S., Fronza, G. and Guardabassi, G., "Periodic Control: A Frequency Domain Approach," *IEEE Transactions on Automatic Control*, Vol. AC-18, No. 1, February 1973, pp. 33-38.

20. Gilbert, E.G. and Parsons, M.G., "Periodic Control and the Optimality of Aircraft Cruise," *Journal of Aircraft*, Vol. 13, No. 10, October 1976, pp. 828-830.
21. Gilbert, E.G., "Vehicle Cruise: Improved Fuel Economy by Periodic Control," *Automatica*, Vol. 12, 1976, pp. 159-166.
22. Speyer, J.L., Dannemiller, D. and Walker, D., "Periodic Optimal Cruise of an Atmospheric Vehicle," *Journal of Guidance, Control and Dynamics*, Vol. 8, No. 2, January-February 1985, pp. 31-38.
23. Grimm, W., Well, K.H. and Oberle, H.J., "Periodic Control for Minimum-Fuel Aircraft Trajectories," *Journal of Guidance, Control and Dynamics*, Vol. 9, No. 2, March-April 1986, pp. 169-174.
24. Ashley, H., "Multiple Scaling in Flight Vehicle Dynamic Analysis - A Preliminary Look," *AIAA Guidance, Control and Flight Mechanics Conference*, Huntsville AL, 1967, Paper 67-560.
25. Ardema, M.D. and Rajan, N., "Separation of Time Scales in Aircraft Trajectory Optimization," *Journal of Guidance, Control and Dynamics*, Vol. 8, No. 2, March-April 1985, pp. 275-278.
26. Ardema, M.D. and Rajan, N., "Slow and Fast State Variables for Three-Dimensional Flight Dynamics," *Journal of Guidance, Control and Dynamics*, Vol. 8, No. 4, July-August 1985, pp. 532-535.
27. Wasow, W., *Asymptotic Expansions for Ordinary Differential Equations*, John Wiley and Sons, New York, 1975.
28. Kelley, H.J., "Reduced-Order Modeling in Aircraft Mission Analysis," *AIAA Journal*, Vol. 9, No. 2, February 1971, pp. 349-350.
29. Kelley, H.J., "Flight-Path Optimization with Multiple Time Scales," *Journal of Aircraft*, Vol. 8, No. 4, April 1971, pp. 238-240.
30. Kelley, H.J., "Aircraft Maneuver Optimization by Reduced-Order Approximation," *Control and Dynamic Systems*, Vol. 10, C. T. Leondes, ed., Academic Press, 1973, pp. 131-178.
31. Kelley, H.J. and Edelbaum, T.N., "Energy Climbs, Energy Turns and Asymptotic Expansions," *Journal of Aircraft*, Vol. 7, No. 1, January-February 1970, pp. 93-95.

32. Ardema M.D., "Solution of the Minimum-Time-To-Climb Problem by Matched Asymptotic Expansions," *AIAA Journal*, Vol. 14, July 1976, pp. 843-850.
33. Ardema, M.D., "Singular Perturbations in Flight Mechanics," NASA TM X-62,320, August 1974 (revised July 1977).
34. Calise, A. J., "Singular Perturbation Methods for Variational Problems in Aircraft Flight," *IEEE Transactions on Automatic Control*, Vol. AC-21, No. 3, June 1976, pp. 345-353.
35. Calise, A. J., "Extended Energy Management Methods for Flight Performance Optimization," *AIAA Journal*, Vol. 15, No. 3, March 1977, pp. 314-321.
36. Calise, A. J., "A New Boundary Layer Matching Procedure for Singularly Perturbed Systems," *IEEE Transactions on Automatic Control*, Vol. AC-23, No. 3, June 1978, pp. 434-438.
37. Uehara, S., Stewart, H.J. and Wood, L.J., "Minimum Time Loop Maneuvers of Jet Aircraft," *Journal of Aircraft*, Vol. 15, No. 8, August 1978, pp. 449-455.
38. Well, K.H., Faber, B.J. and Berger, E., "Optimization of Tactical Aircraft Maneuvers Utilizing High Angles of Attack," *Journal of Guidance and Control*, Vol. 5, No. 2, March-April 1982, pp. 124-130.
39. Bilimoria, K.D., Cliff, E.M. and Kelley, H.J., "Classical and Neo-Classical Cruise-Dash Optimization," *Journal of Aircraft*, Vol. 22, No. 7, July 1985, pp. 555-560.
40. Kumar, R. R., *Singular Optimal Atmospheric Rocket Trajectories*, M.S. Thesis, Virginia Polytechnic Institute and State University, October 1986.
41. De Boor, C., *A Practical Guide to Splines*, Springer-Verlag, New York, 1967.
42. Mummolo, F. and Lefton, L., "Cubic Splines and Cubic Spline Lattices for Digital Computation," Analytical Mechanical Associates Inc. Report No. 72-28, July 1972, (revised 1974).
43. Bryson, A.E. and Ho, Y.C., *Applied Optimal Control*, Blaisdell, 1969.
44. Leitmann, G., *An Introduction to Optimal Control*, McGraw-Hill, New York, 1966.

45. Bell, D.J. and Jacobson, D.H., *Singular Optimal Control Problems*, Academic Press, New York, 1975.
46. Kelley, H.J., Kopp, R.E. and Moyer, H.G., "Singular Extremals," *Topics in Optimization*, G. Leitmann, ed., Academic Press, 1967.
47. Chichka, D.F., *Cruise-Dash Optimization Applied to an Air-breathing Missile*, M.S. Thesis, Virginia Polytechnic Institute and State University, December 1985.
48. Gelfand, I.M. and Fomin, S.V., *Calculus of Variations*, Prentice-Hall, 1963.
49. Ewing, G.M., *Calculus of Variations with Applications*, Dover, 1985.
50. Prussing, J.E., "The Principal Minor Test for Semidefinite Matrices," *Journal of Guidance, Control and Dynamics*, Vol. 9, No. 1, 1986, pp. 121-122.
51. Goh, B.S., "The Second Variation for the Singular Bolza Problem", *SIAM Journal of Control*, Vol. 4, No. 2, 1966, pp. 309-325.
52. Goh, B.S., "Necessary Conditions for Singular Extremals Involving Multiple Control Variables," *SIAM Journal of Control*, Vol. 4, No. 4, 1966, pp. 717-731.
53. McDanell, J.P. and Powers, W.F., "New Jacobi-Type Necessary and Sufficient Conditions for Singular Optimization Problems," *AIAA Journal*, Vol. 8, No. 8, August 1970, pp. 1416-1420.
54. Gabasov, R. and Kirilova, F.M., *Singular Optimal Control*, Nauka, Moscow, 1973 (in Russian).
55. Robbins, H.M., "A Generalized Legendre-Clebsch Condition for the Singular Cases of Optimal Control," *IBM Journal of Research and Development*, Vol. 11, 1967, pp. 361-372.
56. McDanell, J.P. and Powers, W.F., "Necessary Conditions for Joining Singular and Nonsingular Subarcs," *SIAM Journal of Control*, Vol. 9, No. 2, May 1971, pp. 161-173.
57. Keller, H.B., *Numerical Methods for Two Point Boundary Value Problems*, Blaisdell, London, 1968.

58. Keller, H.B., "Numerical Solutions of Two Point Boundary Value Problems," *CBMS-NSF Regional Conference Series in Applied Mathematics*, Vol. 24, SIAM, Philadelphia PA, 1976.
59. Stoer, J. and Bulirsch, R., *Introduction to Numerical Analysis*, Springer, Berlin, 1980.
60. Kwakernaak, H. and Sivan, R., *Linear Optimal Control Systems*, Wiley Interscience, 1972.

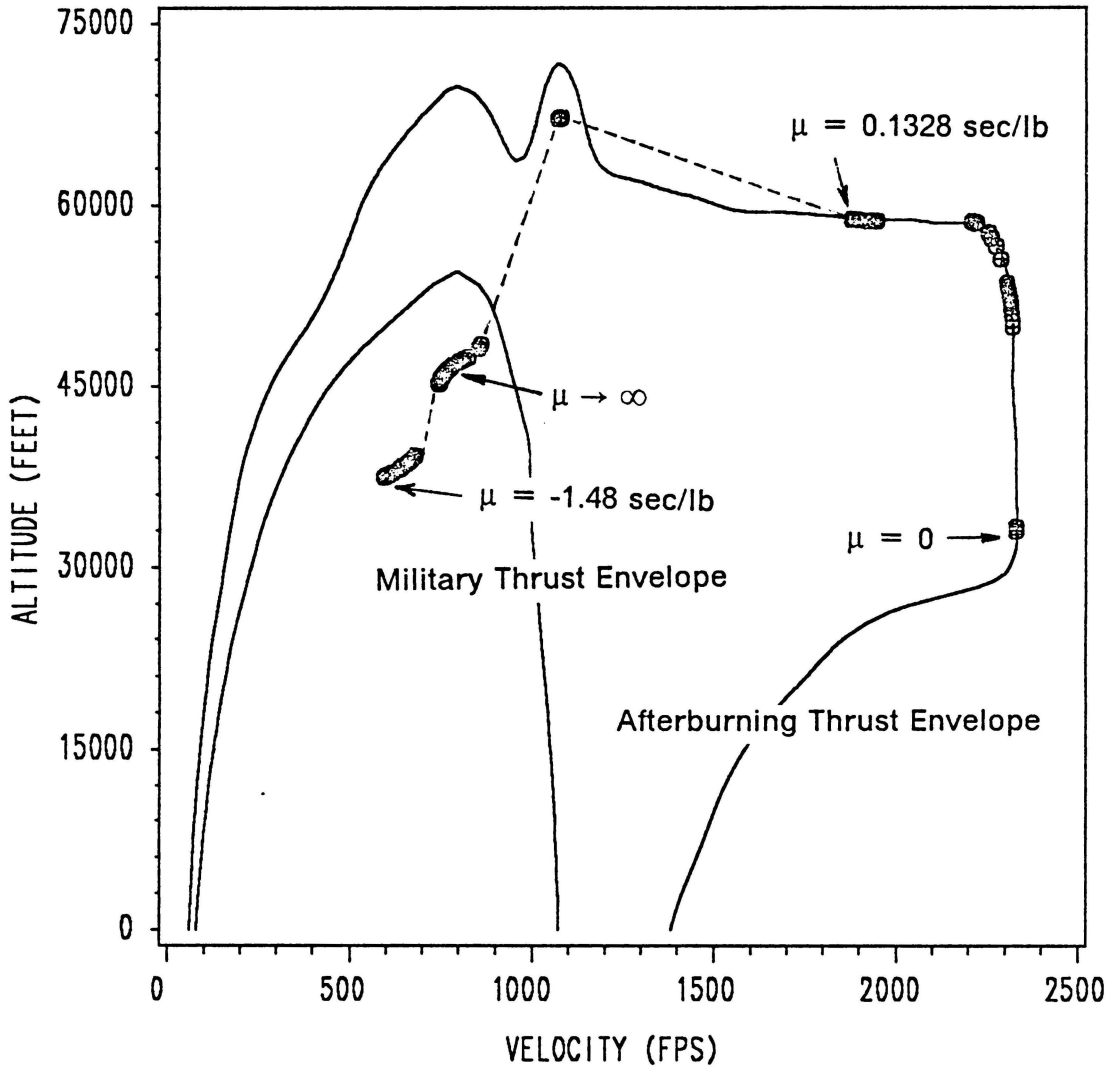


Figure 1. Cruise-Dash Points in the (h,V) Plane

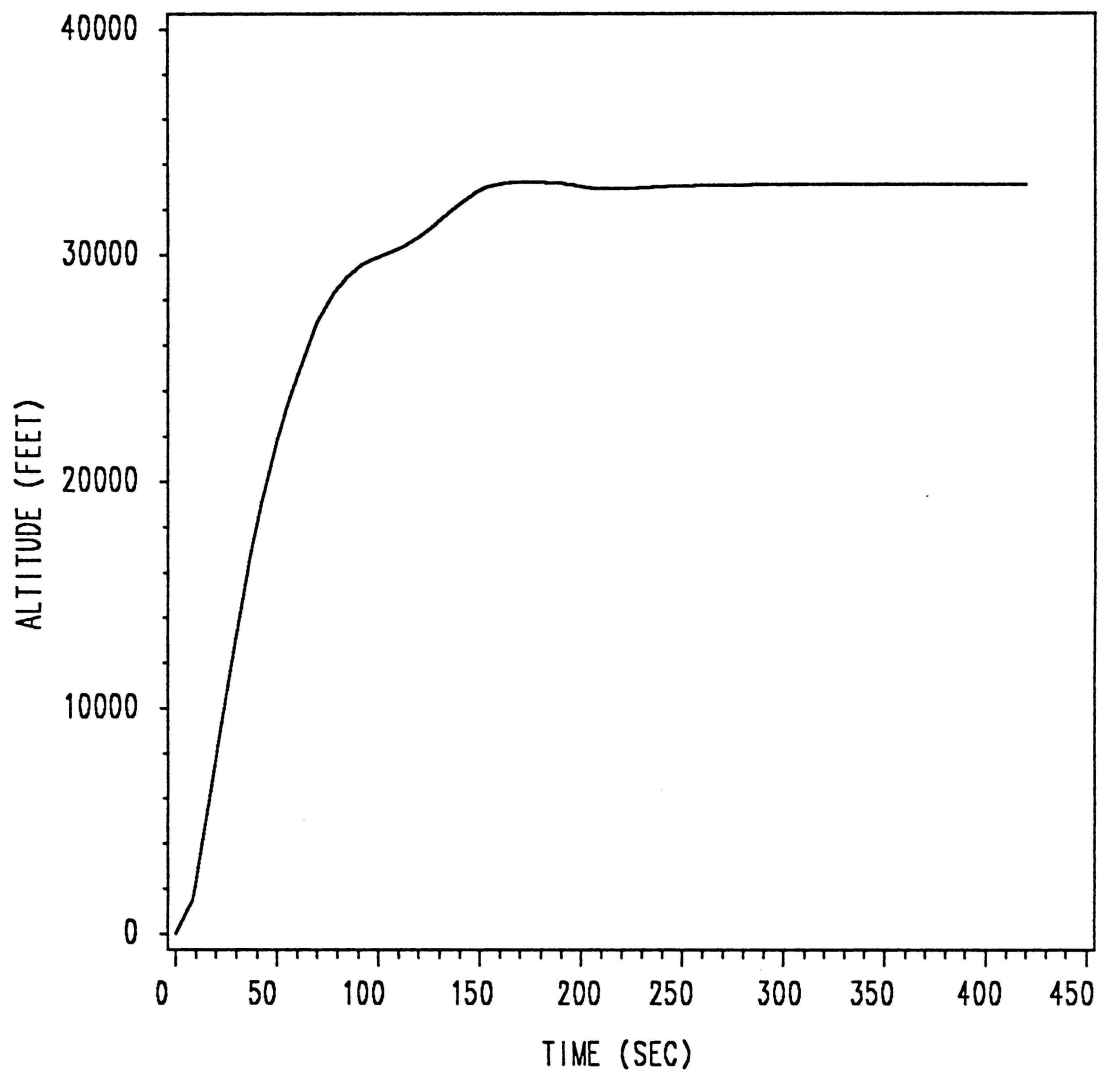


Figure 2. Altitude Time History for  $\mu = 0$  sec/lb

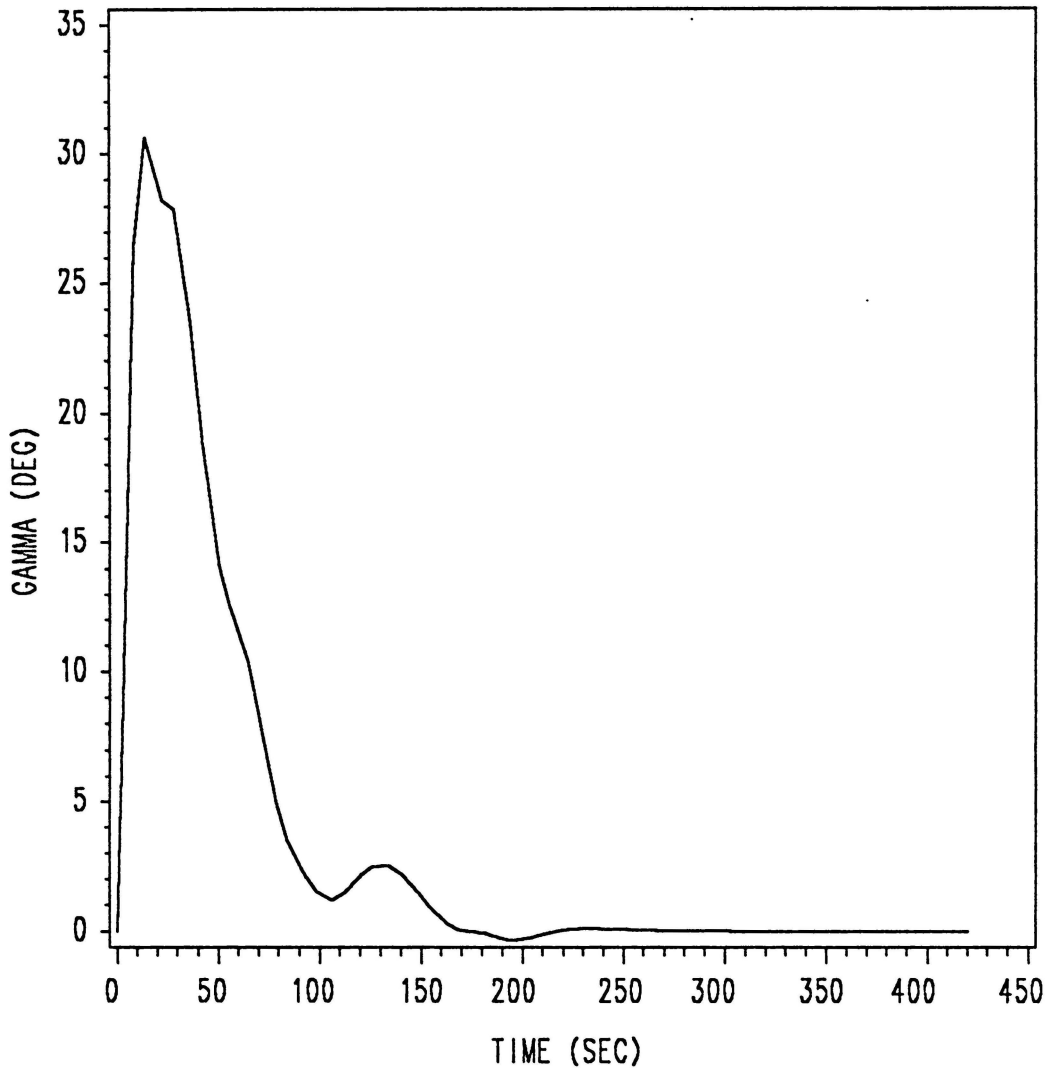


Figure 3. Path-Angle Time History for  $\mu = 0$  sec/lb



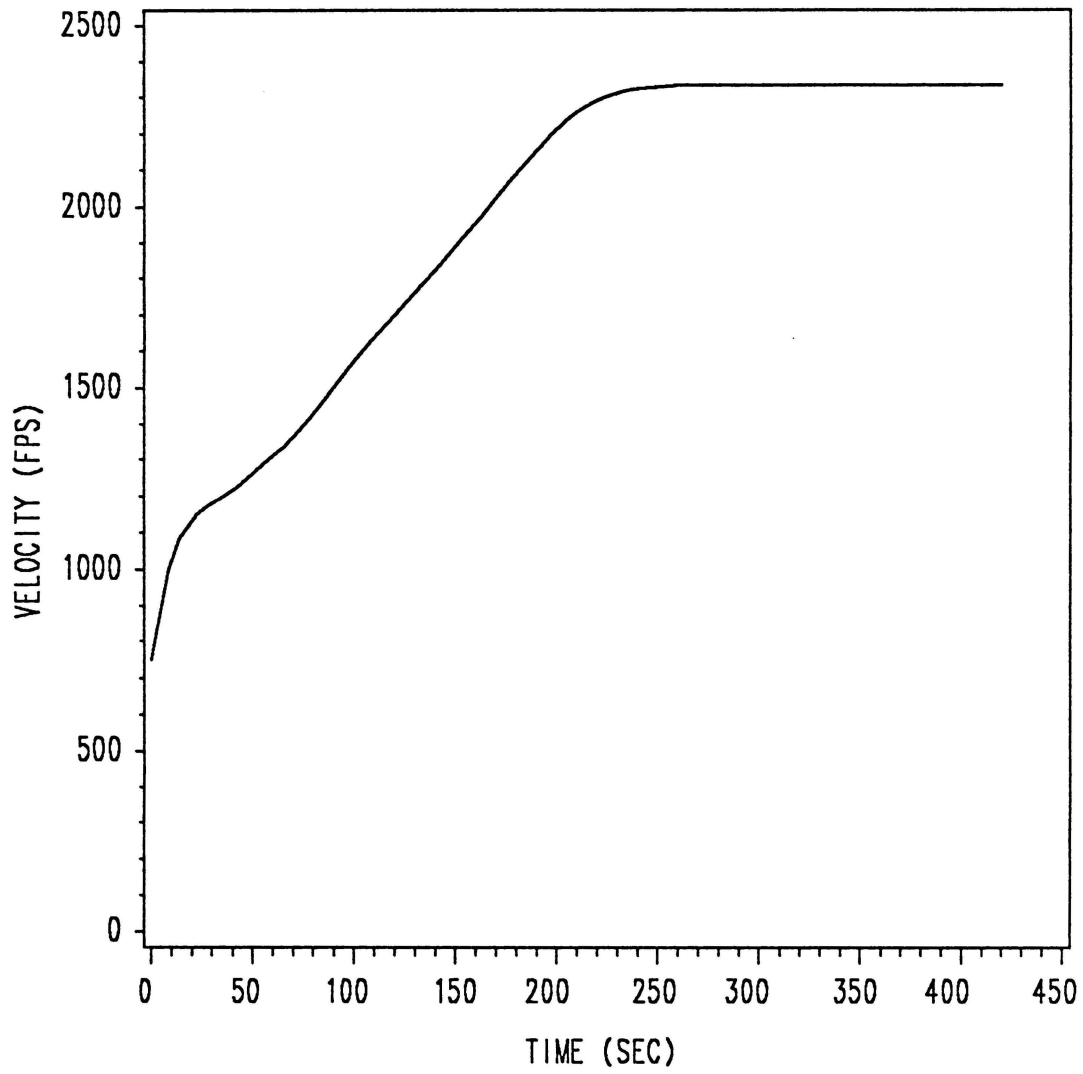


Figure 4. Velocity Time History for  $\mu = 0$  sec/lb

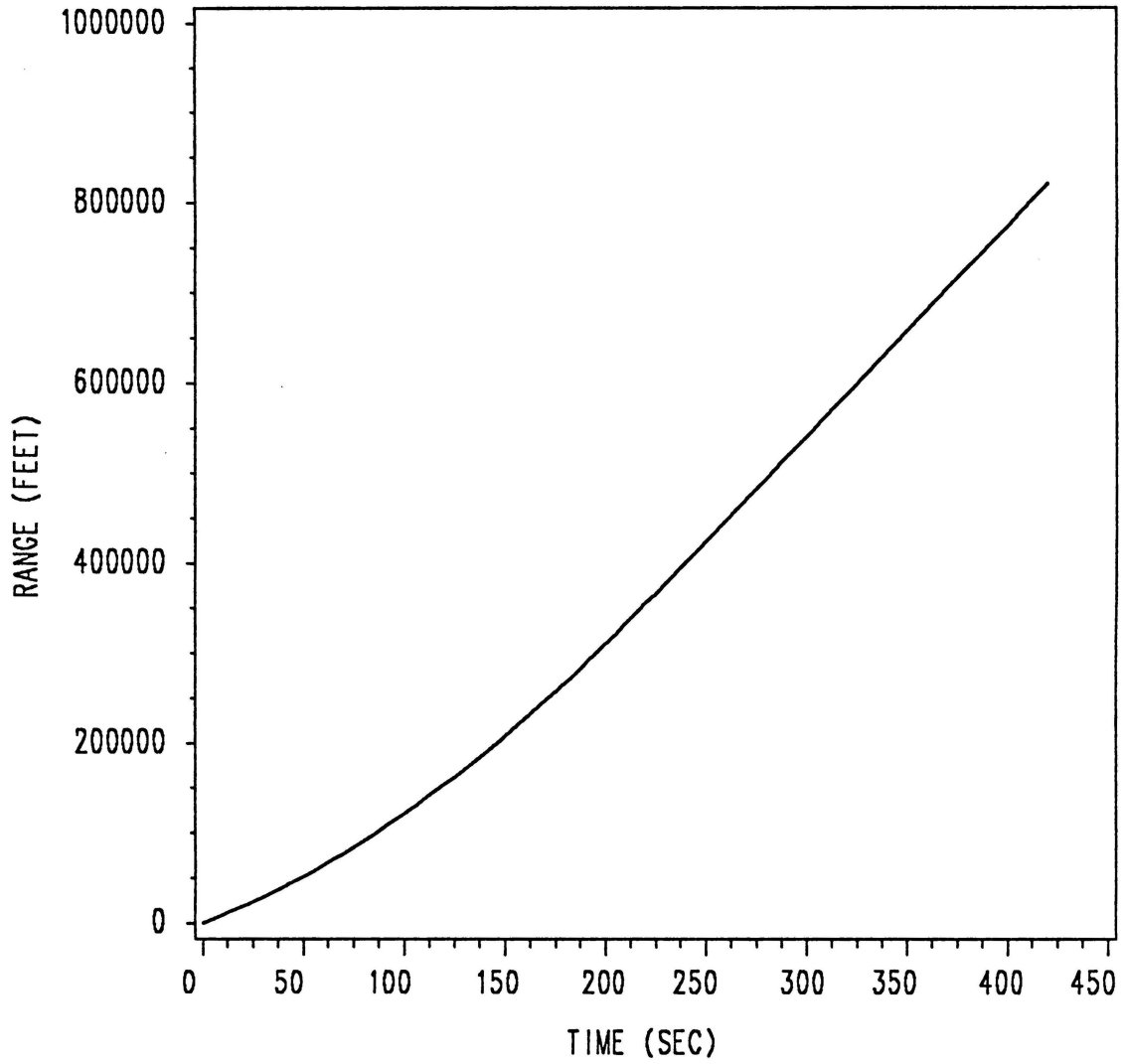


Figure 5. Range Time History for  $\mu = 0$  sec/lb

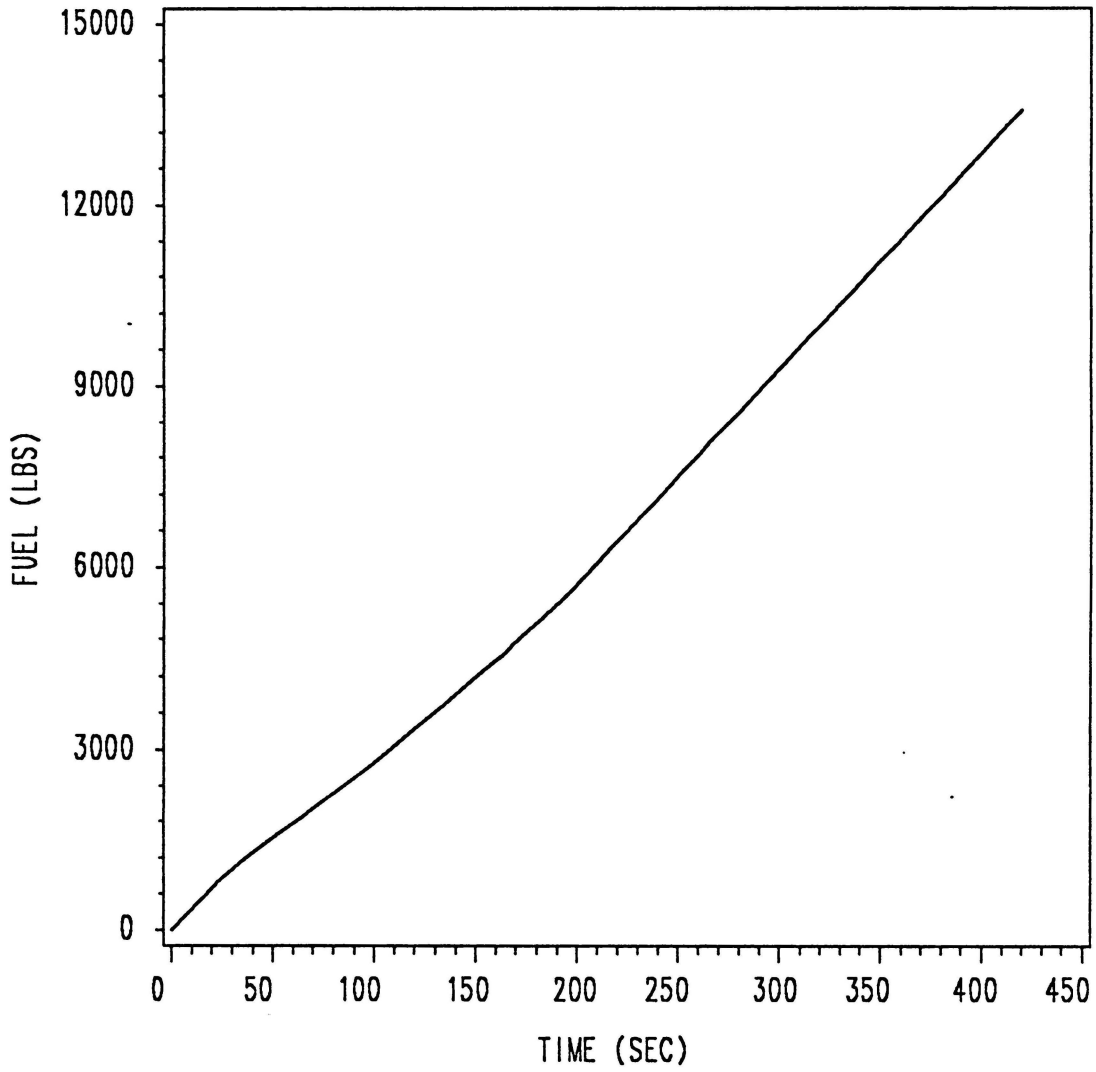


Figure 6. Fuel-Weight Time History for  $\mu = 0$  sec/lb

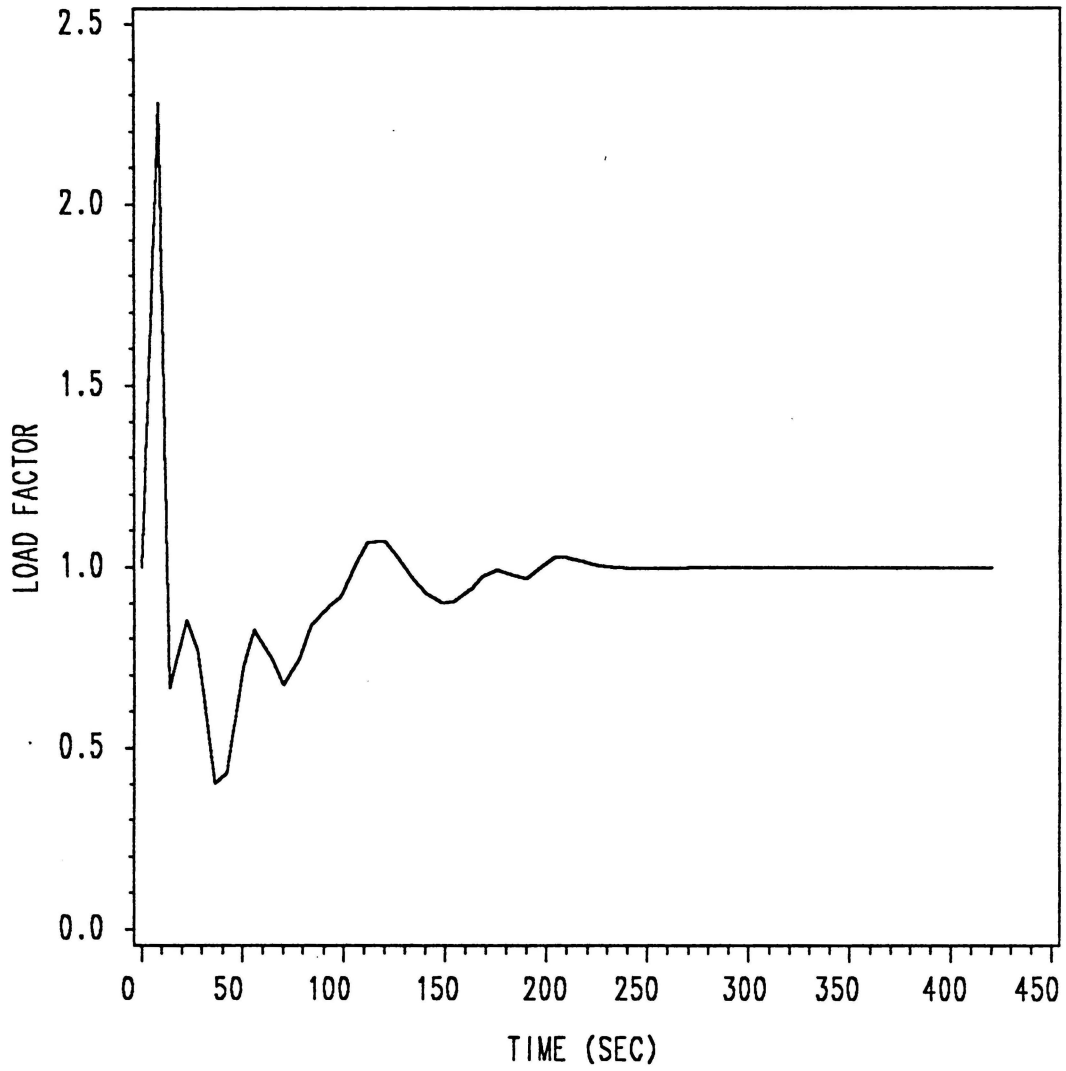


Figure 7. Load-Factor Time History for  $\mu = 0$  sec/lb

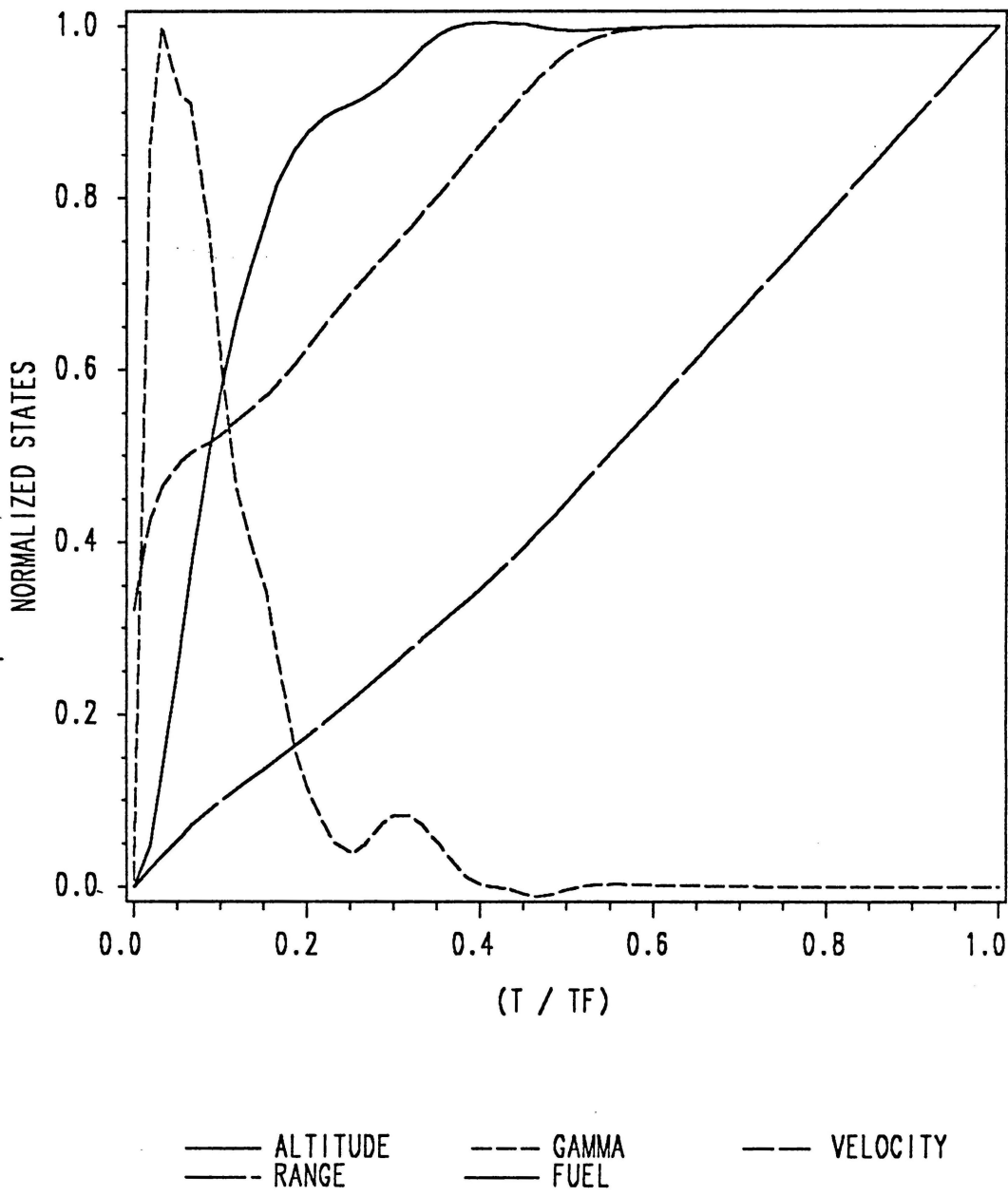


Figure 8. Normalized State Histories for  $\mu = 0 \text{ sec/lb}$

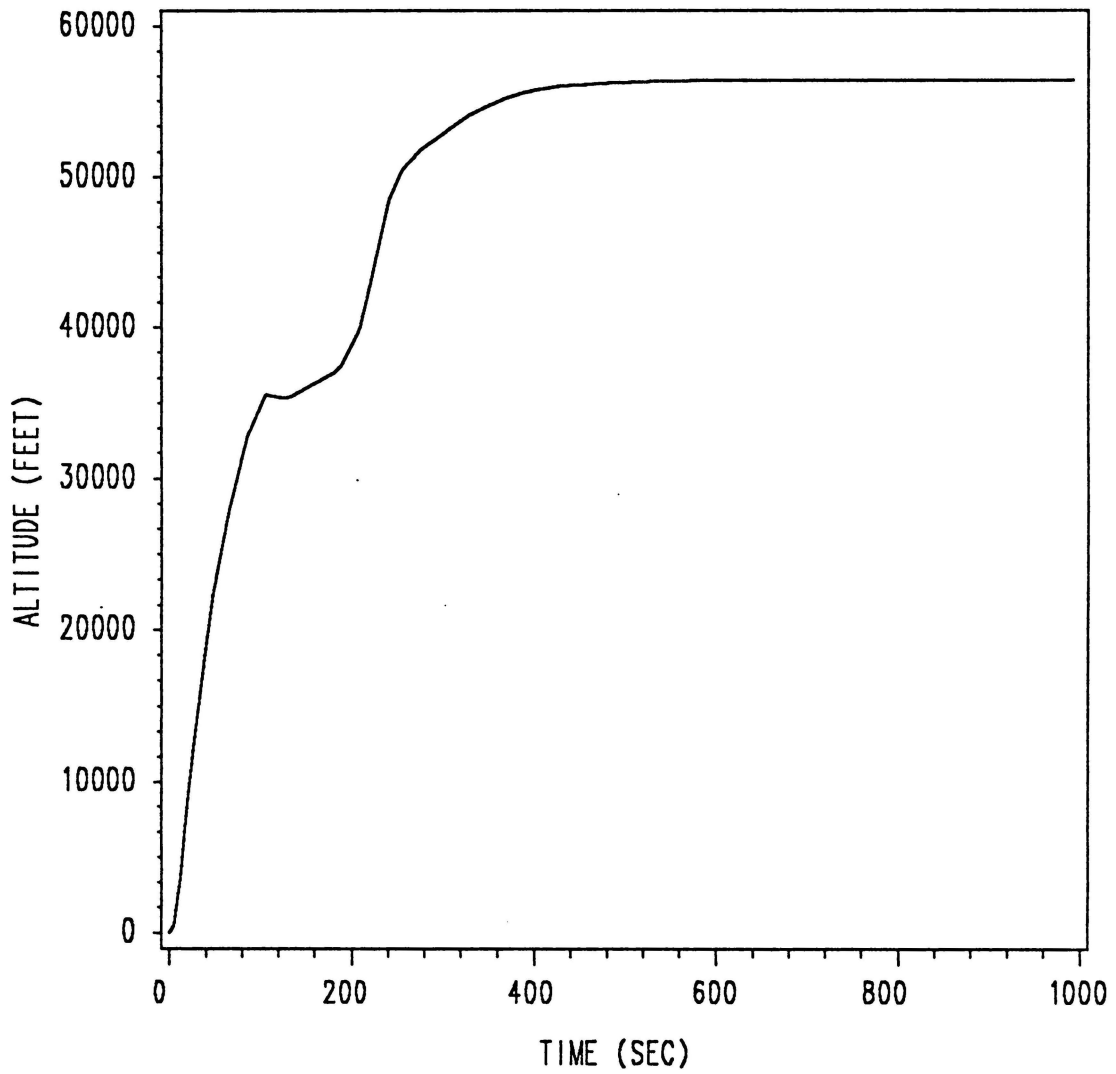


Figure 9. Altitude Time History for  $\mu = 0.0095$  sec/lb

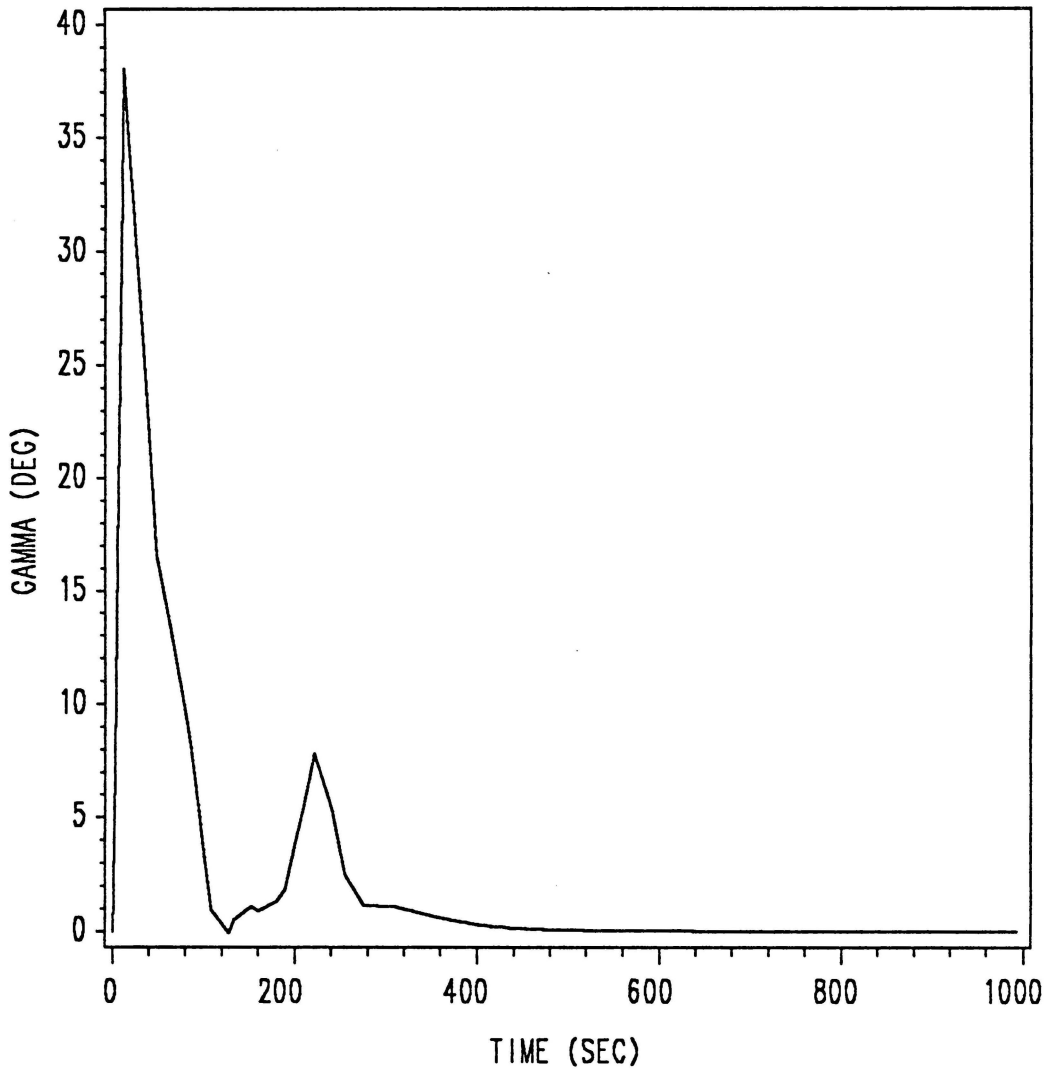


Figure 10. Path-Angle Time History for  $\mu = 0.0095$  sec/lb

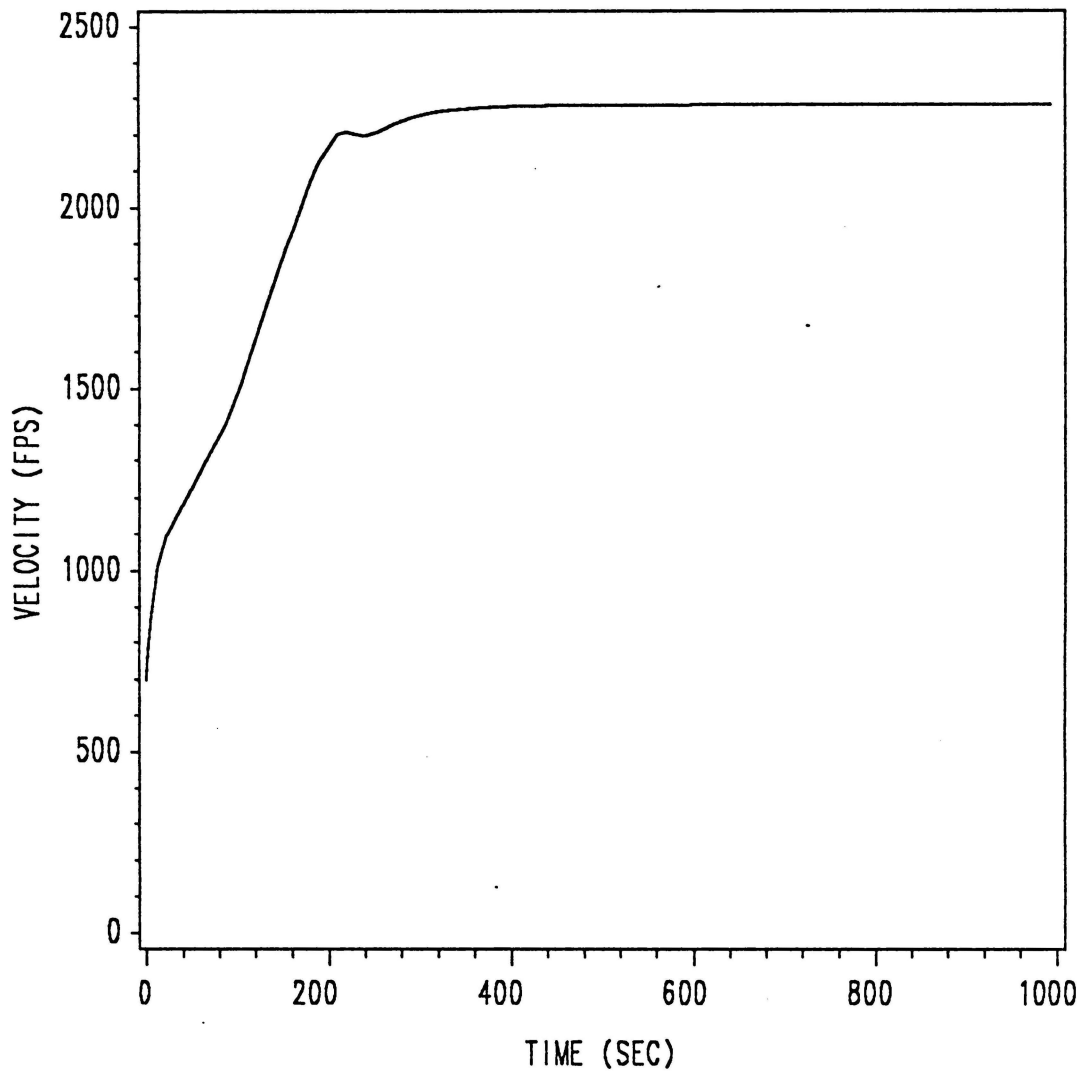


Figure 11. Velocity Time History for  $\mu = 0.0095$  sec/lb



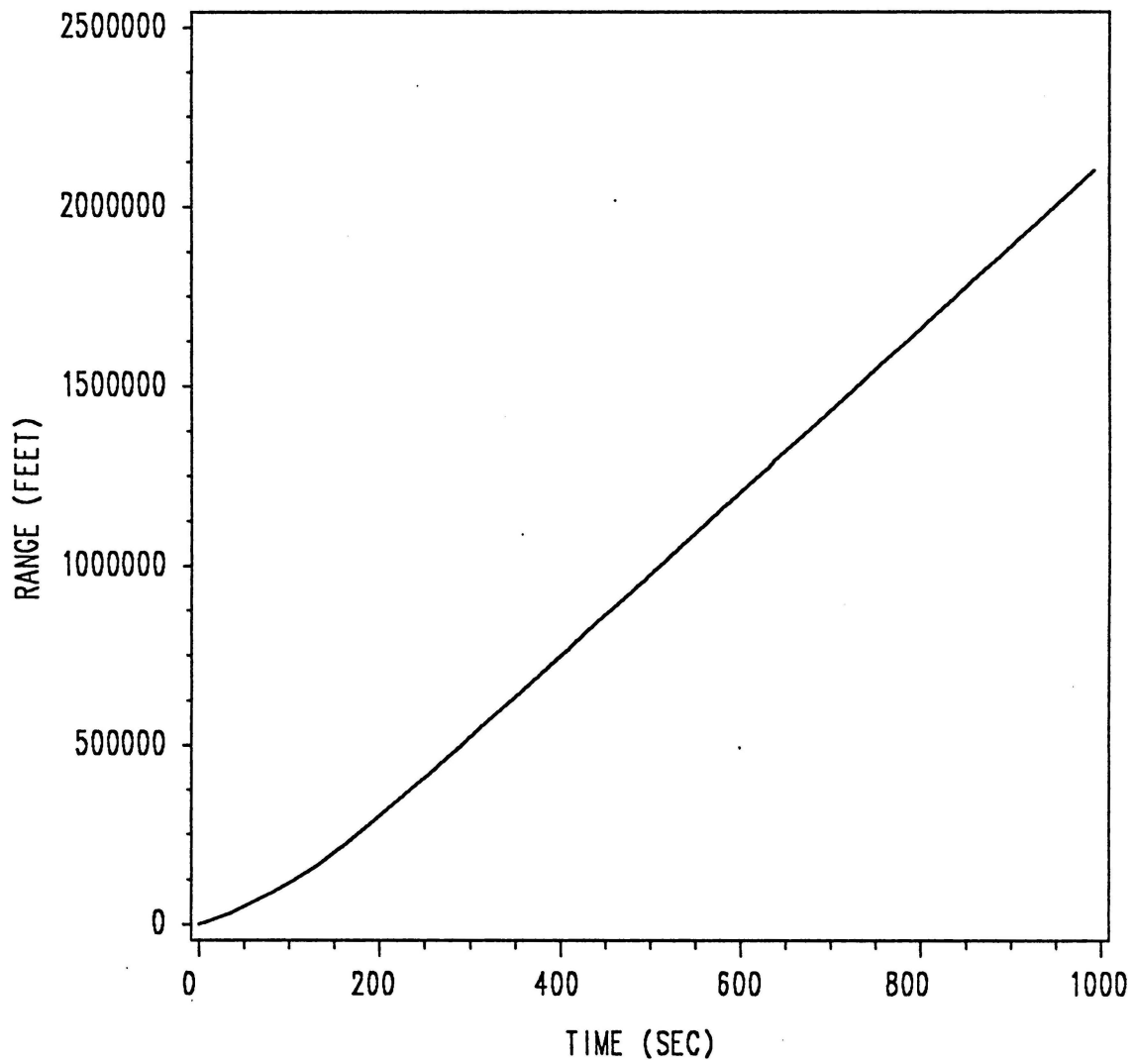


Figure 12. Range Time History for  $\mu = 0.0095$  sec/lb

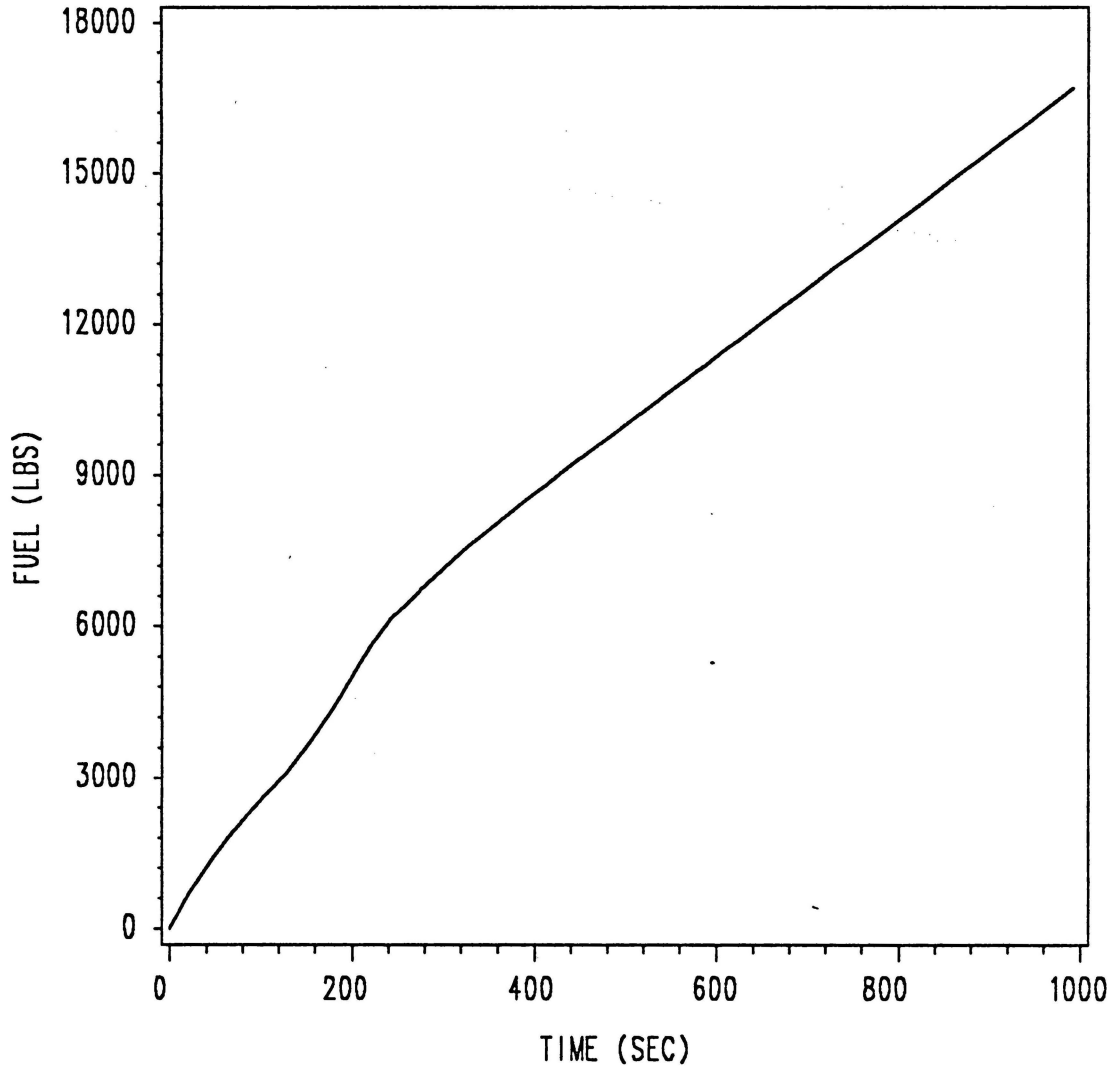


Figure 13. Fuel-Weight Time History for  $\mu = 0.0095$  sec/lb

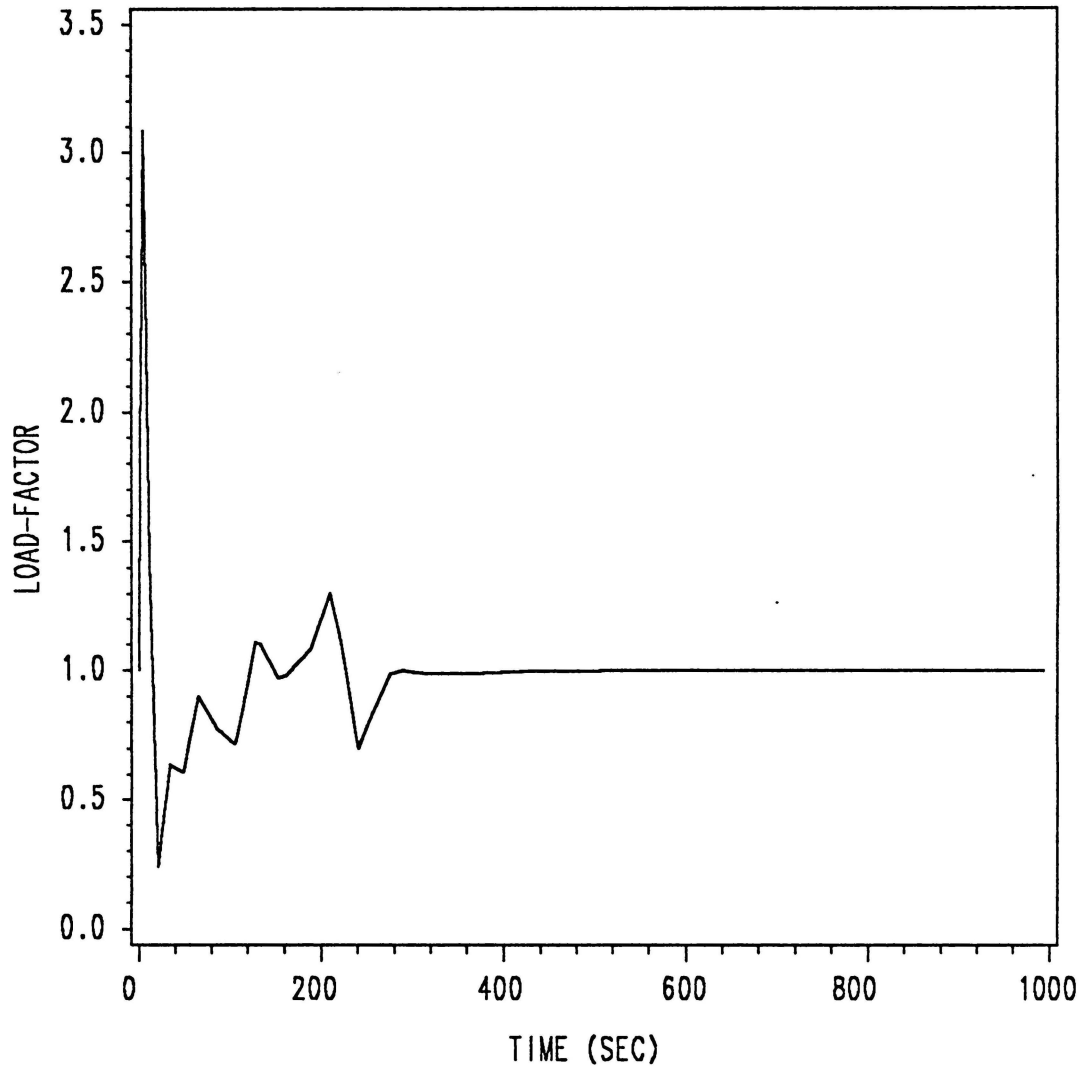


Figure 14. Load-Factor Time History for  $\mu = 0.0095$  sec/lb

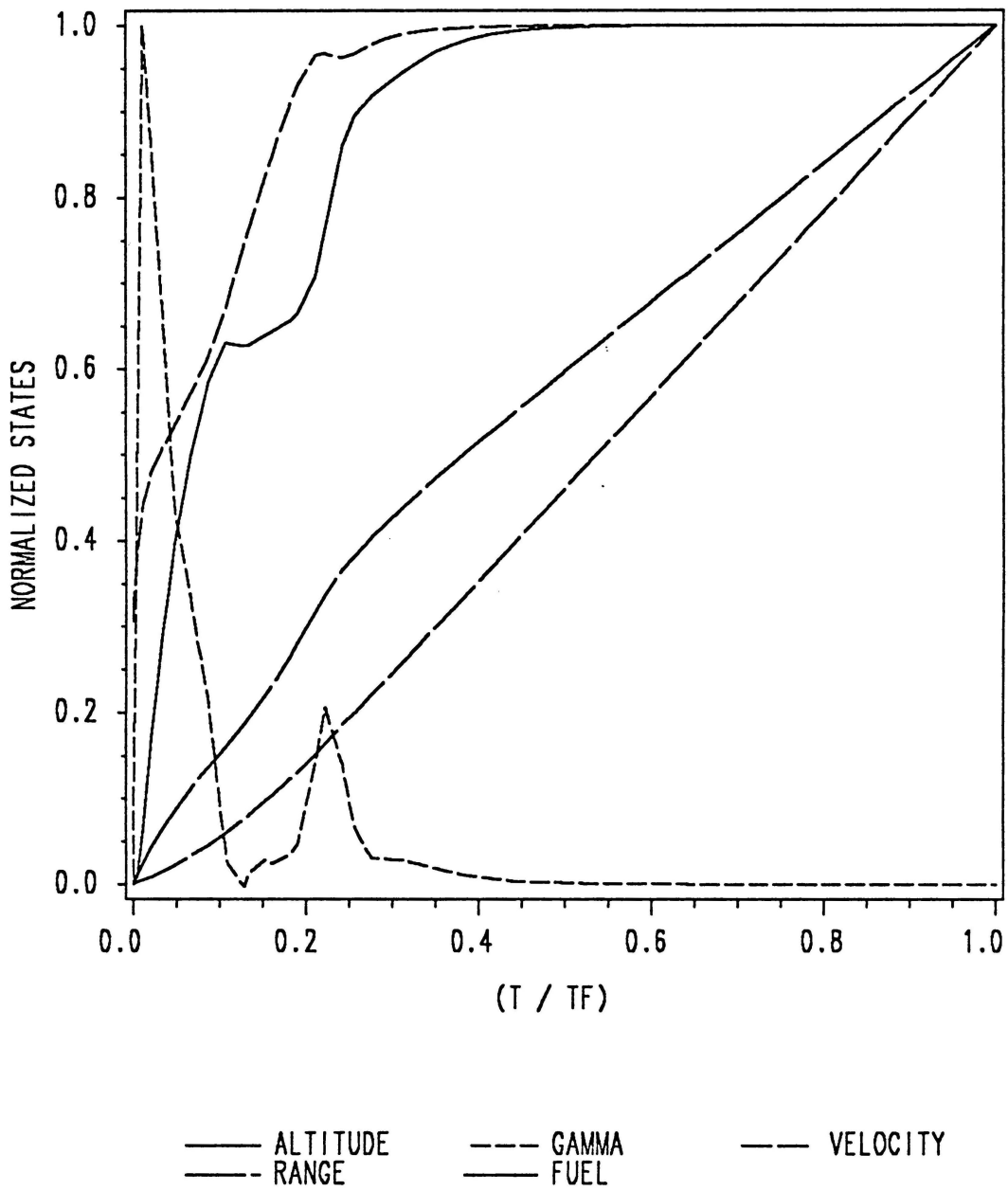


Figure 15. Normalized State Histories for  $\mu = 0.0095$  sec/lb

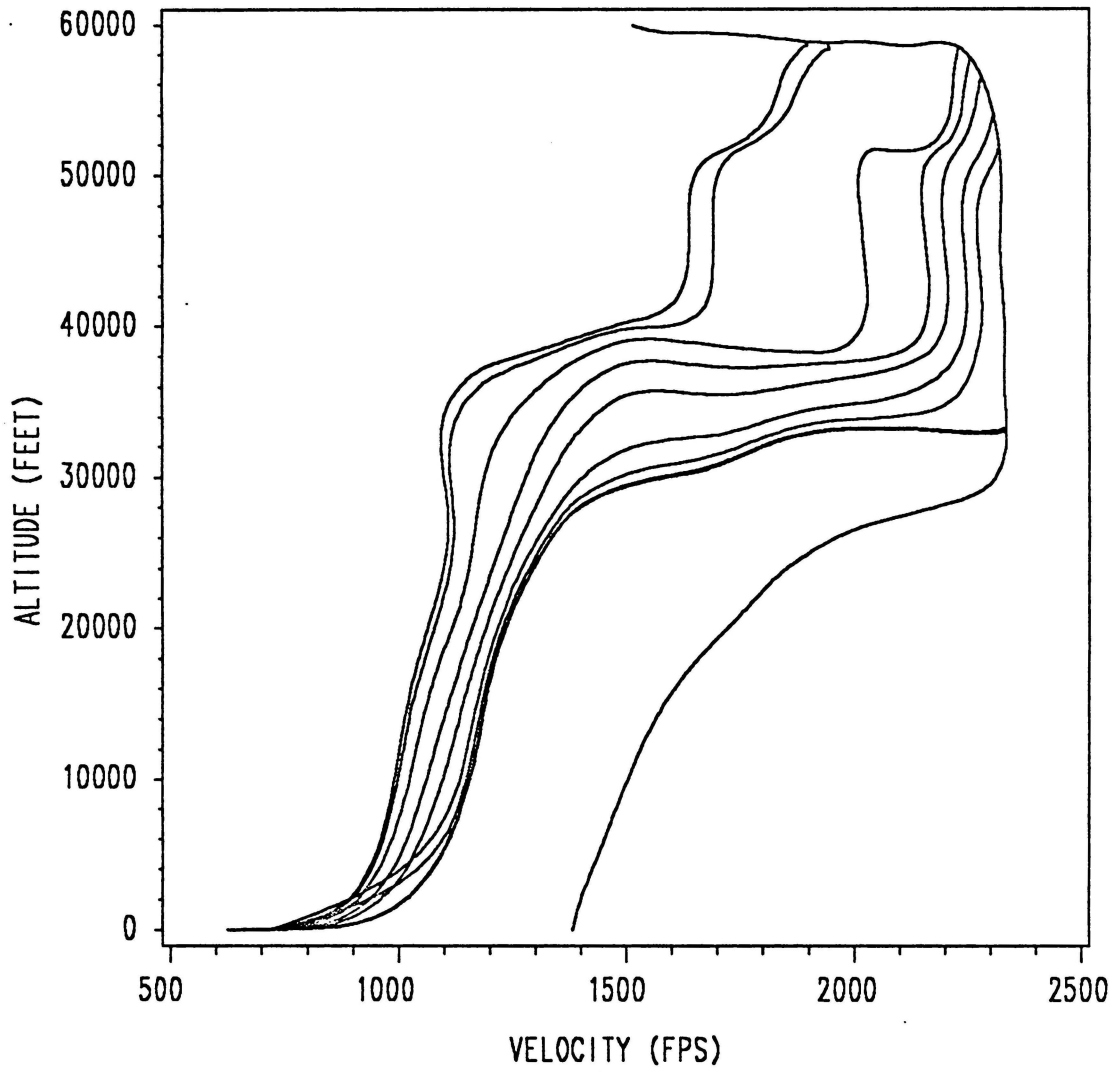


Figure 16. Full-Throttle Cruise-Dash Trajectories in the (h,V) Plane

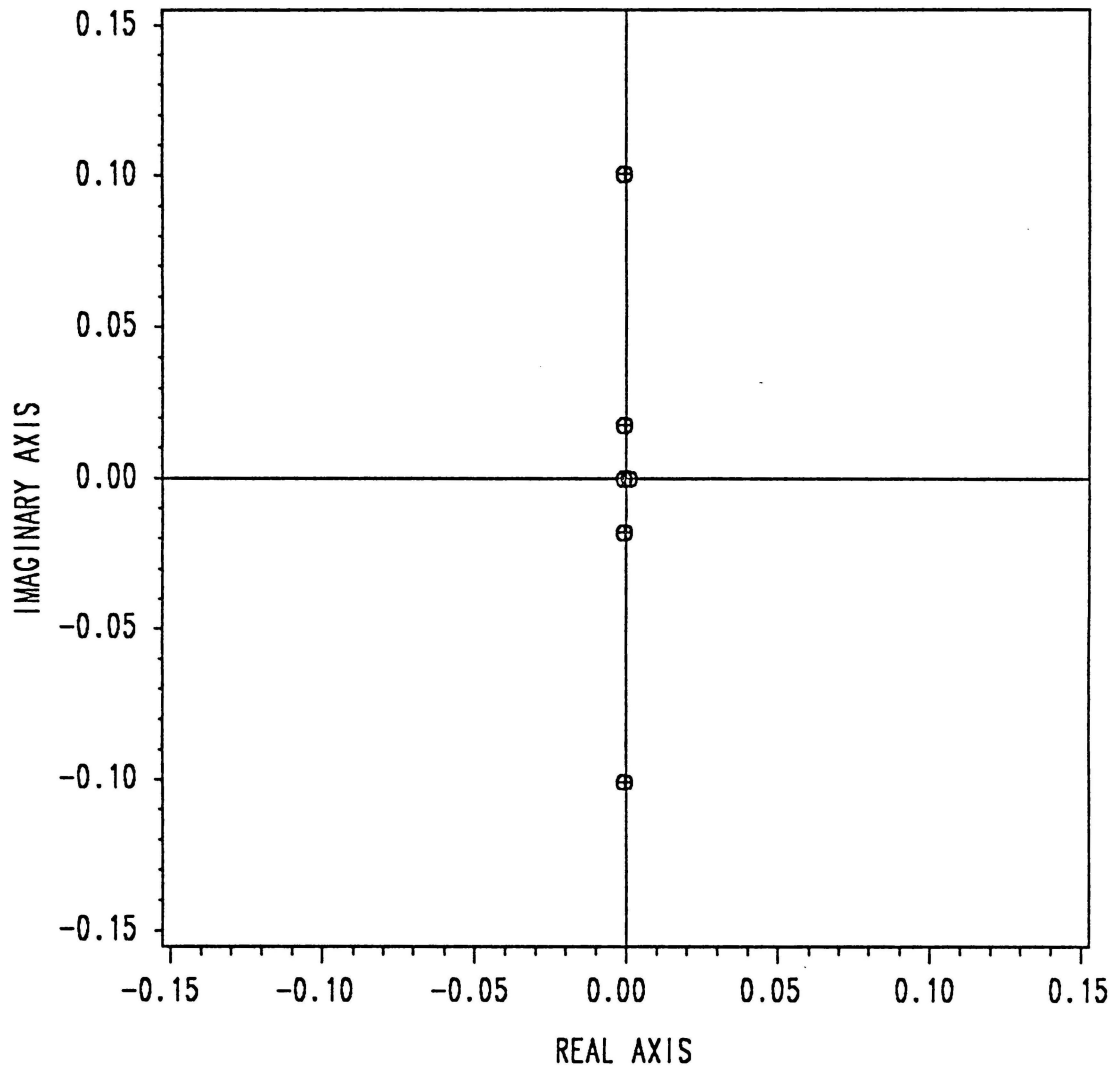


Figure 17. Eigenvalues of Linearized System with  $\mu = 1000$  sec/lb

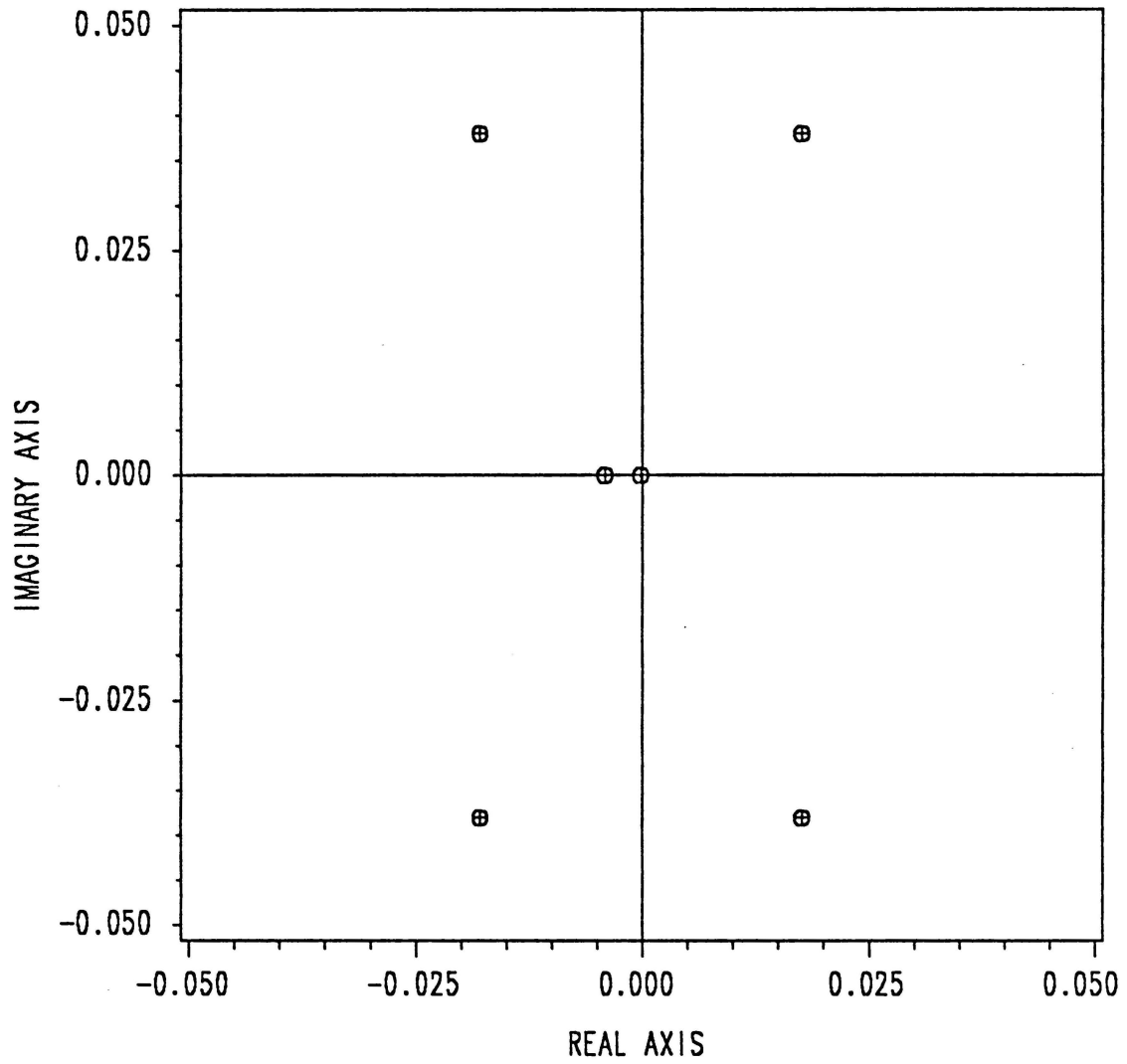


Figure 18. Eigenvalues of Linearized System with  $\mu = 320 \text{ sec/lb}$

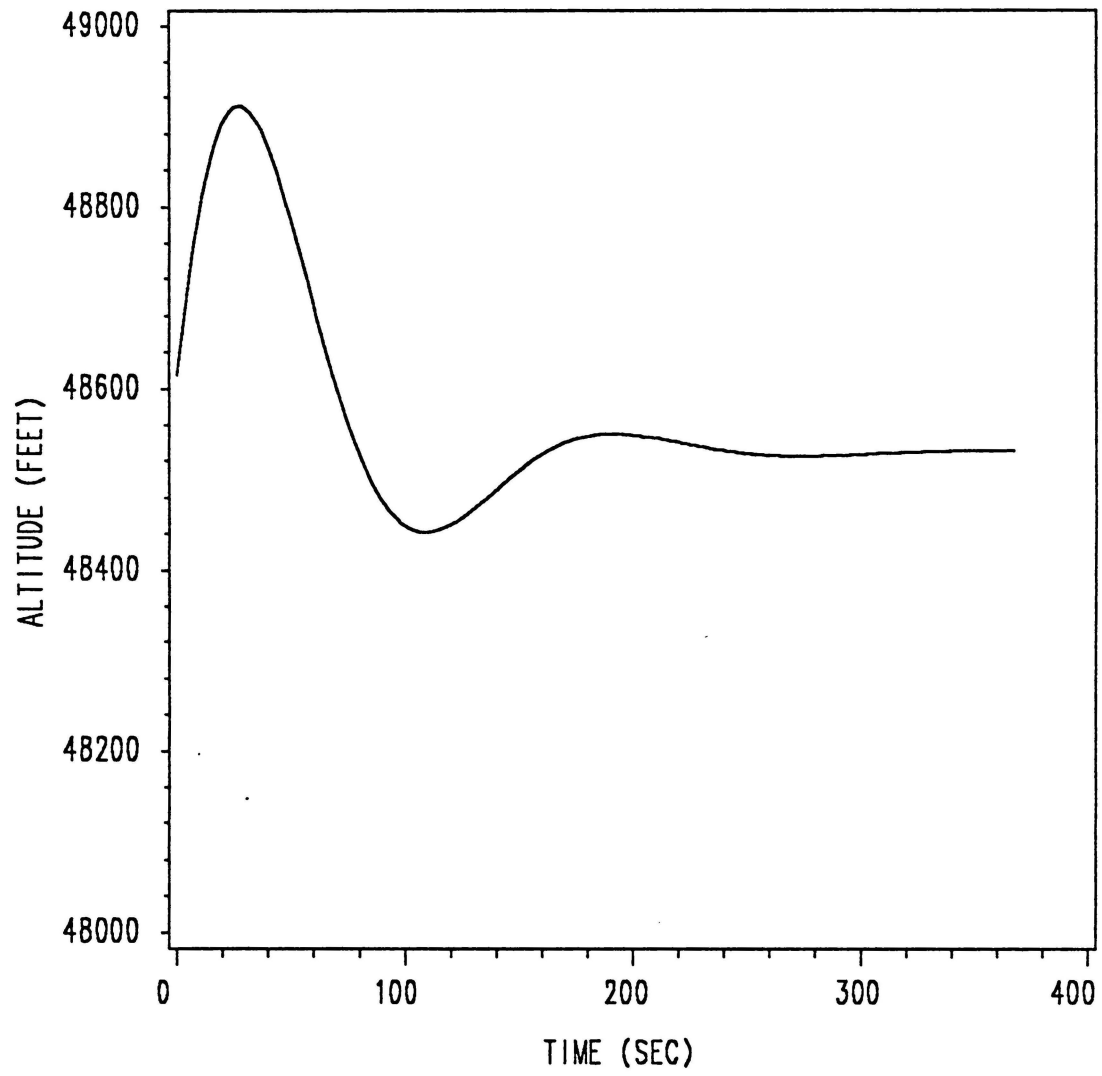


Figure 19. Altitude Time History for  $\mu = 320$  sec/lb



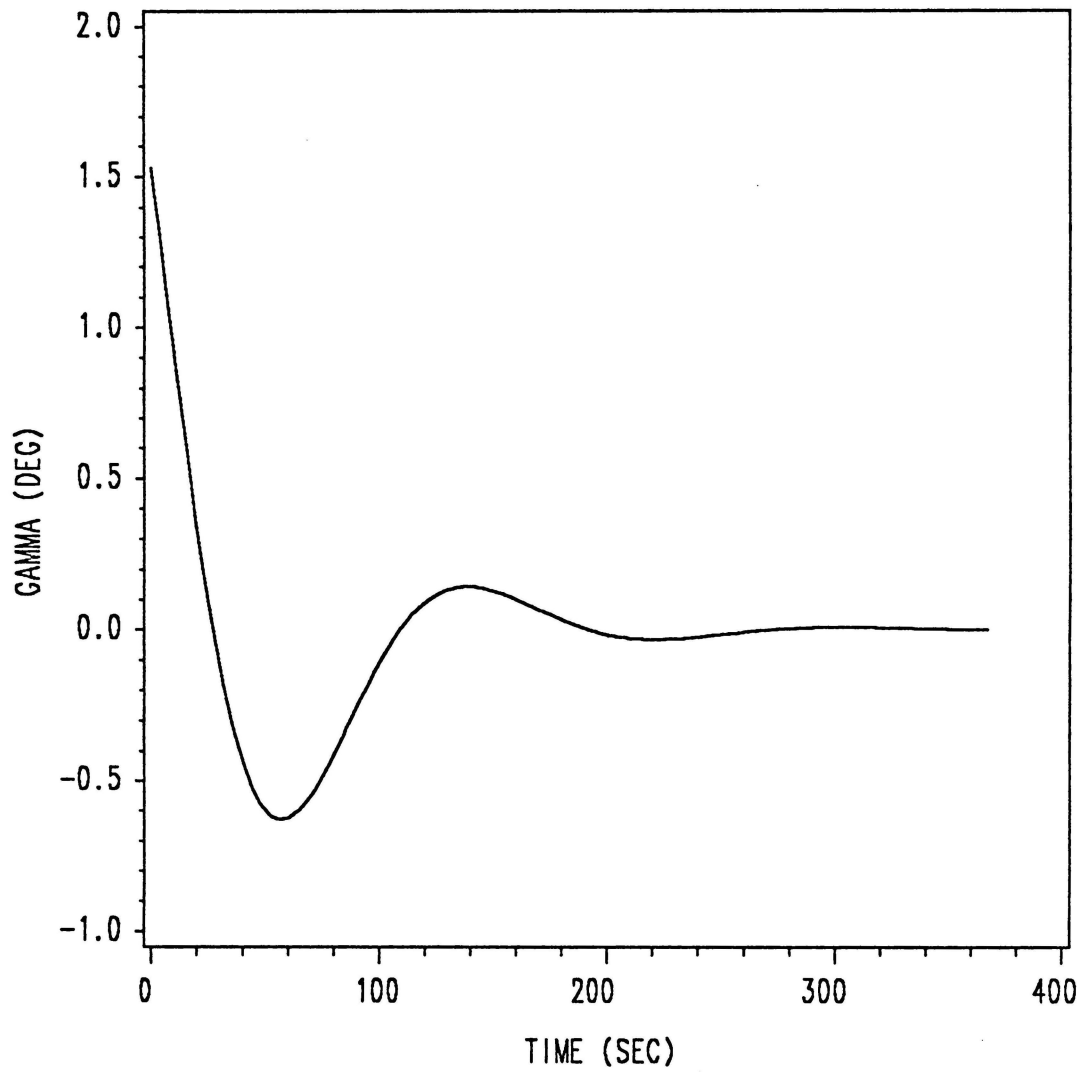


Figure 20. Path-Angle Time History for  $\mu = 320$  sec/lb

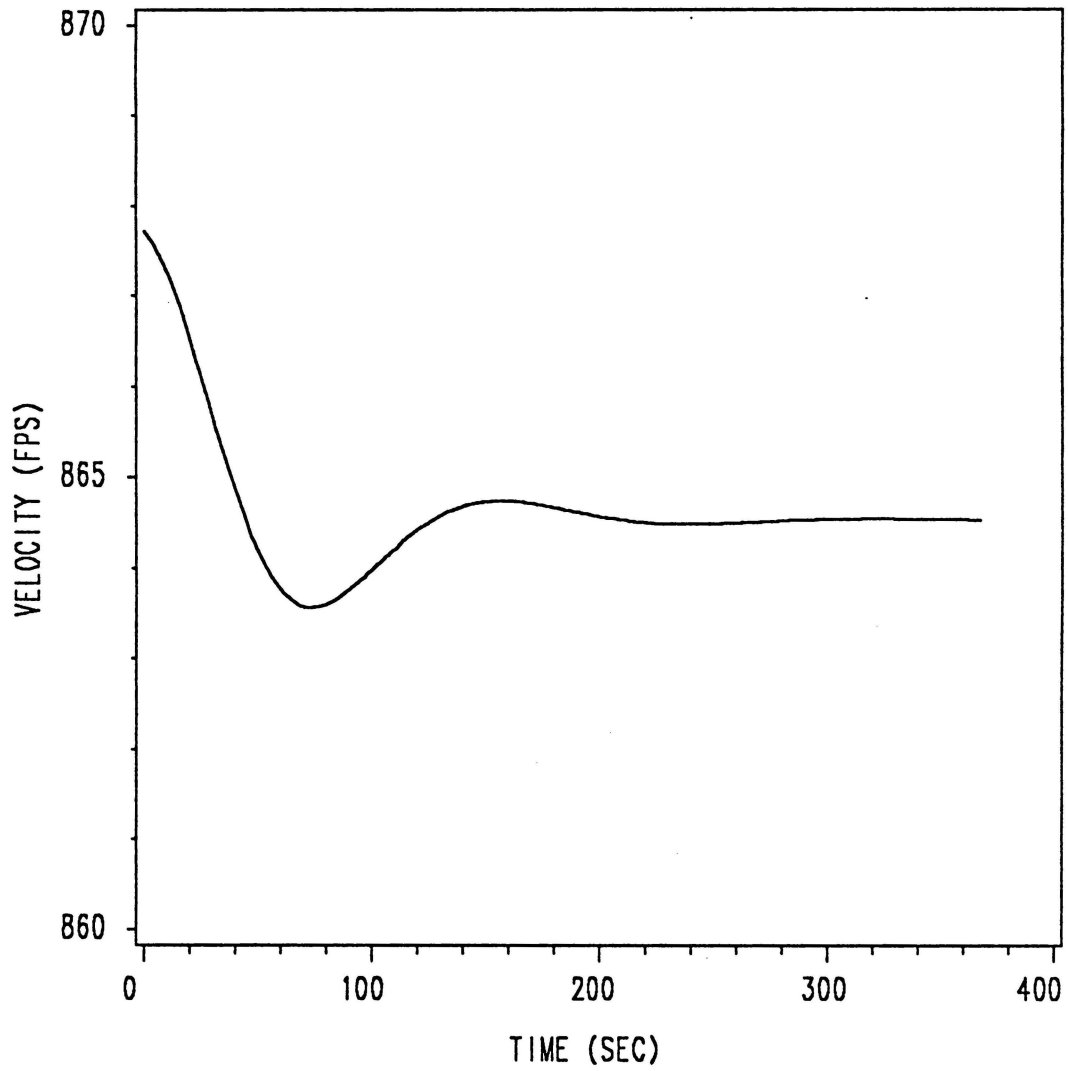


Figure 21. Velocity Time History for  $\mu = 320$  sec/lb

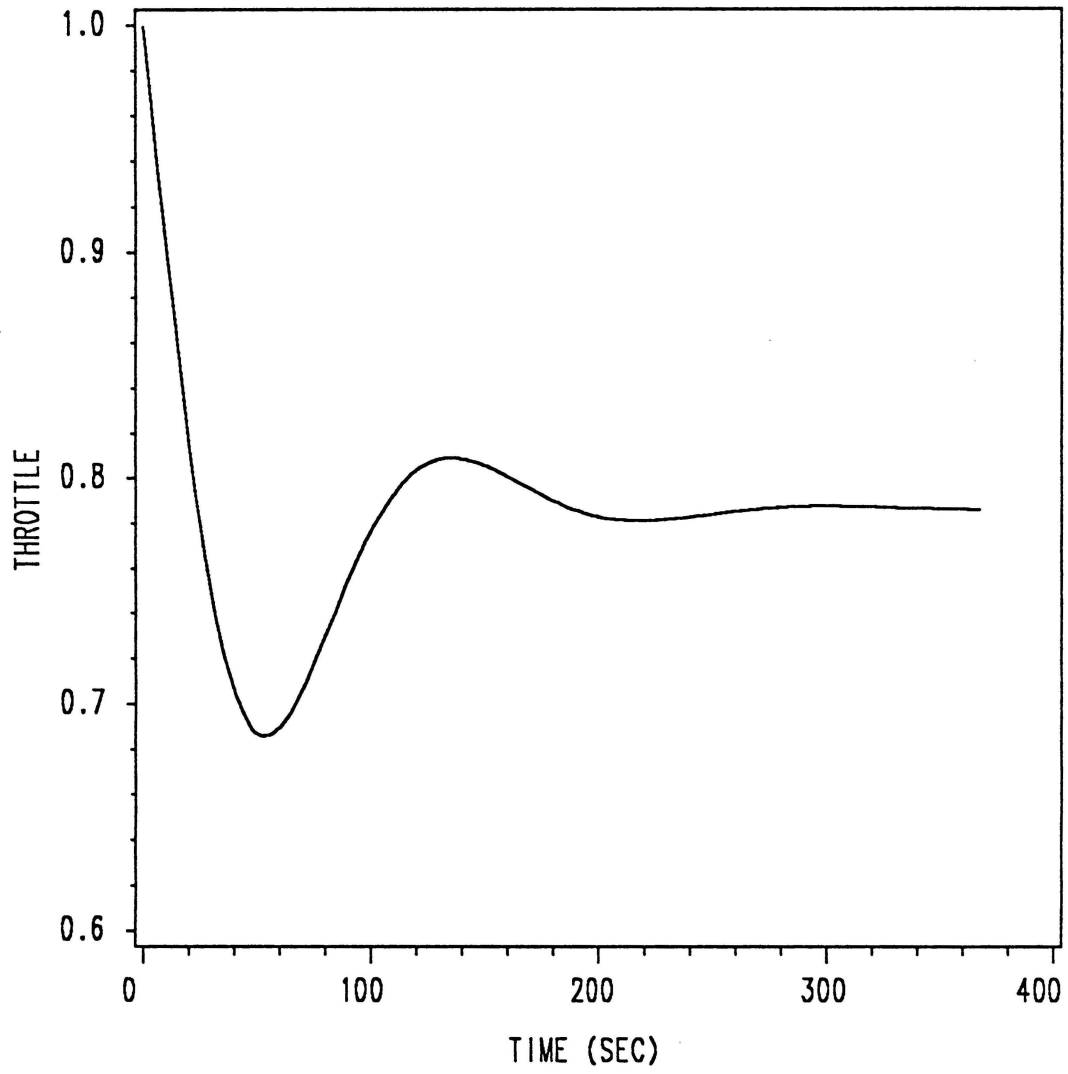


Figure 22. Throttle Time History for  $\mu = 320$  sec/lb

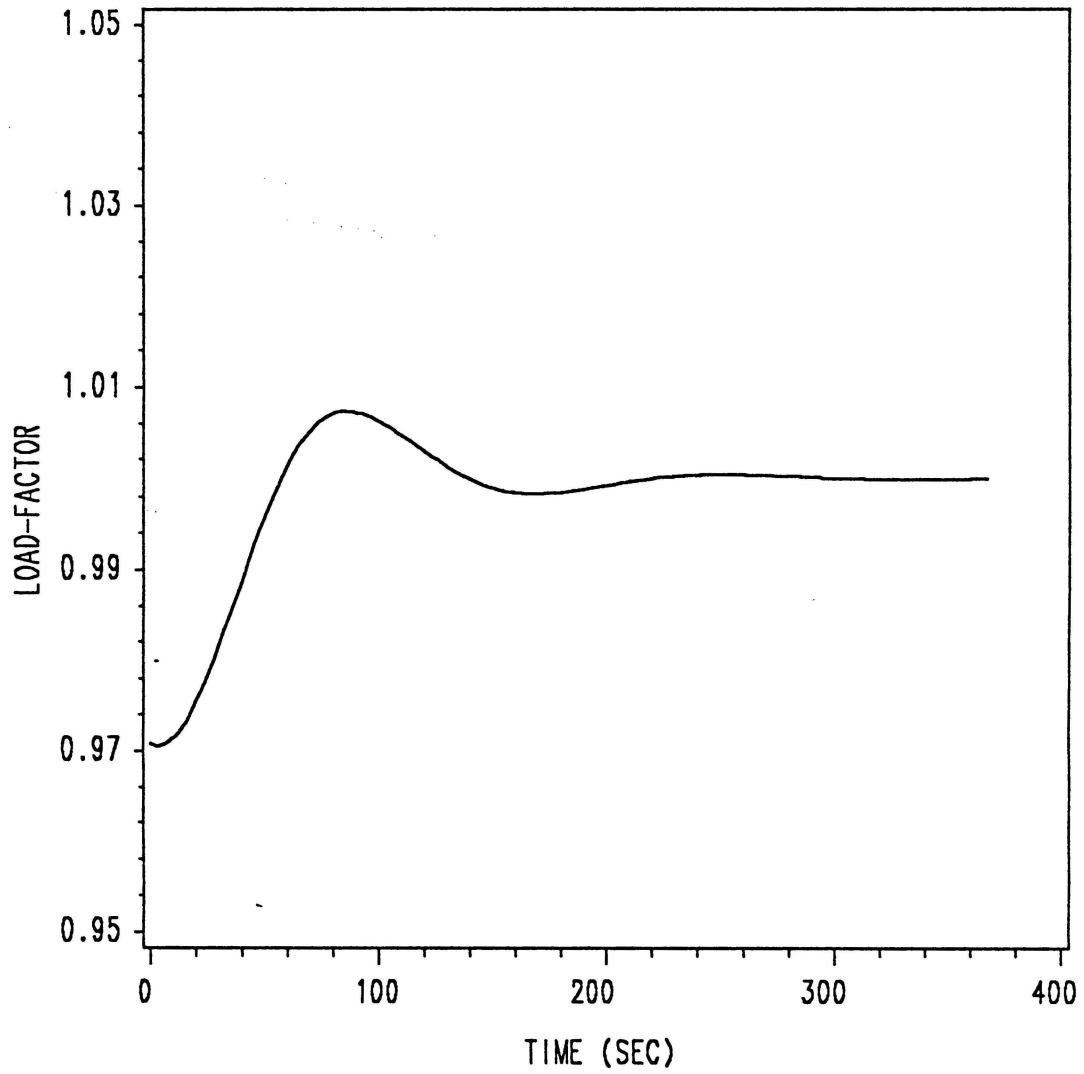


Figure 23. Load-Factor Time History for  $\mu = 320$  sec/lb

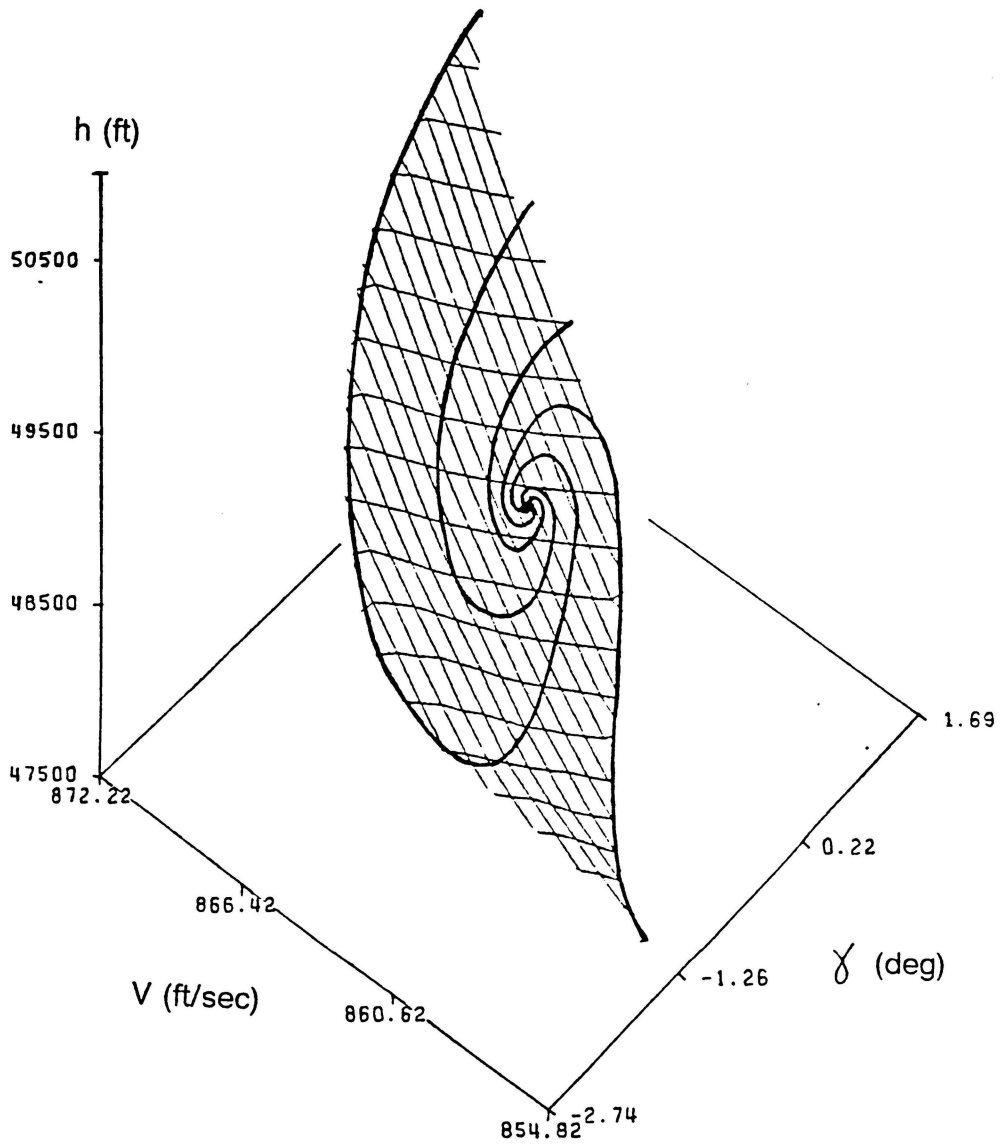


Figure 24. Singular Surface in  $(\gamma, V, h)$  Space

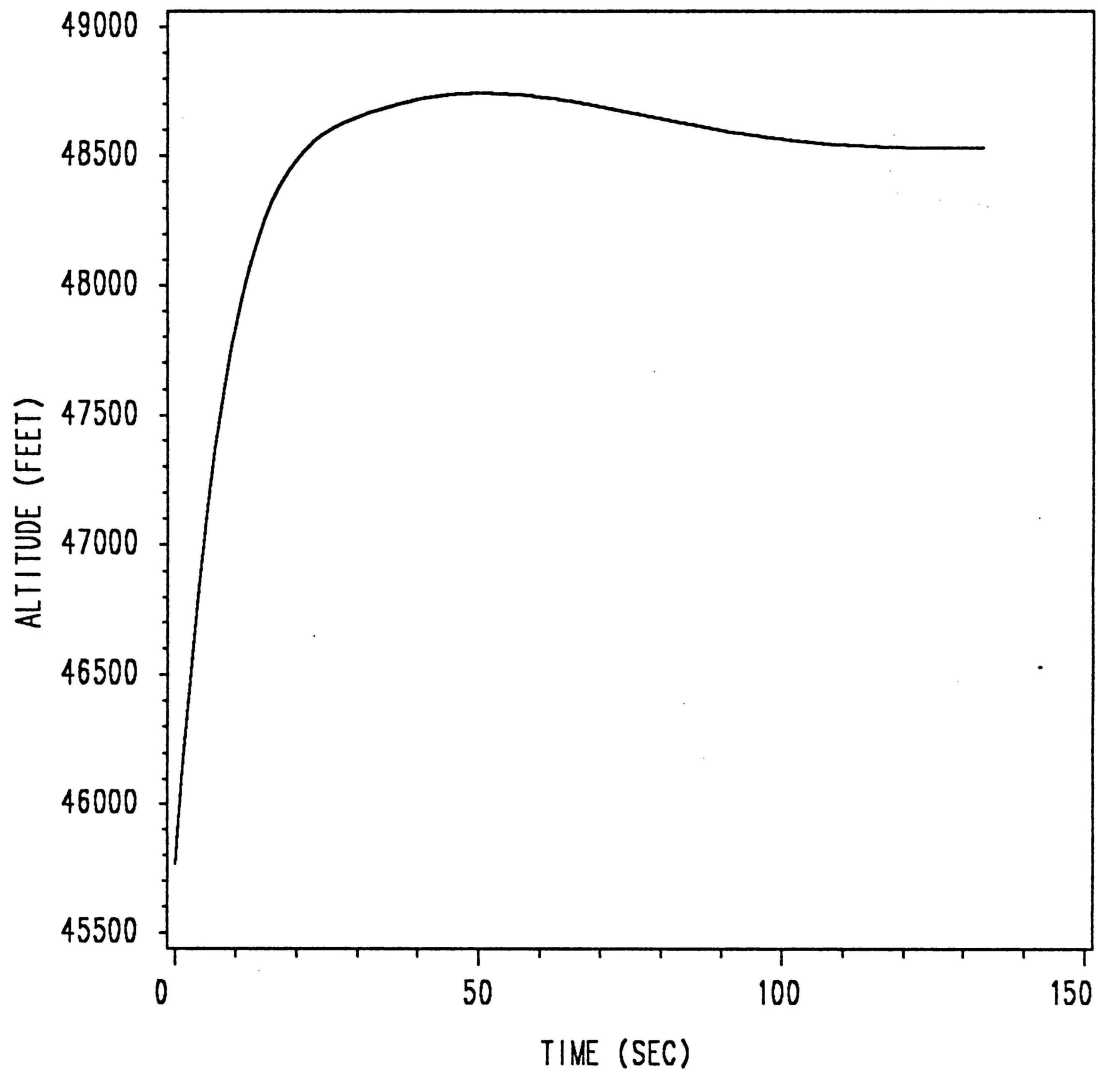


Figure 25. Altitude Time History for (Full)Bang-Singular Control

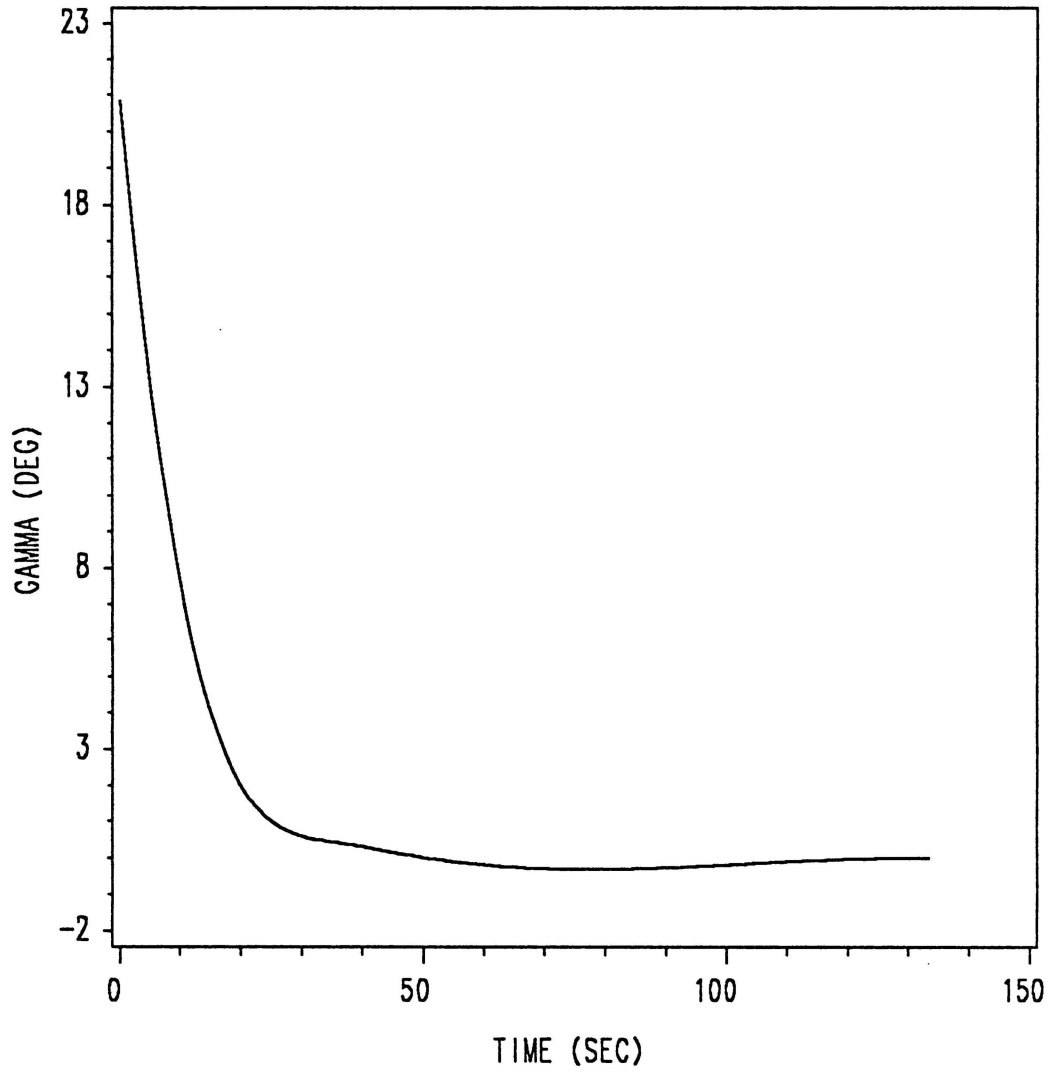


Figure 26. Path-Angle Time History for (Full)Bang-Singular Control

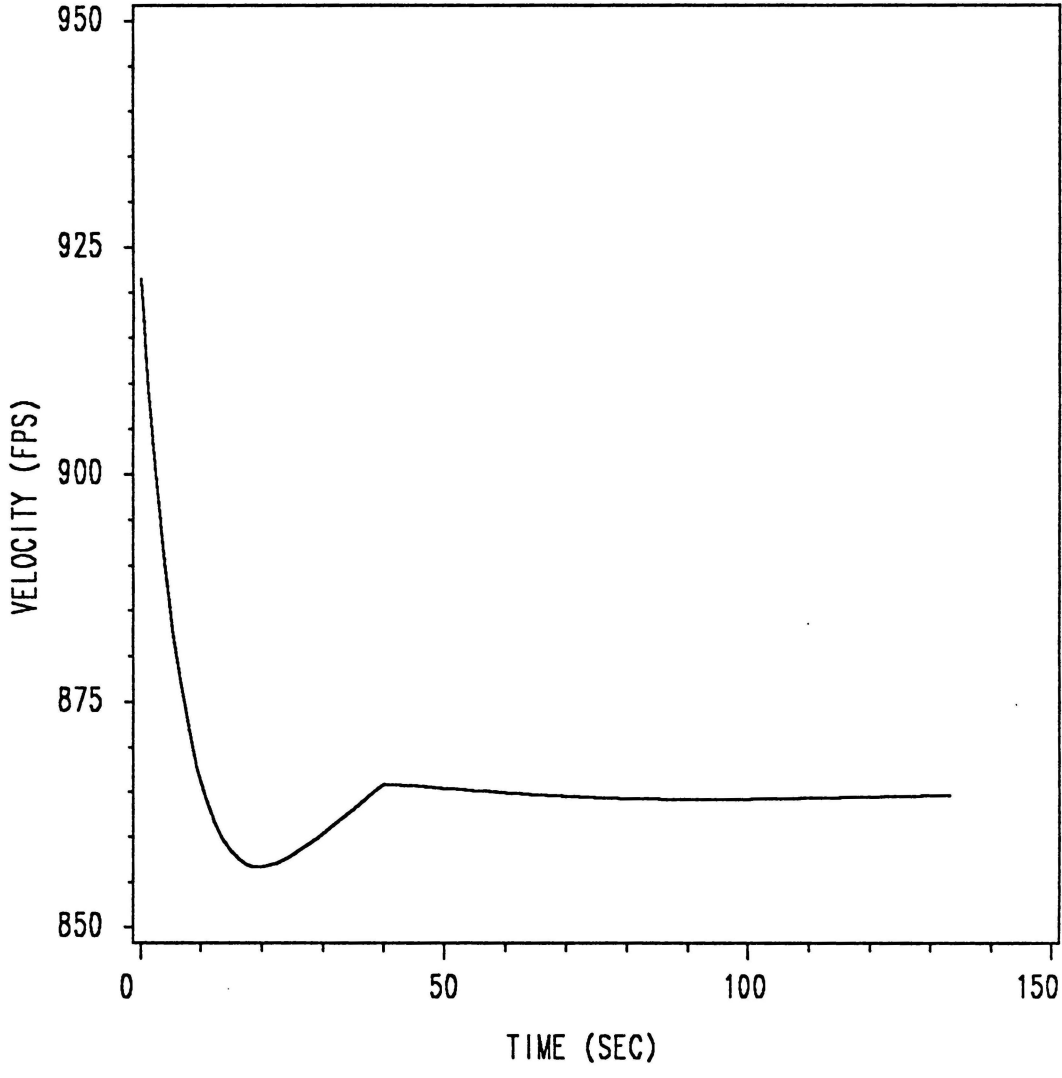


Figure 27. Velocity Time History for (Full)Bang-Singular Control



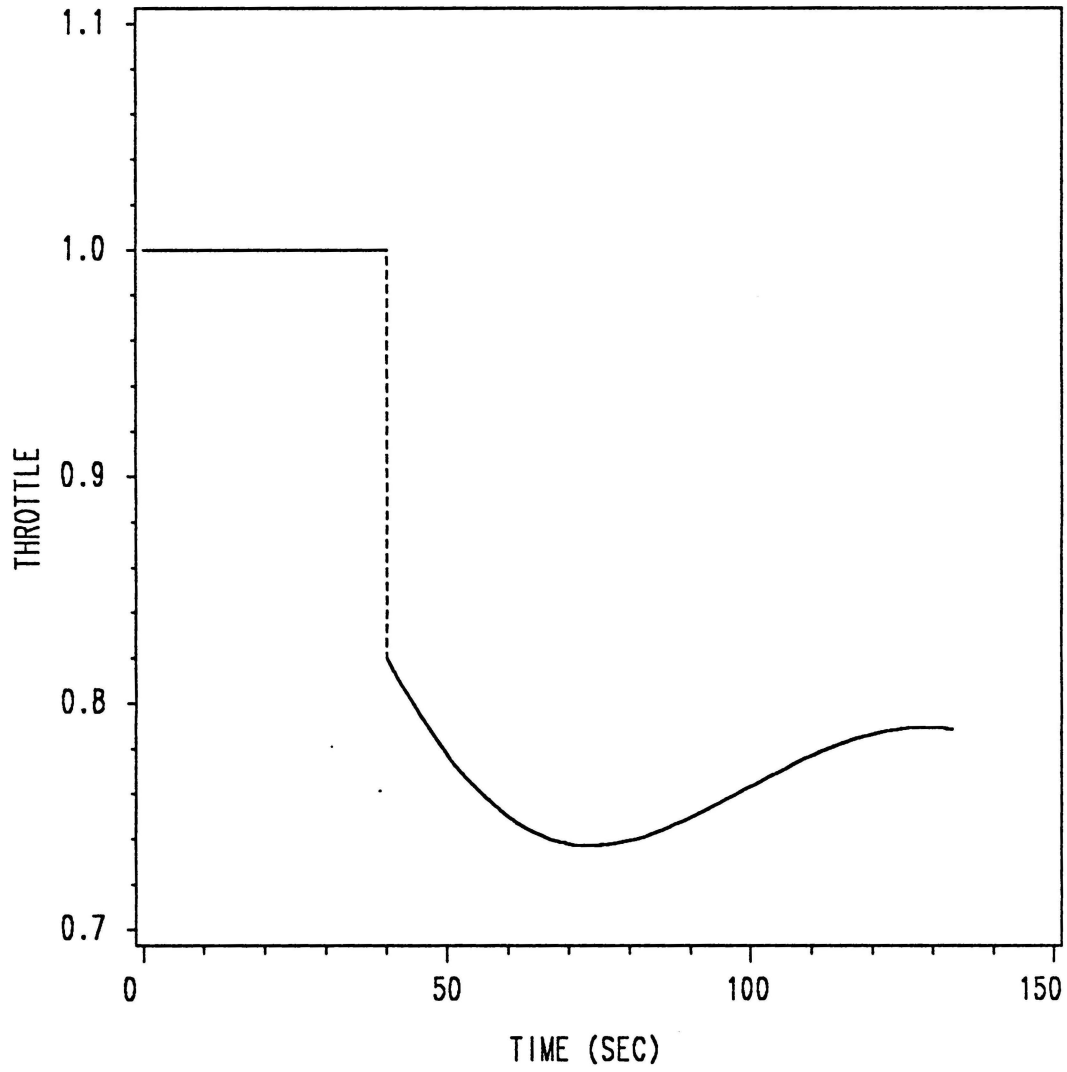


Figure 28. Throttle Time History for (Full)Bang-Singular Control

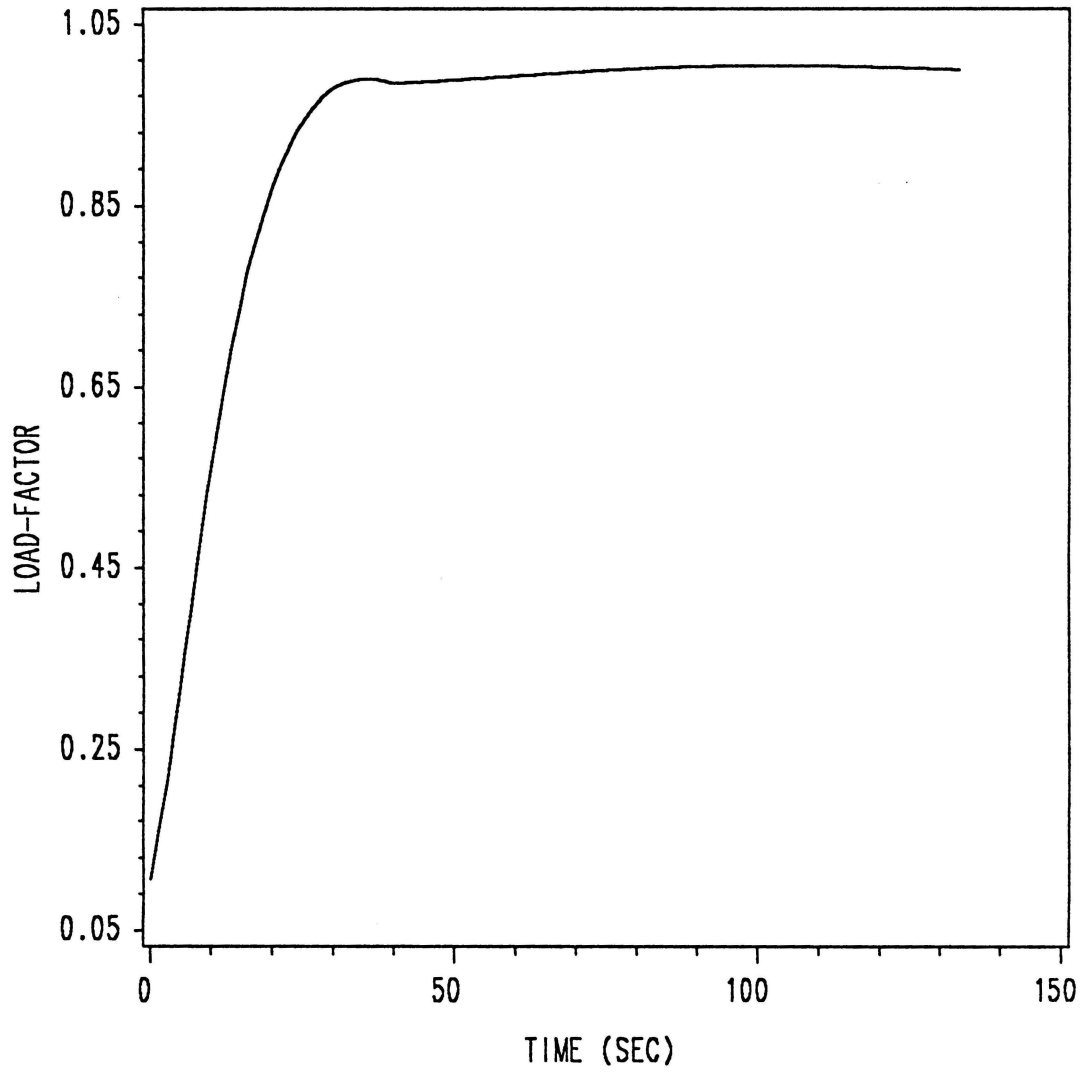


Figure 29. Load-Factor Time History for (Full)Bang-Singular Control

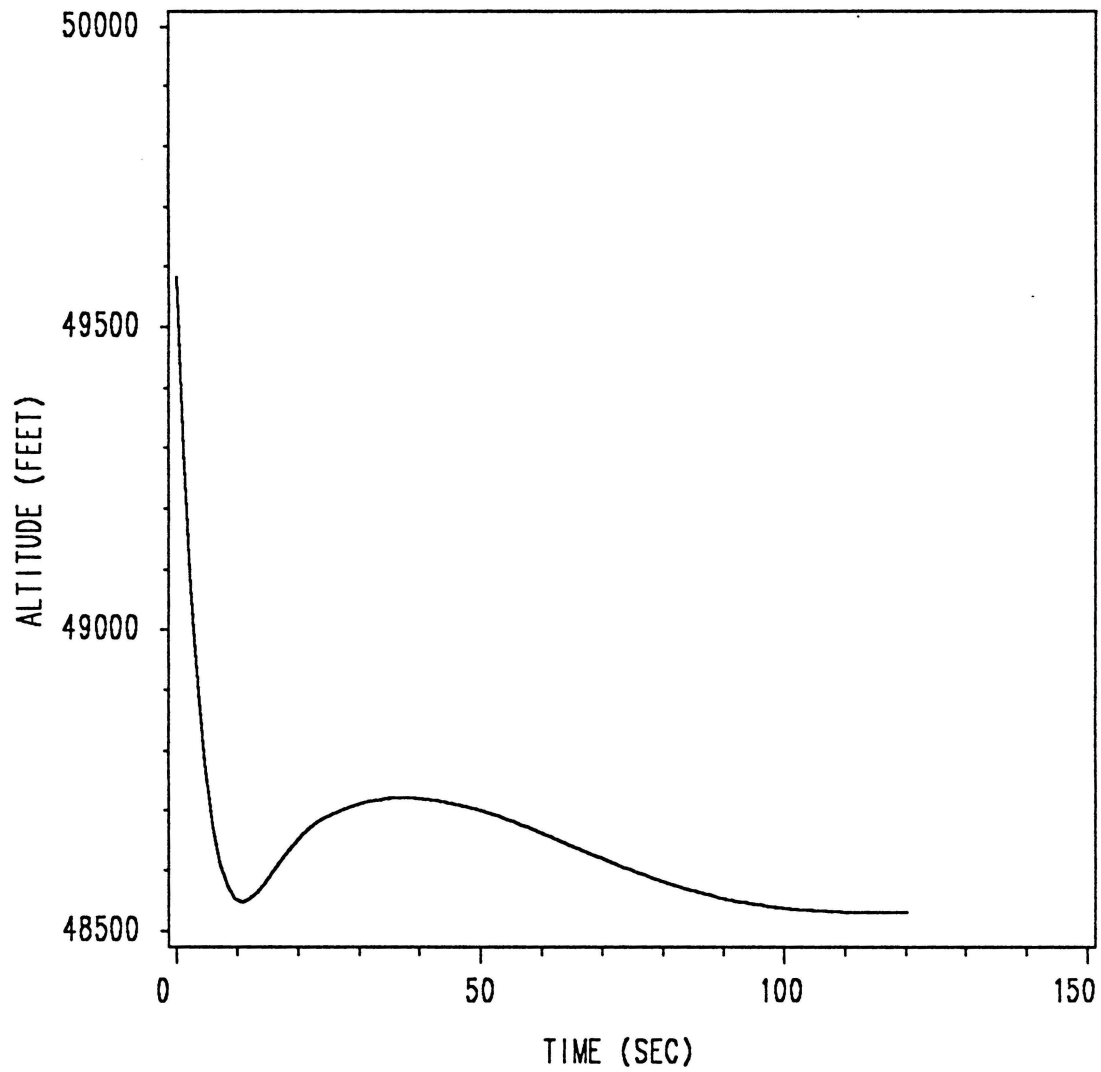


Figure 30. Altitude Time History for (Zero)Bang-Singular Control

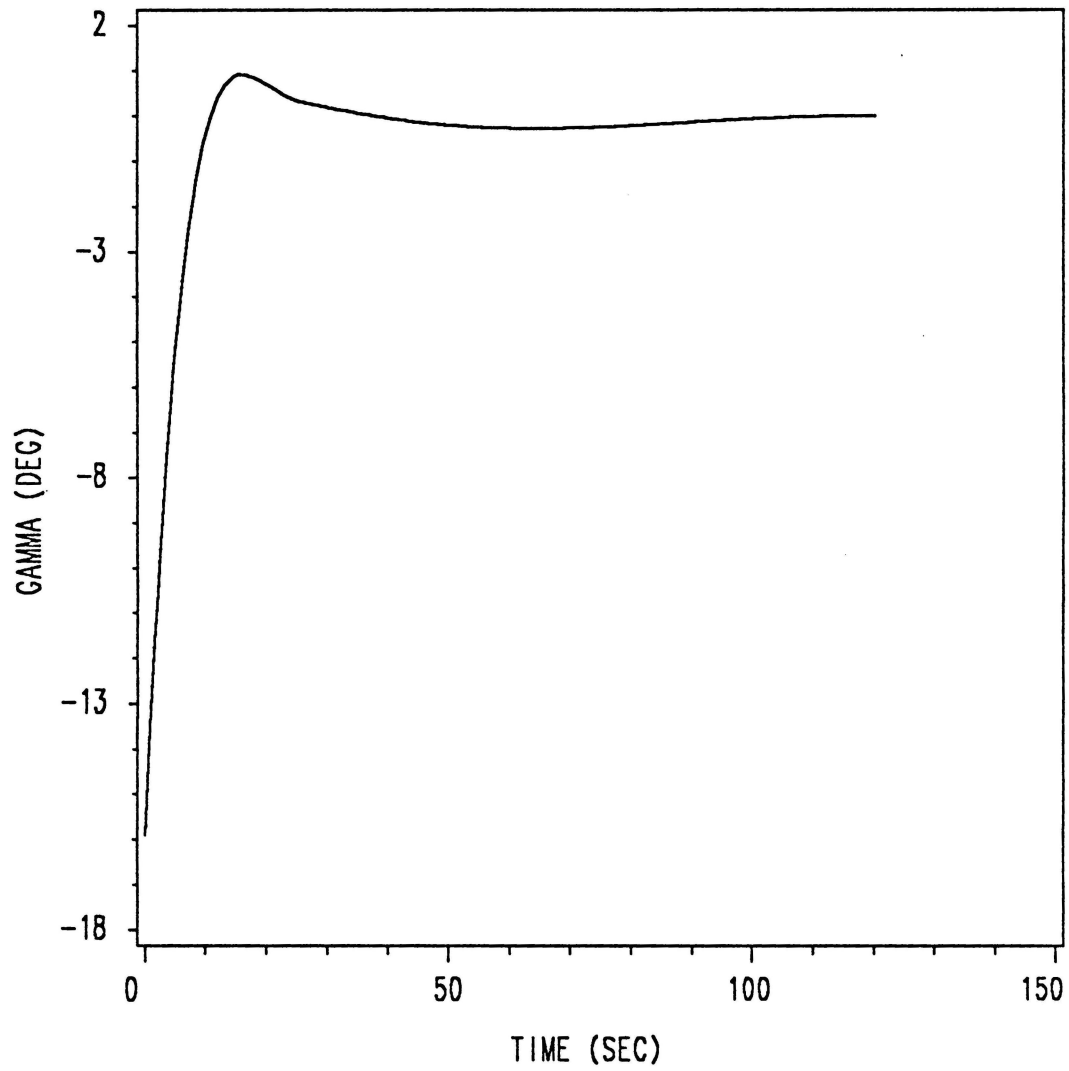


Figure 31. Path-Angle Time History for (Zero)Bang-Singular Control

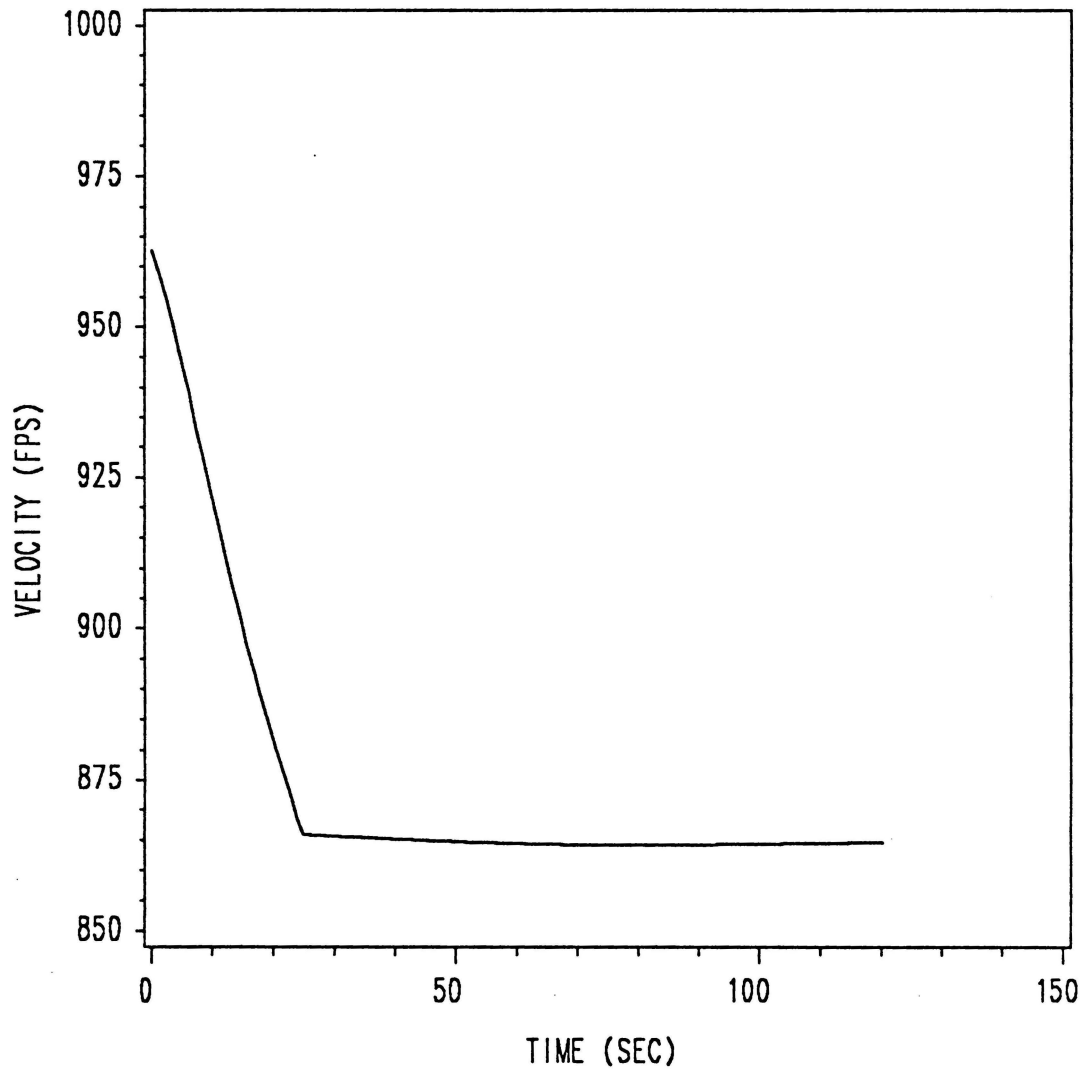


Figure 32. Velocity Time History for (Zero)Bang-Singular Control

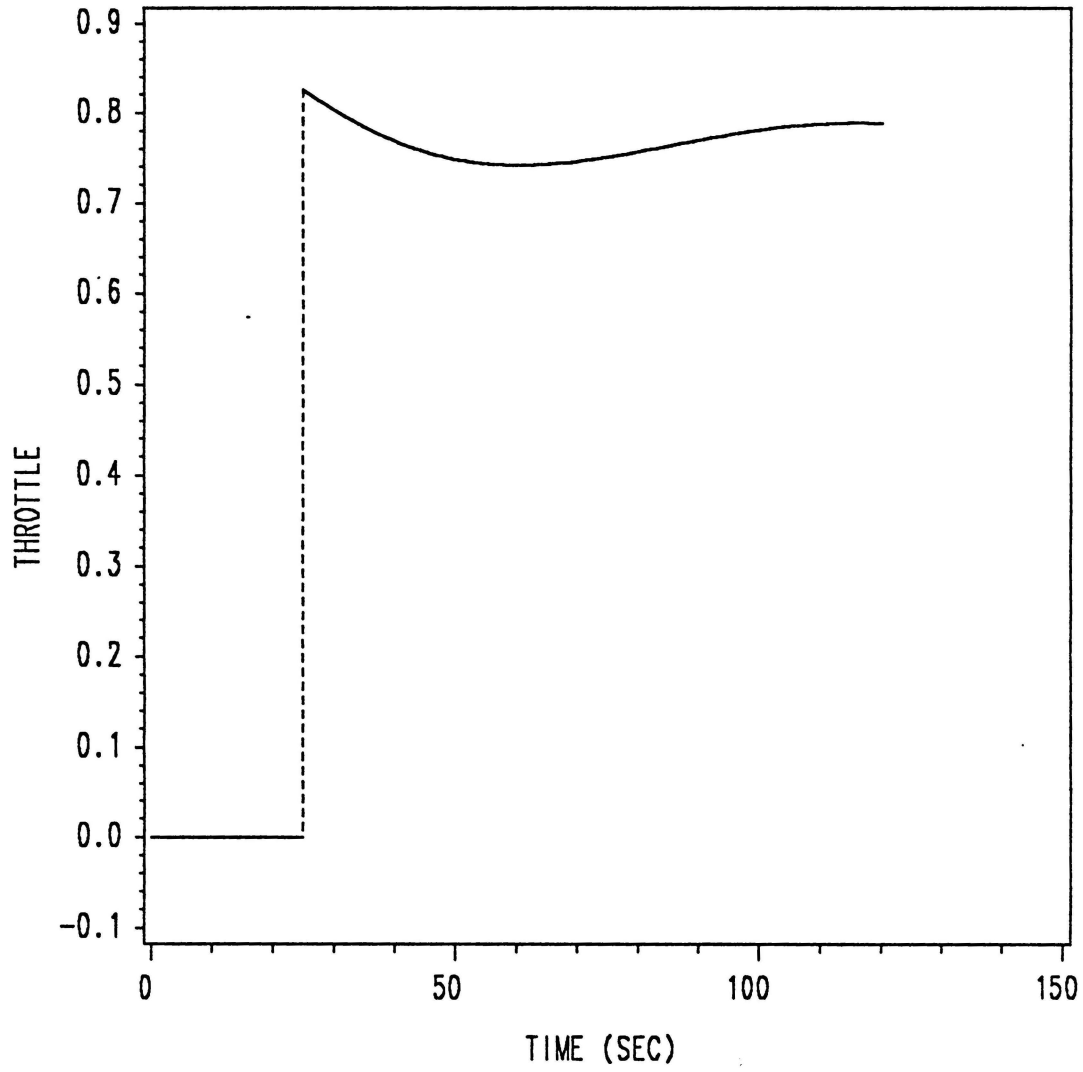


Figure 33. Throttle Time History for (Zero)Bang-Singular Control

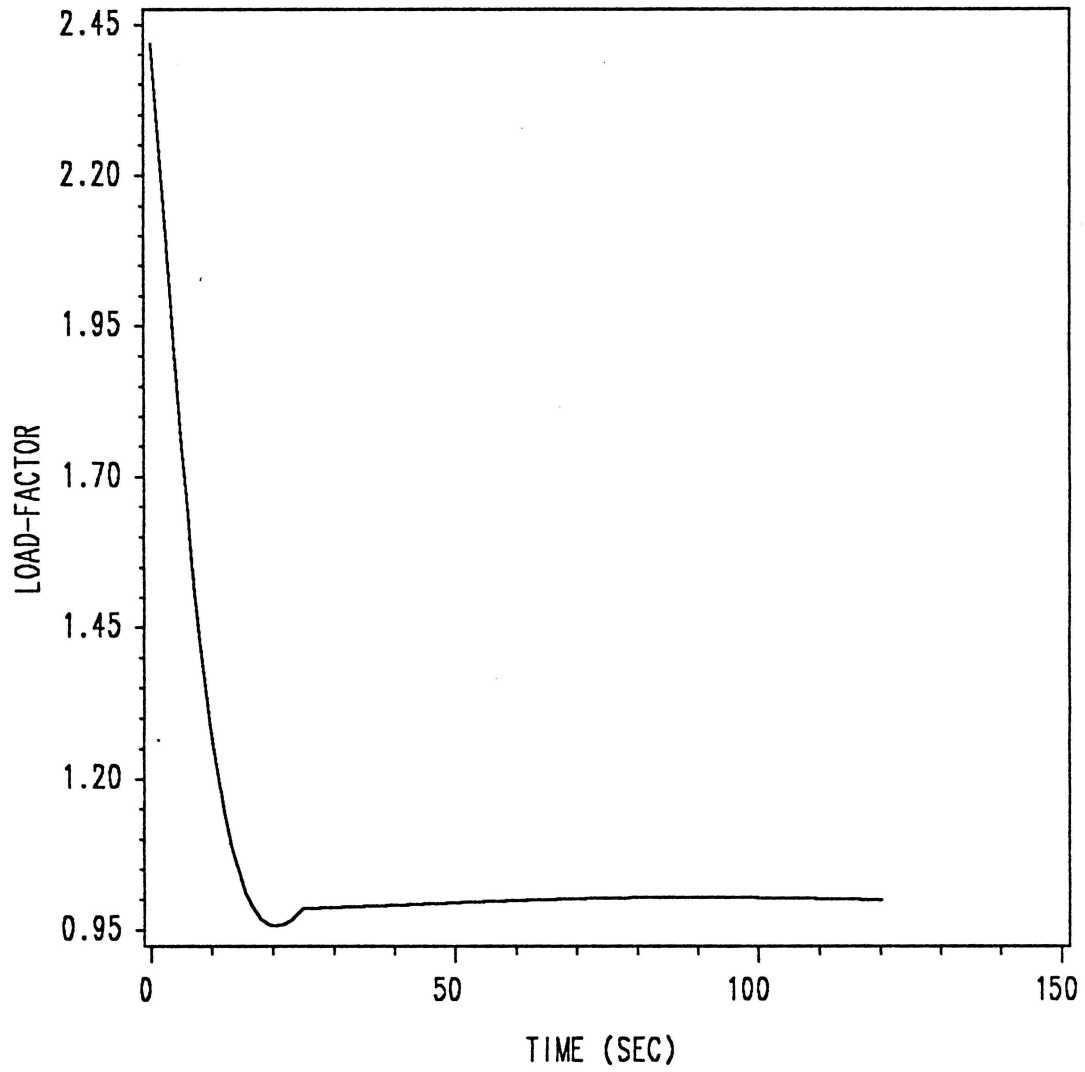


Figure 34. Load-Factor Time History for (Zero)Bang-Singular Control

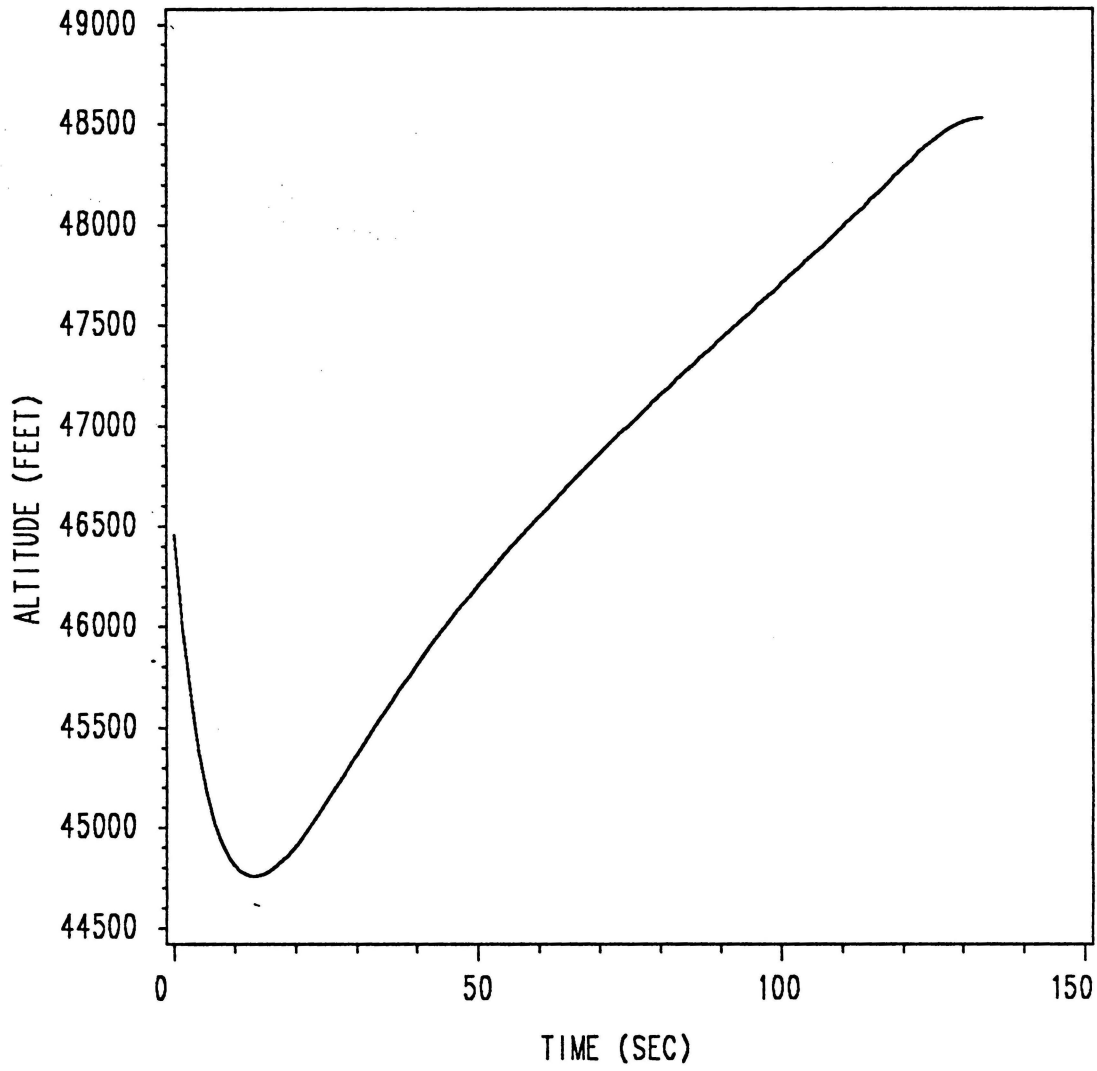


Figure 35. Altitude Time History for Bang-Bang Control



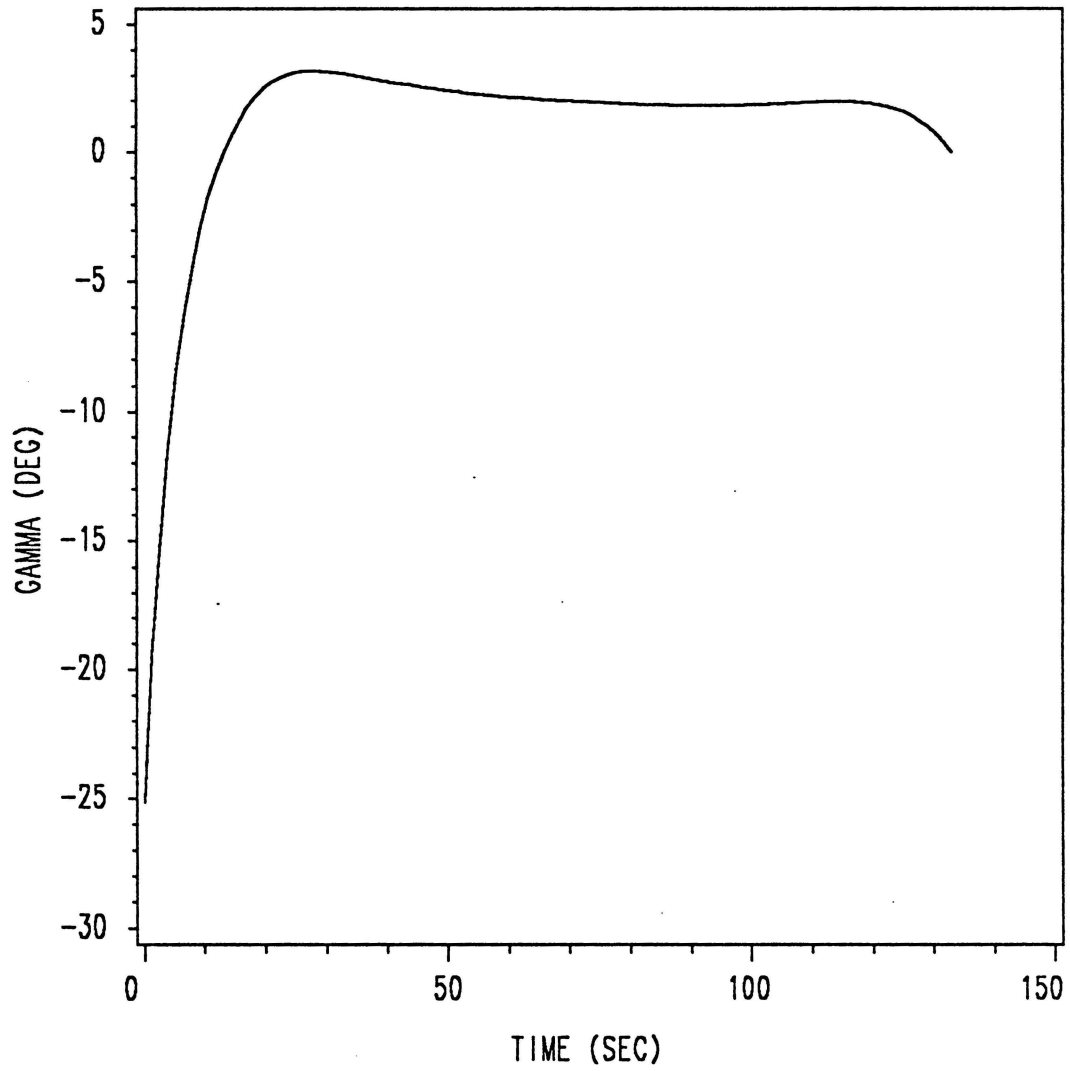


Figure 36. Path-Angle Time History for Bang-Bang Control

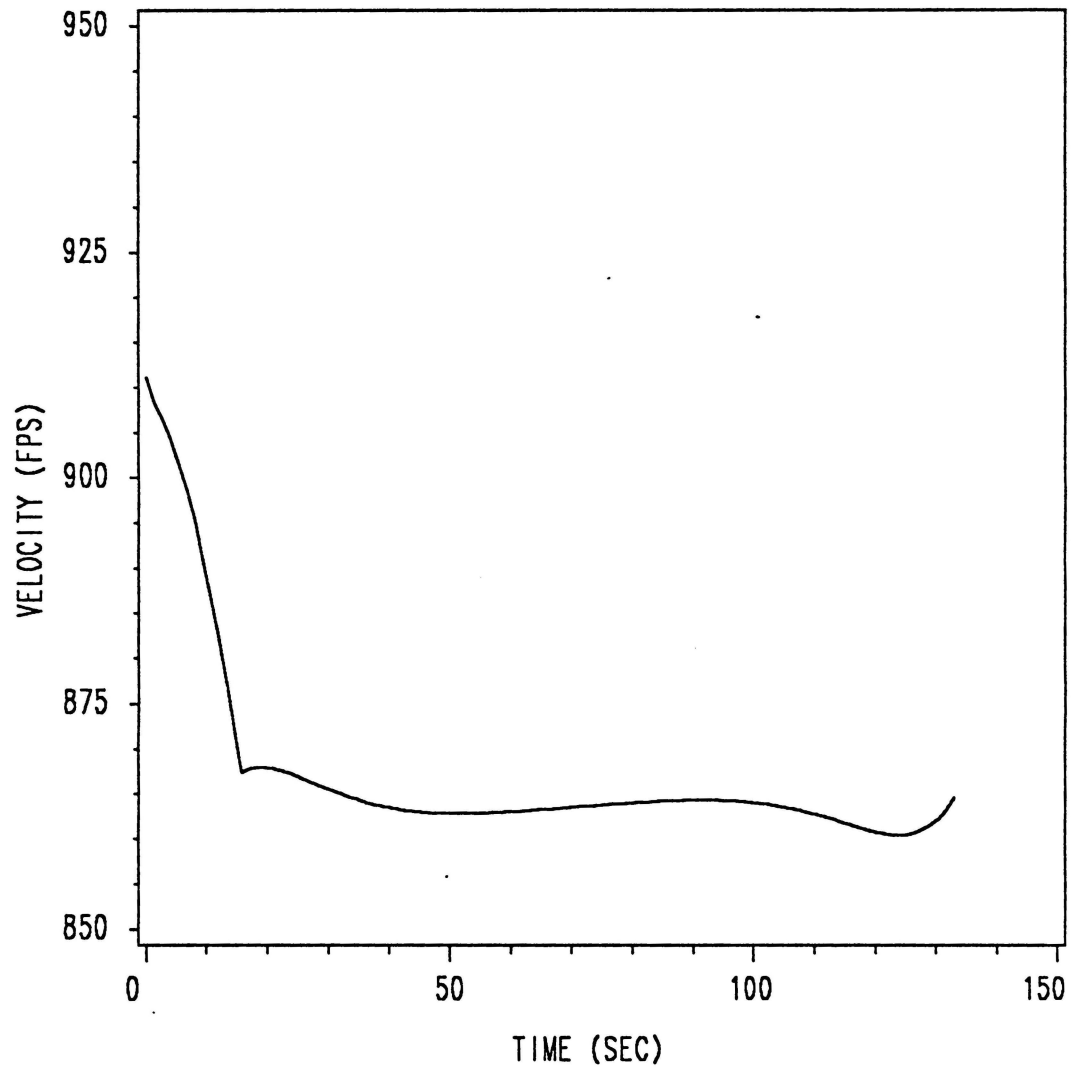


Figure 37. Velocity Time History for Bang-Bang Control

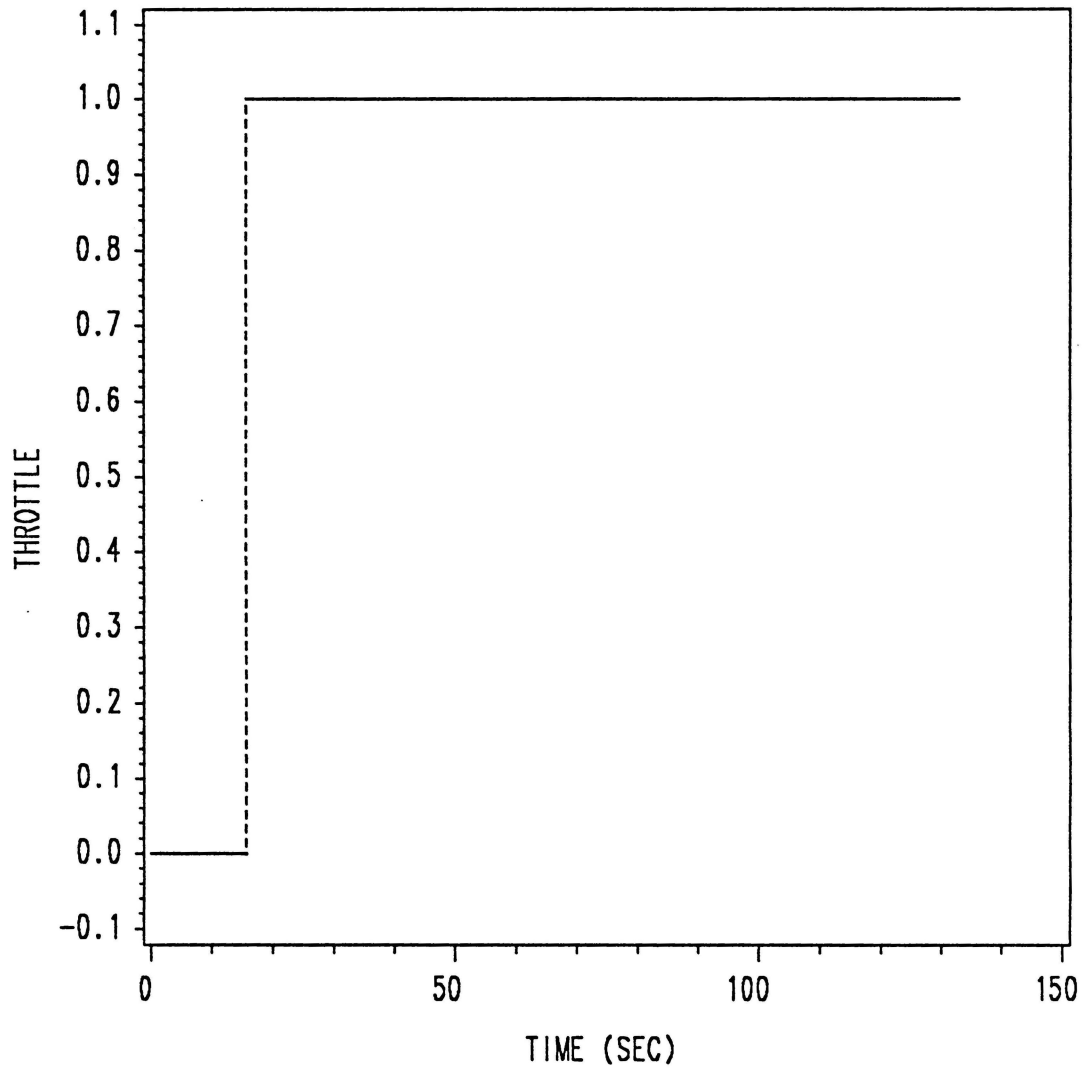


Figure 38. Throttle Time History for Bang-Bang Control

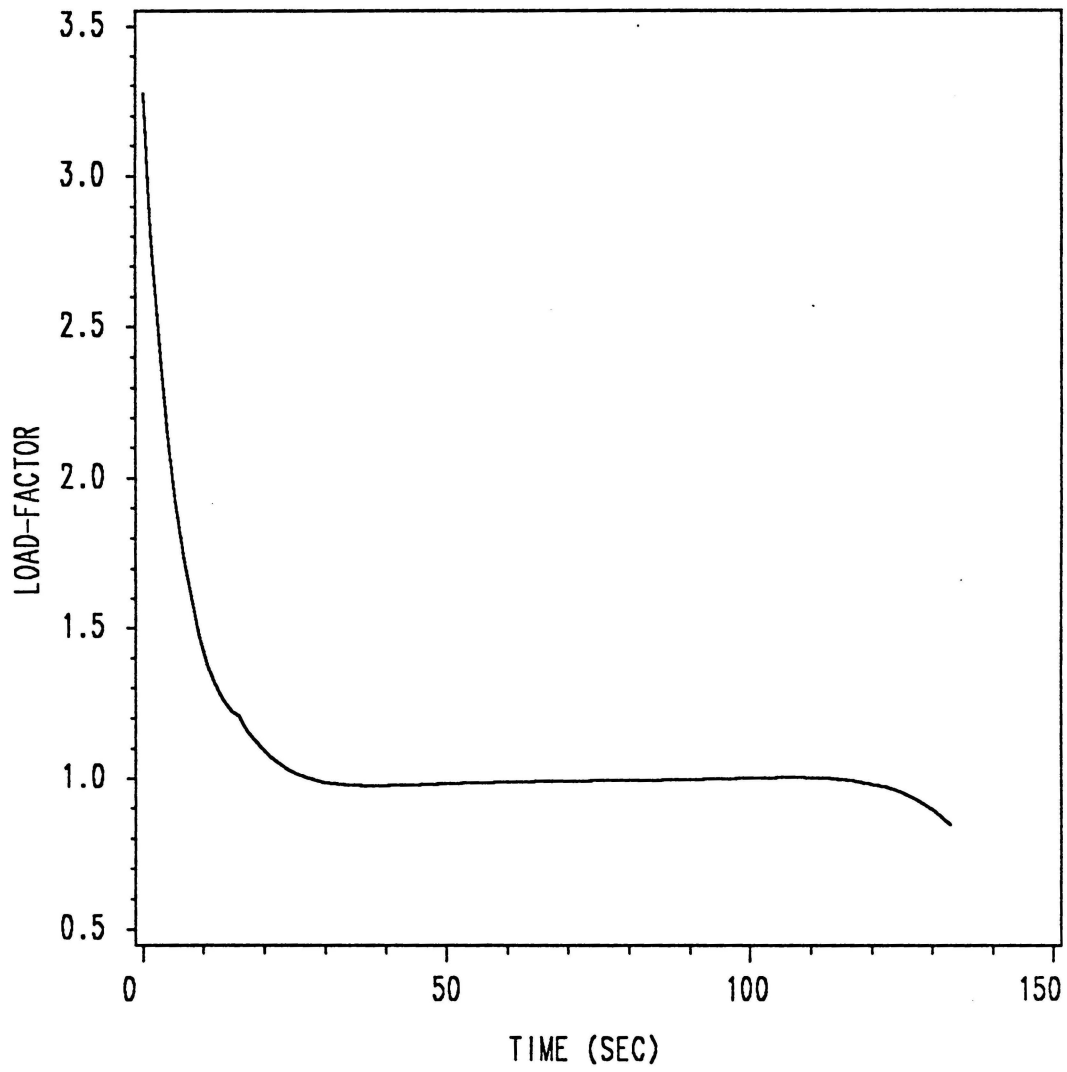


Figure 39. Load-Factor Time History for Bang-Bang Control

**The vita has been removed from  
the scanned document**